Lithosphere

An episodic slab-rollback model for the origin of the Tharsis rise on Mars: Implications for initiation of local plate subduction and final unification of a kinematically linked global plate-tectonic network on Earth

An Yin

Lithosphere 2012;4;553-593
doi: 10.1130/L195.1

Notes

An episodic slab-rollback model for the origin of the Tharsis rise on Mars: Implications for initiation of local plate subduction and final unification of a kinematically linked global plate-tectonic network on Earth

An Yin*
DEPARTMENT OF EARTH AND SPACE SCIENCES AND INSTITUTE FOR PLANETS AND EXOPLANETS (IPLEX), UNIVERSITY OF CALIFORNIA, LOS ANGELES, CALIFORNIA 90095-1567, USA

ABSTRACT

A new tectonic model is proposed for the origin of the Tharsis rise on Mars, which occupies ~25% of the planet. The model invokes initiation of plate subduction by a large impact during the Late Heavy Bombardment at ca. 4.0 Ga. The model explains migration of Tharsis volcanism by slab rollback and the lack of magnetized crust in the bulk of Tharsis by formation of juvenile crust after the Mars dynamo creased to operate. The model also explains (1) the formation of thrust systems as a result of impact-generated crustal thickening (i.e., Thaumasia thrust), retro-arc contraction (i.e., Solis-Lunae fold belt), and plate subduction (Lycus and Ulysses thrusts), (2) the development of dominantly NE-trending grabens and a major east-facing V-shaped conjugate strike-slip system across the Tharsis rise as a result of backarc extension, and (3) crustal thickening of the Tharsis rise as a result of magmatic accretion during protracted construction of arcs above an episodically stalled and thus stationary subducting slab. The model has several implications for the way in which a unified global plate-tectonic network may have been established on early Earth. First, large impacts were common during the Late Heavy Bombardment (ca. 4.2–3.9 Ma), and thus impact-induced plate subduction would have been highly likely in the Hadean period. Such subduction systems must be local in scale and associated only with trench retreat and slab rollback. Localized plate subduction permits other modes of tectonic processes to have occurred simultaneously on early Earth, reconciling conflicting observations for plate-tectonic and non-plate-tectonic processes. Second, the presence of water at the surface of Hadean Earth would have allowed rapid transformation of basaltic crust to eclogite, allowing a sustainable plate subduction process once it started. The Hadean and possibly Archean Earth may only have had localized subduction systems, all characterized by slab rollback and trench retreat. Trench advance and related shallow-angle plate subduction probably did not begin on Earth until Proterozoic time, when a single and united global plate-tectonic network was established. This may have been accomplished by gradual coalescence of formerly independent subduction systems over a significant period of geologic time (>1 b.y.). Incorporation of trench-advance and shallow-angle plate subduction in the Proterozoic may have been induced by complex interactions of multiple subduction systems in a single and kinematically linked global tectonic network. This in turn led to the beginning of the formation of the crustal structures and petrologic assemblages of modern Earth. Based on a simple conductive cooling model, it appears that the most critical factors that control whether plate subduction could have been initiated in a rocky planet during the Late Heavy Bombardment in the inner solar system are its initial crustal thickness and the cooling rate/thickening rate of the lithosphere.

LITHOSPHERE; v. 4; no. 6; p. 553–593 | Published online 14 November 2012 doi: 10.1130/L195.1

INTRODUCTION

With an average elevation of 7–11 km, the Tharsis rise is the largest highland region on Mars and in the solar system (Fig. 1). Although understanding of this large topographic feature, occupying 25% of the Martian surface, has been the focal point of several excellent syntheses (Zuber, 2001; Phillips et al., 2001; Solomon et al., 2005; Nimmo and Tanaka, 2005; Carr and Head, 2010; Golombek and Phillips, 2010), its tectonic origin remains debated. Existing models involve construction of the highland either from below (magmatic underplating–induced hotspot activity or mantle upwelling; Carr, 1974; Wise et al., 1979; Mège and Masson, 1996a, 1996b; Harder and Christensen, 1996; Baker et al., 2007; Dohm et al., 2007; Zhong, 2009) or from above (voluminous volcanic deposits induced by impacts or some forms of lithospheric deformation as inducers; Solomon and Head, 1982; Sleep, 1994; Stevenson, 2001; Reese et al., 2004; Golabek et al., 2011).

In order to appreciate the enormous size of the Tharsis rise, at 3500 km wide and 6000 km long, we may compare it to a few familiar features on Earth. First, the areal extent of Tharsis is >5 times bigger than the combined Himalayan-Tibetan orogen (Yin and Harrison, 2000). Its size is equivalent to the north-south distance of North America (Fig. 2). As the formation of the Tharsis rise has long been related to hotspot activity (e.g., Carr, 1974; Zhong, 2009) and the radius of Mars is only about half that of Earth, it is particularly surprising that the width of the Tharsis rise is up to 10 times greater than the hotspot track of the Hawaiian plume (Fig. 2B).

The existing Tharsis models may be tested by tectonic and igneous features due to their distinctive predictions. The top-construction model requires downward loading and predicts contraction in the center and extension across

*E-mail: yin@ess.ucla.edu; ayin54@ gmail.com.

Editor's note: This article is part of a special issue titled "Initiation and Termination of Subduction: Rock Record, Geodynamic Models, Modern Plate Boundaries," edited by John Shervais and John Wakabayashi. The full issue can be found at http://lithosphere.gsapubs.org/content/4/6.toc.

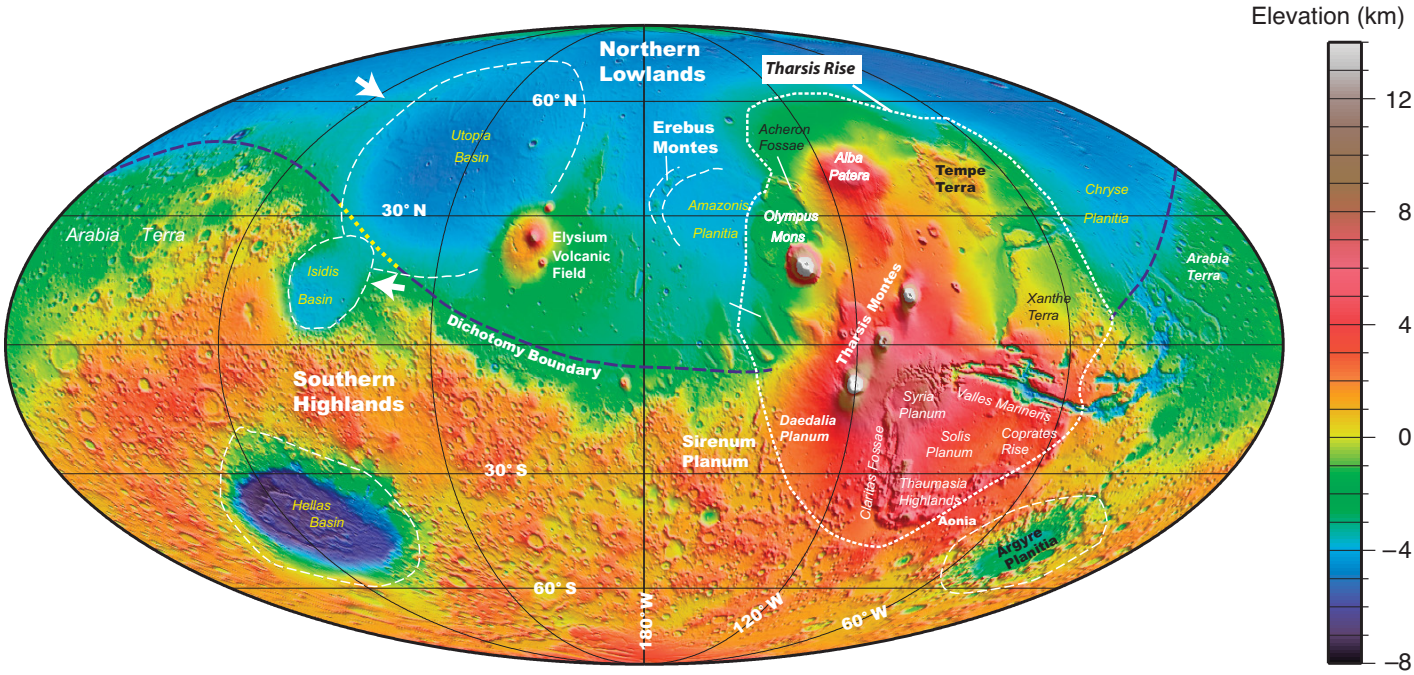

Figure 1. Location of Tharsis rise and major topographic features in and adjacent to the region. Also shown are four largest impact basins on Mars: Hellas, Utopia, Isidis, and Argyre.

the rim of the Tharsis rise at the surface; in contrast, the bottom-construction model requires upward loading and predicts extension in the center and contraction across the rims of the Tharsis rise (e.g., Tanaka et al., 1991; Banerdt et al., 1992). In the stationary hotspot model of Carr (1974), it predicts fixed volcanic centers throughout the evolution of the Tharsis rise, and its development is unrelated to the nearby tectonic features such as major impact basins and highly cratered highlands to the south. The migrating plume model of Zhong (2009) requires volcanism to have swept across the Tharsis rise from southeast to northwest during its evolution (also see Hynek et al., 2011; Šrámek and Zhong, 2010, 2012).

Despite distinctive predictions of the competing Tharsis models in the formation of fault patterns and volcanic evolution, there have been no systematic geologic tests that integrate structural and volcanic data from the Tharsis rise. In this paper, I review the existing knowledge on the temporal evolution of Tharsis volcanism. This is followed by new structural analysis of key fault zones in the Tharsis rise using recently available high-resolution satellite images. This integrated information forms the basis for a new tectonic model of the Tharsis rise that invokes plate subduction induced by a large impact followed by slab rollback, which caused migration of Tharsis volcanism and development of a northeast-trending graben zone in the backarc region.

The new Tharsis model proposed here may provide insights into how and why plate tectonics came to be initiated on Earth. Hansen (2007) and Ruiz (2011) both proposed that plate tectonics on Earth may have been generated by large impacts during the Late Heavy Bombardment in the inner solar system. The best candidates for testing these models are rocky planets such as Mars, where the records of large impact events are still well preserved. Based on our current understanding of the temporal evolution and chronology of Mars (Hartmann and Neukum, 2001), the rates of tectonic deformation and erosion on Mars may be significantly lower than those on Earth. For example, the slip rate on the San Andreas fault is about 35 km/m.y., whereas slip rate on the Valles Mariners left-slip fault that was developed in the past 1–3 Ga and has a total slip of ~150 km is about 50–150 m/m.y. (Yin, 2012). Thus, the evolution of Mars may serve as a slower version of the early history of Earth.

MORPHOLOGY AND LITHOLOGY OF THE THARSIS RISE

The Tharsis rise crosscuts the older hemispheric dichotomy separating the northern lowlands from the southern highlands (Fig. 1; e.g., Carr, 2006; Andrews-Hanna et al., 2008a). Its spatial extent is defined by (1) a sharp topographic front along the edges of the Olympus Mons and Acheron Fossae in the northwest, (2) Gordii Dorsum, Daedalia Terra, and Claritas Fossae in the southwest, (3) the northeastern edges of Tempe Terra, Lunae Planum, and Xanthe Terra in the northeast, and (4) the Thaumasia mountain belt in the southeast (Fig. 2A). Alba Patera (or Alba Mons in more recent literature) marks the northwestern corner of the Tharsis rise. Within the rise, the northeast-trending Tharsis Montes, consisting of Ascraeus, Pavonis, and Araia Montes, and Valles Marineris dominate its morphology (Fig. 2A).

Scott and Tanaka (1986) and Skinner et al. (2006) recognized the following geologic units across the Tharsis rise: (1) heavily cratered and highly fractured Early Noachian basement (Nf) that is exposed at Thaumasia Highlands, Coprates rise, Clarita Fossae, Ceraunius Fossae, Tempe Fossae, and Noctis Labyrinthus, (2) minor Hesperian highly fractured terranes (unit Hf), (3) Late Noachian to Late Amazonian volcanic flows that were deposited during the construction of the Tharsis rise, and (4) minor surface deposits (Fig. 3; also see Dohm et al., 2001a, 2001b, 2001c; Williams et al., 2003; Plescia, 2004; Skinner et al., 2006; Baptista et al., 2008). Among these units, volcanic rocks occupy ~80% of the total area of the Tharsis rise (e.g., Skinner et al., 2006; Hauber et al., 2009).

THARSIS VOLCANISM

Tharsis volcanic fields and eruption centers can be broadly grouped into four zones,

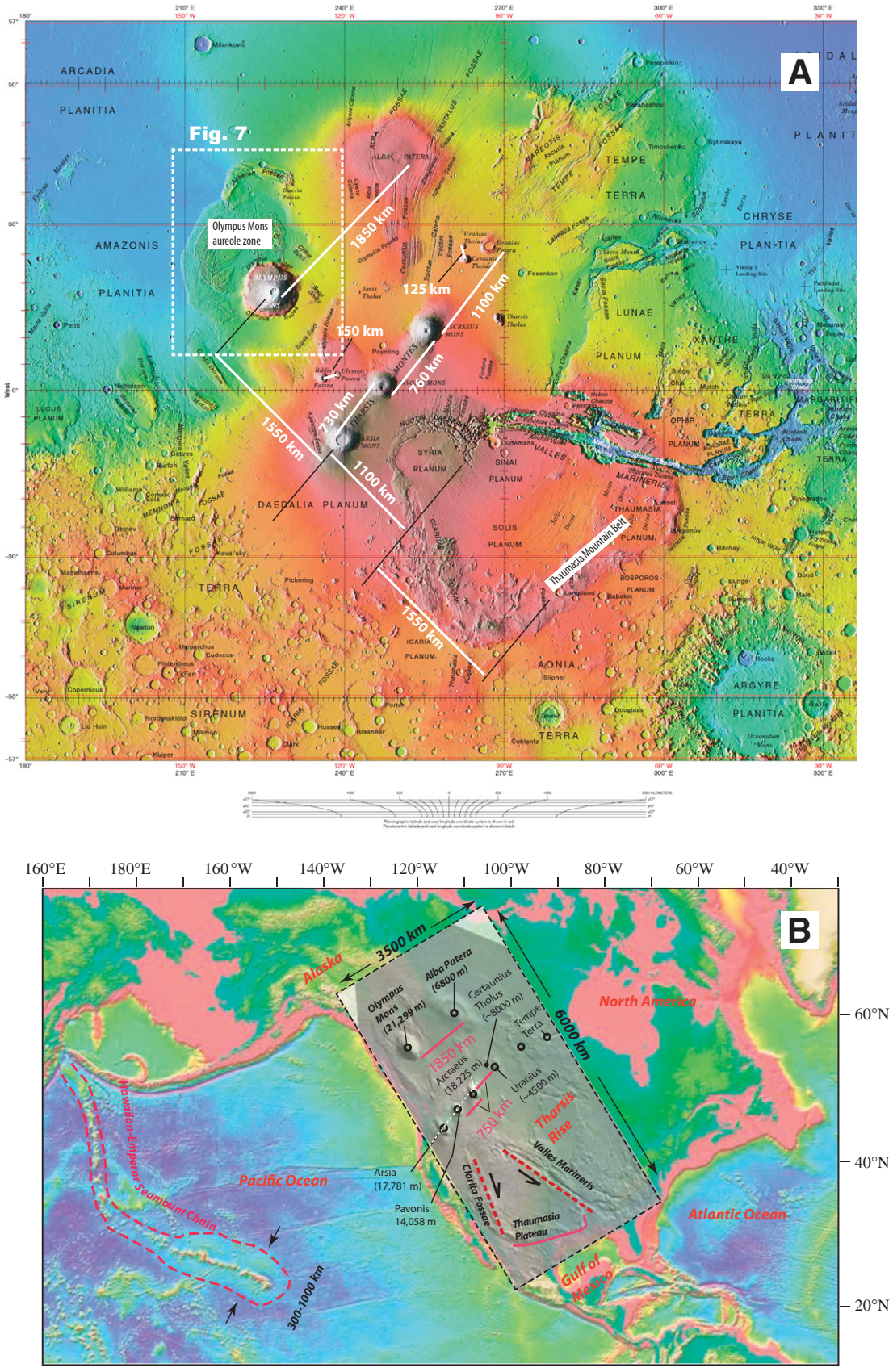

Figure 2. (A) Geographic map of Tharsis rise, with location names mentioned in the text. (B) Superposition of Tharsis rise over North America at the same scale.

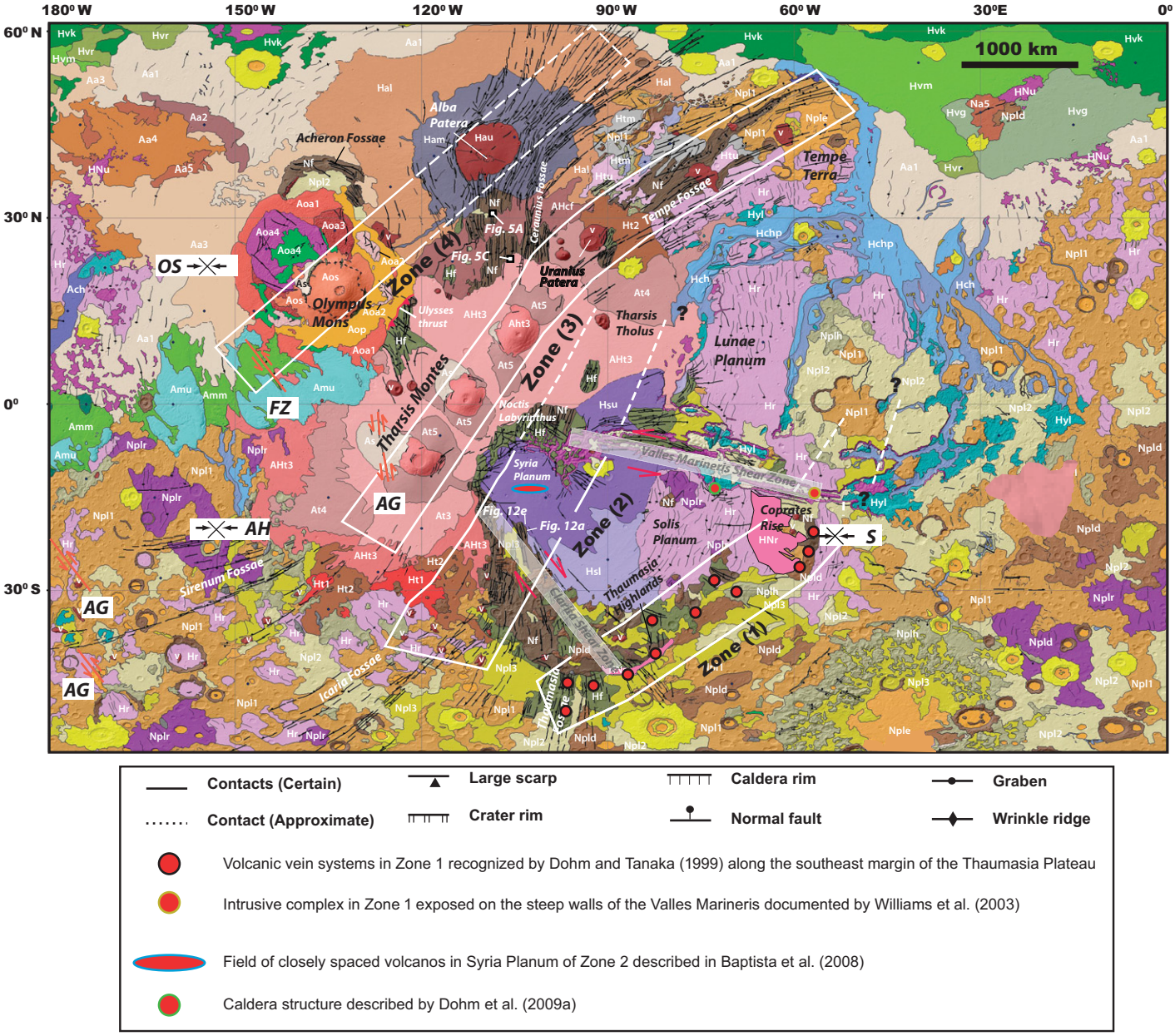

Figure 3. Geologic map of the Tharsis rise from Scott and Tanaka (1986). White boxes are four volcanic zones discussed in the text. AG, FZ, AH, OS, and S—locations where strike-slip faults were documented around the rim of the Tharsis rise. AG—study site by Anguita et al. (2001), FZ—study site by Forsythe and Zimbelman (1988), OS—study site by Okubo and Schultz (2006), AH—study site by Andrews-Hanna et al. (2008b), and S—study site by Schultz (1989). Age assignments of lithologic units are as follows, according to Scott and Tanaka (1986) and Skinner et al. (2006): N—Noachian; H—Hesperian; A—Amazonian. Main units relevant to this study: Nf—highly fractured Noachian terrane; Npld—highly eroded crater unit consisting of a mixture of lava flows, pyroclastic material and impact breccias; Nplh—relics of highland volcanic rocks and impact breccia; Hr—extensive flows of low viscosity erupted in the Early Hesperian; Ht1, Ht2, AHt3, At4, At5, At6—volcanic units in the Tharsis Montes region; Aoa1, Aoa2, Aoa3, Aoa4—units in the Olympus aureole zone; Aos, Aop—lava flow units from Olympus Mons; Hal, Aam, Aau—volcanic units of the Alba Patera; Htl, Htm, Htu—Tempe Terra Formation consisting of many small (<10 km in diameter) central volcanoes and collapsed structures. Locations of Figures 5A and 5C are also shown. Also shown are volcanic fields and intrusive features mapped by Dohm and Tanaka (1999), Williams et al. (2003), Baptista et al. (2008), and Dohm et al. (2009a).

all trending northeast, with their initiation and termination ages generally becoming younger from southeast to northwest based on crosscutting relationships and crater statistics (Fig. 3; Scott and Tanaka, 1986; Skinner et al., 2006). As volcanism overlaps in time between adjacent volcanic zones (e.g., Dohm et al., 2001a) and the basal units of initial volcanic deposits are commonly covered by younger flows in the Tharsis rise (Scott and Tanaka, 1986; Skinner et al., 2006), the available geologic relationships in most cases provide only upper and lower bounds. What is more readily discernible is the termination age of volcanic zones from crosscutting relationships of lava flows originating from different eruption centers. Note that the description and discussion of Tharsis volcanism herein focus only on volcanic rocks deposited on top of Early Noachian basement (i.e., unit Nf in Fig. 3). This does not preclude that pre-Noachian basement is composed of igneous rocks, as shown by Dohm et al. (2001a, 2001b) in the southeastern Tharsis region.

Zone 1 Volcanism

In zone 1, most volcanic centers lie in a 200–300-km-wide belt along the southeast margin of the Thaumasia Plateau, including the Thaumasia Plateau and Coprates rise mountain ranges, although the volcanic flows extend much farther to the northwest (Figs. 1 and 3). Volcanic rocks in zone 1 were emplaced in the Late Noachian and Early Hesperian via effusive eruption from vein-like sources (Fig. 3; Dohm et al., 2001a, 2001b). Intrusive centers may be exposed on the walls of Valles Marineris (Fig. 3; Williams et al., 2003). Gravity modeling requires the existence of a thick volcanic pile in this zone (Williams et al., 2008).

Zone 2 Volcanism

In zone 2, volcanic fields migrated northward, as indicated by sequential replacement of older smooth-ridged volcanic flows by younger and lobate volcanic-plain units in the Late Hesperian (Fig. 3; Dohm and Tanaka, 1999). A cluster of closely spaced (20–40 km) Hesperian shield volcanoes (diameters of 5–20 km) is present across Syria Planum (Fig. 3; Baptista et al., 2008). These rocks overlie Early Hesperian units (Dohm and Tanaka, 1999), providing a lower age bound for their emplacement. However, their upper age limit is not constrained. Zone 2 volcanism may locally record later-stage volcanism possibly into the Amazonian Period (Dohm et al., 2001a). The Hesperian volcanic rocks around Tharsis Tholus are also grouped into zone 2 in this study (Fig. 3).

Zone 3 Volcanism

In zone 3, volcanic rocks are closely related to the central volcanoes of Arsia Mons, Pavonis Mons, Ascraeus Mons, Uranius Patera, and those in northern Tempe Terra (Fig. 3) based on geologic mapping of Scott and Tanaka (1986) and Skinner et al. (2006). The calderas of the central volcanoes in zone 3 are spaced between 750 km and 850 km apart (Fig. 3). According to geologic mapping and crater counts, most volcanic rocks in zone 3 were emplaced between the Late Hesperian and the Late Amazonian, although volcanism at Uranius Patera appears to have finished earlier than other volcanoes in the Early Amazonian (Scott and Tanaka, 1986; Skinner et al., 2006; Werner, 2009). Similar age relationships have also been documented for volcanic centers at Ceraunius Tholus, Uranius Tholus, Biblis Patera, Ulysses Tholus, and Tharsis Tholus (Figs. 2 and 3), where volcanic flows appear to predate the voluminous, late-stage flows emplaced from the Tharsis Montes (Plescia, 2000; Murray et al., 2010; Platz et al., 2011; Brož and Hauber, 2012). North of Biblis Patera and at the foothills of Ascraeus Mons (Fig. 2A), small volcanic cones displaying steep slopes are interpreted to have been generated by explosive eruptions (Murray et al., 2010; Brož and Hauber, 2012). Explosive eruption at a much larger scale from the Tharsis Montes was inferred from theoretical considerations and the observation that extensive ash-like deposits are present within and around the Tharsis rise (e.g., Head and Wilson, 1998a, 1998b; Mouginis-Mark, 2002; Hynek et al., 2003; Squyres et al., 2007). The style of volcanic eruption in the Tharsis Montes changed from main-flank construction to diffusely distributed effusion along small volcanic veins controlled by rifts (Crumpler and Aubele, 1978; Bleacher et al., 2007, 2009). At Tharsis Tholus, the composite shield volcano and its neighboring plain regions were affected by 1.7–0.4 Ga (Late Amazonian) NE-trending graben structures (Platz et al., 2011).

The shape of individual volcanoes in zone 3 changes along strike, from the high (14–18 km) eruption centers in the southwest (i.e., Tharsis Montes) to low volcanic centers in the northeast (i.e., Uranius Patera at 4.5 km and Ceraunius Tholus at 8 km) (Fig. 2). Carr (2006) noted that the caldera of Uranius Patera is much larger than those associated with the three volcanic centers of the Tharsis Montes. As the size of calderas is proportional to the amount of eruptions, Carr (2006) proposed that Uranius Patera was developed into a flat and aerially extensive volcano much like younger Alba Patera; its gentle flanks are now buried by young volcanic flows.

Zone 4 Volcanism

Zone 4 consists of Olympus Mons and Alba Patera and was initiated in the latest Hesperian and Early Amazonian (ca. 3.4 Ga; Fig. 3; Scott and Tanaka, 1986; Mouginis-Mark et al., 1988; Hiesinger and Head, 2002; Werner, 2009). Eruption at Alba Patera, a late-stage (Hesperian and younger) regional center of magmatic-tectonic activity within the Tharsis rise (Anderson et al., 2001), occurred as recently as ca. 200 Ma, whereas Olympus volcanism may have continued in the past few million years (Fig. 3; Scott and Tanaka, 1986; Hartmann and Neukum, 2001; Werner, 2009).

An extensive Early Hesperian volcanic unit has been mapped around Alba Patera (Fig. 3; unit Hal of Scott and Tanaka, 1986). The edge of this unit extends more than 1500 km from the volcanic center of Alba Patera, and its Early Hesperian age has been used by all previous workers as evidence to support an earlier initiation of volcanism at Alba Patera than that in Olympus Mons (e.g., Wise et al., 1979; Scott and Tanaka, 1986; Morris and Tanaka, 1994; Ivanov and Head, 2006). This age assignment would place the initiation of Alba Patera volcanism synchronous with that along the Tharsis Montes, as implied in the geologic map of Scott and Tanaka (1986).

Unit Hal is associated with exceedingly low-slope topography (e.g., Carr, 2006). This unit lies below a cone-shaped and more steeply dipping volcanic unit (Fig. 3; unit Ham of Scott and Tanaka, 1986). Although the source of volcanic flows in unit Hal has been assigned to Alba Patera, this is by no means a unique interpretation. Carr (2006) noted that the caldera size of the central volcano at Uranius Patera directly southeast of Alba Patera is larger than the caldera size of Alba Patera. Based on this observation, Carr (2006) suggested that the volcanic construct of Uranius Patera was perhaps even greater than that of Alba Patera when it was active. Despite this interesting insight, the existing geologic map does not relate any volcanic units to this volcano at Uranius Patera except unit v in Figure 3, which defines the remaining volcanic cone mostly buried by younger volcanic flows (Scott and Tanaka, 1986). As units At4 and At5 are clearly related to volcanic eruption of the Tharsis Montes (that is, they can be traced to the eruption centers; see Fig. 3), it raises the question: Where are the volcanic flows erupted from the large caldera at Uranius Patera? Here, I suggest that unit Hal was derived from early eruption at Uranius Patera rather from Alba Patera. This interpretation implies that volcanism at Alba Patera did not start until the Late Hesperian and Early Amazonian, coeval with

the initiation of volcanism at Olympus Mons. I further suggest that the Early Hesperian volcanic unit Hr in Tempe Terra was also derived from Uranius Patera. The hypothesis of a greater Uranius Patera volcanic system is tentative and requires further investigation into the paleoflow directions of units Hal and Hr in the northern Tharsis rise using recently available high-resolution satellite images.

Similar to the observation in zone 3, the shapes of central volcanoes change along strike from tall and narrow Olympus Mons (peak elevation at 21 km) in the southwest to short and wide Alba Patera (peak elevation at 6.8 km) in the northeast (Fig. 2). Such a difference in morphology requires the lava viscosity of Alba Patera to be lower than that of Olympus Mons. This in turn requires different magmatic sources for the two volcanoes. Eruption style of Alba Patera has been considered to be effusive, with its average viscosity constrained to be ~4×10^6 Pa (Hiesinger et al., 2007). However, pyroclastic deposits were also proposed for volcanism at Alba Patera by Mouginis-Mark et al. (1988).

The style of eruptions at Olympus Mons has not been well determined. For example, Morris (1982) proposed that the Olympus aureole zone may have been produced by explosive eruption due to flank failure. This interpretation is among many other interpretations for the origin of the Olympus aureole zone, which include (1) erosional remnants (Carr, 1973), (2) gravitational spreading and thrusting induced by magma push (Harris, 1977; Tanaka, 1985; McGovern et al., 2004), (3) subglacial flows (Hodges and Moore, 1979), (4) submarine processes (Blasio, 2011), (5) volcanic spreading (Borgia et al., 1990; McGovern and Morgan, 2009), and (5) mass wasting at the base of Olympus Mons (Lopes et al., 1980, 1982; Shea and van Wyk de Vries, 2008). Effusive volcanism at Olympus Mons was also reported by Carr et al. (1977), Wadge and Lopes (1991), and Rawling et al. (2003).

The aforementioned synthesis of literature indicates that Alba Patera and Olympus Mons both were constructed by explosive and effusive eruptions. This mixed mode of eruption could be a result of temporal evolution of a volcanic system, for example, with explosive eruption first, followed by effusive eruption due to a progressive decrease in volatiles inside magma chambers. As the Olympus aureole zone is cut by normal faults (Scott and Tanaka, 1986), its basal contact must have stopped moving. In contrast, the Olympus volcanic cone preserves nearly pristine young volcanic flows that are only a few million years old (Hartmann and Neukum, 2001; Werner, 2009). Thus, if the aureole zone was indeed created by pyroclastic explosion, as proposed by Morris (1982), the change in eruption style could have been controlled by the proposed degassing mechanism mentioned above.

An advantage of interpreting the large scarps (with a relief of 5–8 km) at the base of Olympus Mons (e.g., Lopes et al., 1980) as the sources of pyroclastic deposits (Morris, 1982) is that this interpretation results in the least mechanical and physical difficulties in explaining the large sizes (>1000 km long) and long transport distances (>1000 km from the sources) of individual spoon-shaped sheets around Olympus Mons. That is, the lateral transport of these rocky materials via air should have been much easier than transport on the ground surface.

Summary of Tharsis Volcanism

In summary, volcanism in the Tharsis rise is zonal, trending dominantly in the northeast direction. The initiation ages of zonal volcanism become younger from southeast to northwest. Early volcanism in the southwest was dominated by effusive eruption without clearly defined centers (i.e., in zone 1 of Fig. 3). This was followed by the development of closely spaced (20–30 km) clusters of central volcanoes in zone 2 to the northwest. The linear zoning of volcanism became well defined when zone 3 volcanism was developed along the Tharsis Montes. In comparison to zone 2, major central volcanoes are spaced ~750–800 km, which is ~30–40 times greater than volcano spacing in zone 2. Finally, zone 4 volcanoes were developed along the currently northwestern edge of the Tharsis rise, with the central volcanoes spaced at ~1800 km apart. In both zone 3 and zone 4, central volcanoes change morphology along strike, from tall and narrow in the southwest to flat and wide in the northwest. In addition, volcanism in zone 3 and zone 4 is locally expressed in the form of pyroclastic eruption, which may indicate the presence of volatiles inside magma chambers. More recent volcanic eruptions in both zone 3 and zone 4 were dominated by effusive eruption, suggesting that the late stage volcanism has less influence from volatiles inside the magma chamber.

As explained later herein by the proposed *episodic* slab rollback model, the zonal volcanism and its northwestward migration are interpreted as a result of slab rollback with the "trench" currently bounding the northwestern edge of the Tharsis rise. The inferred possible temporal change in eruption style in zone 3 and zone 4 from explosive to effusive eruption may be explained by episodic rapid subduction and slab rollback of Martian lithosphere that carried hydrous minerals at its surface down to the deep mantle. Once the subduction became stable and no more hydrous minerals were carried down to the mantle, volcanism was maintained by pressure-released melting due to mantle upwelling; the dominance of the latter would have switched the style of volcanic construction from explosive to effusive eruption. As detailed herein, the along-strike change in volcano morphology in zone 3 and zone 4 is best explained by mantle delamination in the northeast and whole-lithosphere subduction in the southwest across the Tharsis rise. The overlapping of volcanic activity between zone 3 and zone 4 can be explained as a result of arc migration and sustained backarc volcanism. That is, zone 3 volcanism changed from central-volcano eruption (arc) to fissure eruption (backarc) (Bleacher et al., 2009).

STRUCTURAL GEOLOGY AND SEQUENCE OF THARSIS DEFORMATION

Extensional, contractional, strike-slip, and transtensional structures have all been documented across the Tharsis rise (e.g., Wise et al., 1979; Plescia and Saunders, 1982; Scott and Tanaka, 1986; Schultz and Tanaka, 1994; Dohm and Tanaka, 1999; Mangold et al., 1998, 2000; Schultz, 2000; Anderson et al., 2001, 2004; Cailleau et al., 2003; Mueller and Golombek, 2004; Márquez et al., 2004; Anderson et al., 2001, 2004, 2008; Andrews-Hanna et al., 2008b; Yin, 2010a, 2010b, 2011a, 2011b, 2012). These structures may be grouped into: (1) the Main Tharsis graben zone (e.g., Carr, 2006), (2) the Solis-Lunae fold belt (e.g., Mueller and Golombek, 2004), (3) the Thaumasia thrust (e.g., Schultz and Tanaka, 1994), (4) the Valles Marineris fault zone (e.g., Schultz, 1998), (5) the Lycus thrust (Harris, 1977; this study), (6) the Gordii Dorsum fault zone (Forsythe and Zimbelman, 1988), (7) the Acheron fault zone (Kronberg et al., 2007), and (8) the Ulysses fault zone (Scott and Dohm, 1990; this study) (Fig. 4).

Although the synthesis presented here was based mostly from existing literature, new observations aiming at establishing the kinematics of major fault systems in the Tharsis rise are provided in this study. Data sources and methods for analysis of satellite images can be found in Schultz et al. (2010) and Yin (2012).

Main Tharsis Graben Zone

The >6000 km Main Tharsis graben zone, displaying large S-shaped geometry in map view, extends from Tantalus Fossae, Mareotis Fossae, and Tempe Fossae in the north to Daedalia Planum and Terra Sirenum in the south (Figs. 3 and 4; Scott and Tanaka, 1986; Carr, 2006; Skinner et al., 2006). The graben zone passes through the Tharsis rise diagonally, cutting through Alba Patera, Ceraunius Fossae, the

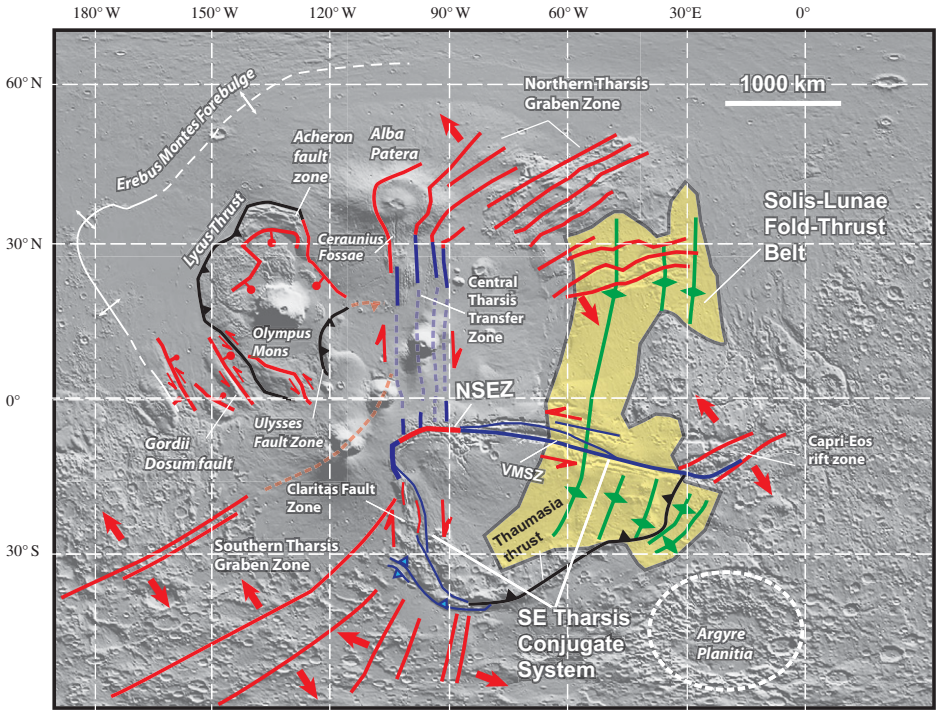

Figure 4. Tectonic map of Tharsis rise. NSEZ—Noctis Labyrinthus–Syria Planum extensional zone; VMSZ—Valles Marineris shear zone. Red lines represent locations and trends of major extensional structures, black lines represent thrusts, blue lines represent transtensional strike-slip fault zones, and white lines represent the inferred trace of forebulge. Green lines define the traces of major folds expressed as wrinkle ridges.

Tharsis Montes, and Claritas Fossae (Figs. 2, 3, and 4; e.g., Scott and Tanaka, 1986; Borraccini et al., 2005; Hauber and Kronberg, 2005; Carr, 2006; Dohm et al., 2009b). Individual grabens are expressed by closely spaced topographic depressions either bounded by normal faults or underlain by dikes (e.g., Anderson et al., 2001; Wyrick et al., 2004; Schultz et al., 2006, 2008; Polit et al., 2009; Wilson and Head, 2002; Scott et al., 2002; Wyrick and Smart, 2009).

Based on its local trend, the graben zone may be divided into the northern, central, and southern segments. The northern segment trends northeast and cuts across Alba Patera and northern Tempe Terra (Hauber and Kronberg, 2001). The semicircular patterns around volcanic centers at Alba Patera and Ascuris Planum indicate that graben formation was coeval with pluton emplacement (Fig. 4; e.g., Comer et al., 1985; Cailleau et al., 2003; Anderson et al., 2004). The central segment of the Main Tharsis graben zone trends north, extending from Claritas Fossae to the southern flank of Alba Patera. Its trace is disrupted by younger volcanic flows issued from Ascraeus Mons and Syria Planum and cut by younger northeast-tending grabens at Noctis Labyrinthus that link with the Valles Marineris fault zone (Figs. 3 and 4; Tanaka and Davis, 1988).

As the Main Tharsis graben zone has two dominant trends in the northeast and north directions, an obvious question is: In what direction was the extension accommodated? A preliminary structural analysis was carried out in this study across portions of Ceraunius Fossae, where right-slip transtensional faults can be established as detailed next. First, right-slip motion of north-trending faults in this segment of the graben zone is clearly indicated by right-lateral offsets of older and obliquely trending linear depressions that could either represent grabens or stream channels (Figs. 5A and 5B). A graben origin for the offset depressions would imply a much more complex history of deformation in the area. Second, right-lateral strike-slip faulting is also suggested by stream deflection patterns *across faults* in this graben zone (Figs. 5C–5I). The consistent "dog-leg" patterns of stream deflection in a right-lateral sense along the same fault strengthen the interpretation that the studied fault shown in Figures 5A and 5C is a right-slip structure; such a deflection pattern is commonly seen across active strike-slip faults on Earth (e.g., Burbank and Anderson, 2001). Note that we are only concerned with drainage patterns across identifiable fault traces rather than examining the geometry of naturally occurring streams in regions without tectonic disturbance. For example, at the east side of Figures 5F and 5G, an interpreted north-trending stream curves into the main east-west–trending stream as a tributary. As no fault trace can be found across the curved segment of the north-trending stream, its curvature cannot be caused by tectonics.

If stream deflection in Figures 5C–5G was a result of strike-slip faulting, and a minimum slip on individual faults of 200 m and 1000 m can be determined from restoring the drainage systems. For the deflected drainage system shown in Figures 5H and 5I, the required minimum slip from stream restoration is ~800 m (Fig. 5J).

The southern segment of the Main Tharsis graben zone starts from western Claritas Fossae and fans out southwestward across Terra Sirenum and western Daedalia Planum (Figs. 3 and 4; Hauber and Kronberg, 2005). The graben system cuts across the Thaumasia mountain belt and wrinkle ridges of the Solis-Lunae fold belt (Fig. 3; Scott and Tanaka, 1986; Dohm et al., 2001c), indicating that extension postdates folding and the development of the mountain belt.

The right-slip Ceraunius fault zone established in this study and the right-slip Claritas fault zone of Montgomery et al. (2009) to the south are structures linking NE-trending grabens in the Main Tharsis graben zone to the north and south. Together, the right-slip and graben structures accommodate dominantly NW-SE extension across the northwestern, central, and southeastern Tharsis rise (Fig. 3).

Solis-Lunae Fold Belt

The 400–600-km-wide and 2500–3000-km-long Solis-Lunae fold belt extends from easternmost Claritas Fossae to western Tempe Terra (Figs. 3 and 4; e.g., Watters, 1991, 1993; Schultz, 1998; Dohm and Tanaka, 1999; Anderson et al., 2001; Dohm et al., 2009b; Anguita et al., 2001, 2006; Okubo and Schultz, 2004; Mueller and Golombek, 2004; Borraccini et al., 2007; Williams et al., 2008; Montgomery et al., 2009). Folds are expressed as wrinkle ridges spaced at ~30–60 km and may have been created by blind thrusting (Watters, 1991; Okubo and Schultz, 2004; Mueller and Golombek, 2004). The fold belt may have initiated in the Early Hesperian (Watters, 1993), but it predates faults of Valles Marineris that were active from the Late Hesperian to the Late Amazonian (e.g., Witbeck et al., 1991; Schultz, 1998). Detailed geologic mapping of the Thaumasia and Terra Sirenum regions indicates that the fold belt likely began to initiate during the Noachian (Dohm et al., 2001a), possibly prior to the embryonic stage of Tharsis (Anderson et al., 2012) and/or coeval

with its incipient development (Karasozen et al., 2012); this region has also been reported to display characteristics of Basin and Range morphology of the southwest United States (Anderson et al., 2012; Karasozen et al., 2012).

Ancient Thaumasia Thrust

The Thaumasia mountain belt, comprising the Thaumasia Plateau in the west and Coprates rise in the east, was developed in the Early Noachian (Dohm et al., 2001a, 2001b; Baker et al., 2007; Dohm et al., 2007). Gravity modeling indicates a 70–90-km-thick crust in the region, which is 2–3 times thicker than that of the nearby northern lowlands crust at ~32 km (Zuber et al., 2000; Neumann et al., 2004; Andrews-Hanna et al., 2008a). The formation of the mountain belt may have been created by motion on the east-directed Thaumasia thrust (Plescia and Golombek, 1986; Schultz and Tanaka, 1994; Anguita et al., 2001, 2006; Borraccini et al., 2007; Montgomery et al., 2009; Nahm and Schultz, 2010), assisted by the deposition of a thick volcanic pile in the Early Noachian (Williams et al., 2008).

Eastern Tharsis Conjugate Strike-Slip System

According to Montgomery et al. (2009), a conjugate set of strike-slip fault zones occurs in the eastern Tharsis rise: the left-slip Valles Marineris fault in the north and the right-slip Clarita fault zone in the south (Fig. 3). The Valles Marineris fault zone bounds the Valles Marineris trough system, which has long been considered to have originated from rifting (Blasius et al., 1977; Masson, 1977, 1980, 1985; Frey, 1979; Plescia and Saunders, 1982; Lucchitta et al., 1992; Peulvast and Masson, 1993; Peulvast et al., 2001; Schultz and Lin, 2001). Its presence has been a key piece of evidence for hotspot-induced radial extension (e.g., Carr, 2006). This simple rift model was later modified to account for early development of an ancestral basin (Lucchitta et al., 1994; Schultz, 1998) and the role of interactions among a Europe-sized basin, magmatism, tectonism, and surface water activites (Dohm et al., 2001a, 2009a). Formation of Valles Marineris has also been related to right-slip (Courtillot et al., 1975; Anguita et al., 2001; Bistacchi et al., 2004) or left-slip faulting (Purucker et al., 2000; Webb and Head, 2002), dissolution of bedrock via subsurface flow (Sharp, 1973; Spencer and Fanale, 1990; Tanaka and MacKinnon, 2000; Montgomery and Gillespie, 2005; Adams et al., 2009), and melting of ground ice via dike emplacement (McKenzie and Nimmo, 1999). In the context of the original

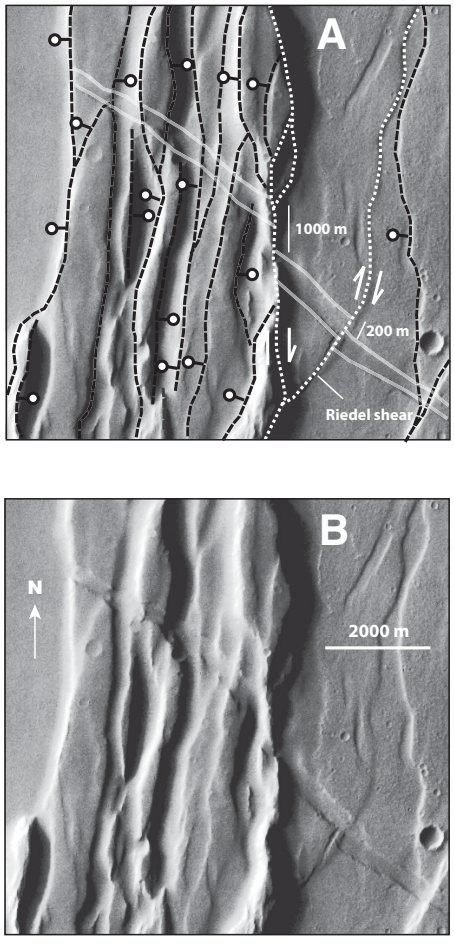

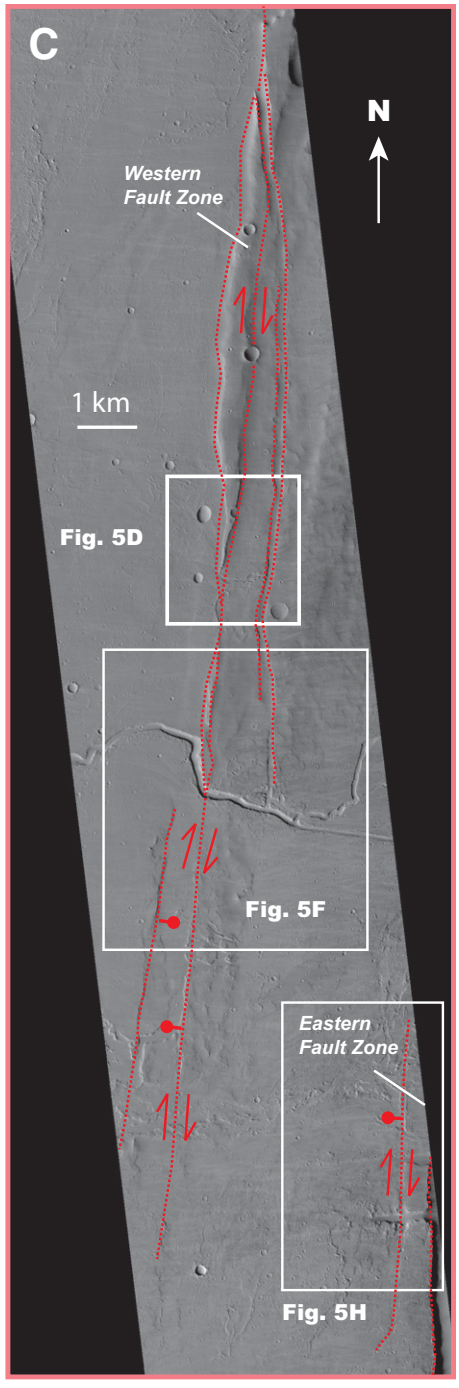

Figure 5. (A) Structural interpretations of Thermal Emission Imaging System (THEMIS) image V29021007 from Ceraunius Fossae. See Figure 3 for location. An early linear depression, which was either a graben or a stream channel, is offset by a series of north- and northeast-striking right-slip faults. (B) Same THEMIS image as in A without interpretation. (C) Interpreted High Resolution Imaging Science Experiment (HiRISE) image PSP_006877_2085_RED showing a north-northeast–striking right-slip fault. See Figure 3 for location. Also shown are locations of Figures 5D, 5G, and 5H. (*Continued on following page.*)

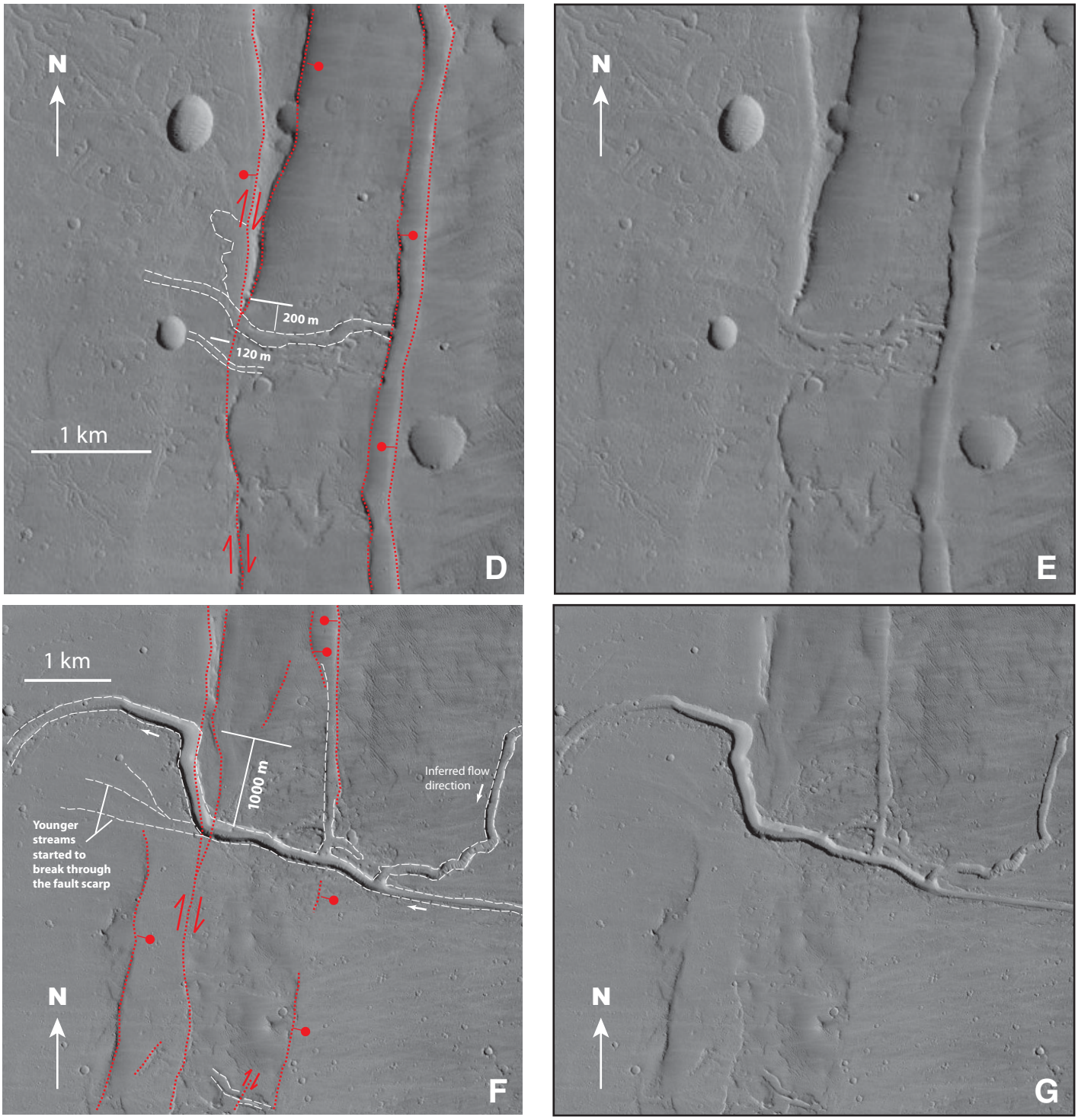

Figure 5 (*Continued*). (D) Interpreted HIRISE image, a portion of C, showing right-lateral drainage deflections across a right-slip transtensional fault. The deflection indicates at least 200 m of right slip on the fault. (E) Same image as D without interpretations. (F) Drainage deflection across a right-slip fault zone. The fault also appears to offset a crater. (G) Same image as F without interpretation. (*Continued on following page.*)

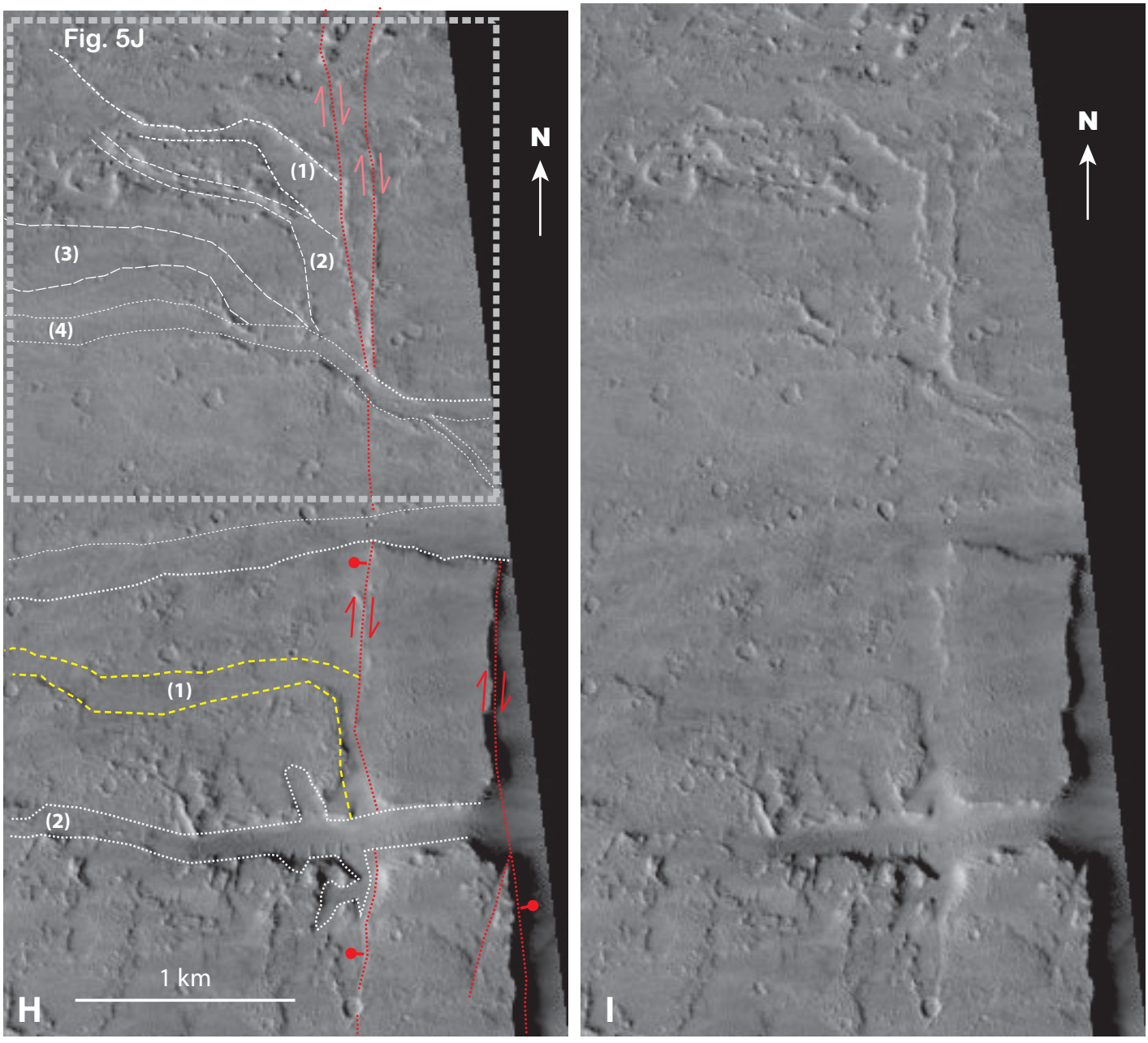

Figure 5 (*Continued*). (H) Right-lateral stream deflections along right-slip fault zone. (I) Same image as H without interpretations. (*Continued on following page.*)

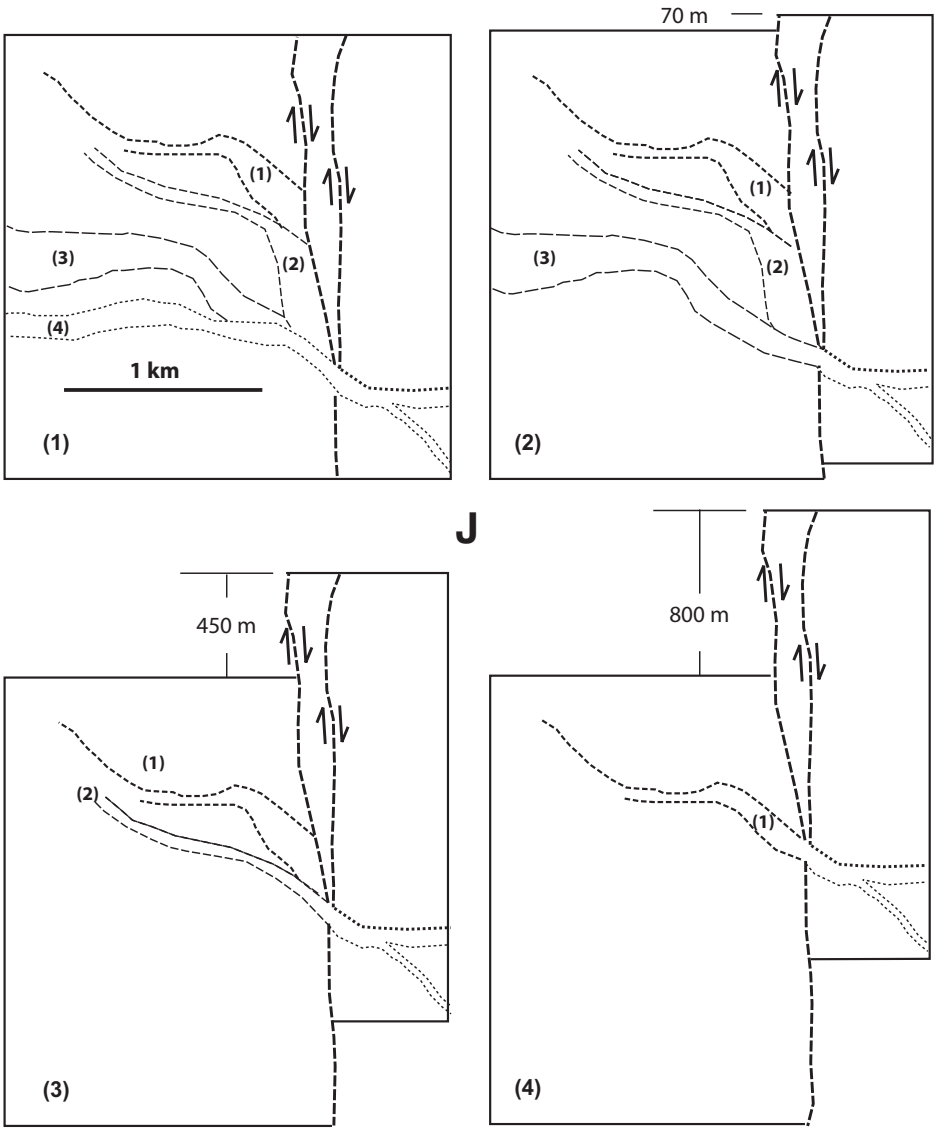

Figure 5 (*Continued*). (J) Palinspastic restoration of deflected streams across the right-slip fault zone shown in H.

left-slip fault models, the Valles Marineris fault zone is linked with the east-directed Thaumasia thrust (Webb and Head, 2002; Montgomery et al., 2009). These models face two problems: (1) the Valles Marineris fault zone does not terminate at the Thaumasia thrust, but extends 800 km farther east of their intersection, and (2) the Thaumasia thrust formed in the Early Noachian (Dohm et al., 2001a, 2001b), i.e., much earlier than the incipient development of the Valles Marineris trough zone during the Late Noachian, based on detailed stratigraphic relations among rock materials and tectonic structures along the western margin of the tectonic province, Thaumasia Planum (Dohm and Tanaka, 1999; Dohm et al., 2001a), as well as the Late Hesperian and Amazonian development observed by Witbeck et al. (1991) and Schultz (1998).

All pure strike-slip models for the origin of the Valles Marineris fault zone are also problematic in that they cannot create the large trough volumes during fault motion. Recent mapping of Valles Marineris indicates the fault zone to be a left-slip transtensional structure with a total left-slip motion of 150–160 km (Figs. 6A, 6B, and 6C; Yin, 2012). This result is broadly consistent with 200–250 km of left-lateral offset of magnetic anomalies across the fault (Fig. 6D; Purucker et al., 2000; Lillis et al., 2009). The left-slip Valles Marineris fault zone links the Noctis Labyrinthus–Syria extensional zone with the Capri-Eos rift zone to have accommodated NW-SE extension (Masson, 1977, 1980). The Noctis Labyrinthus–Syria extensional zone constitutes a series of northeast-trending arcuate-shaped extensional structures (Masson, 1977, 1980), whereas the Capri-Eos rift zone is bounded by the Capri and Eos normal faults (Witbeck et al., 1991; Yin, 2012).

Right-slip shear on the north-trending central segment of the graben zone south of Syria Planum was documented by Montgomery et al. (2009) across Claritas Fossae. This generally north-trending strike-slip zone links with complex northeast-trending extensional faults in Syria Planum and Noctis Labyrinthus in the north (e.g., Anderson et al., 2001) and the broad southern segment of the Main Tharsis graben zone that trends northeast and extends into the Icaria Fossae region (Fig. 3). As the Valles Marineris left-slip fault zone also links with the extensional faults in Syria Planum and Noctis Labyrinthus, the Valles Marineris left-slip and Claritas right-slip faults form a V-shaped conjugate strike-slip system (for the mechanics of this class of fault system, see Yin and Taylor, 2011), which opens to the southeast direction. In addition, because the Icaria Fossae grabens are part of the Main Tharsis graben zone and link with the Claritas right-slip fault system, the operation of the V-shaped conjugate faults in the eastern Tharsis rise should have been coeval with the development of the Main Tharsis graben zone.

Lycus Thrust

The Olympus Mons aureole zone marks the northwestern edge of the Tharsis rise. Its deposits have been related to (1) the development of long-runout landslides originated from the cliff-forming bases of Olympus Mons (Fig. 7; Carr et al., 1977; Lopes et al., 1982; Morris, 1982; McGovern and Solomon, 1993), (2) formation of a thrust belt (Harris, 1977; McGovern and Morgan, 2009), and (3) emplacement of pyroclastic flows during explosive eruptions (Morris, 1982). According to Scott and Tanaka (1986), the aureole zone consists of four Amazonian units: Aoa1a, Aoa2, Aoa3, and Aoa4, of which coarse-textured Aoa2, Aoa3, and Aoa4 can be clearly traced to spoon-shaped escarpments at the base of Olympus Mons (Lopes et al., 1982). These units could be composed of either landslide or pyroclastic flow materials. Surprisingly, Aoa1, the most extensive and structurally lowest unit, has never been discussed in the literature. Regardless of the origin of the deposits for the basal unit Aoa1, it is marked by a sharp contact against plain deposits of Amazonis Planitia, which is referred to as the Lycus thrust (Figs. 3 and 7). Evidence for the proposed thrust

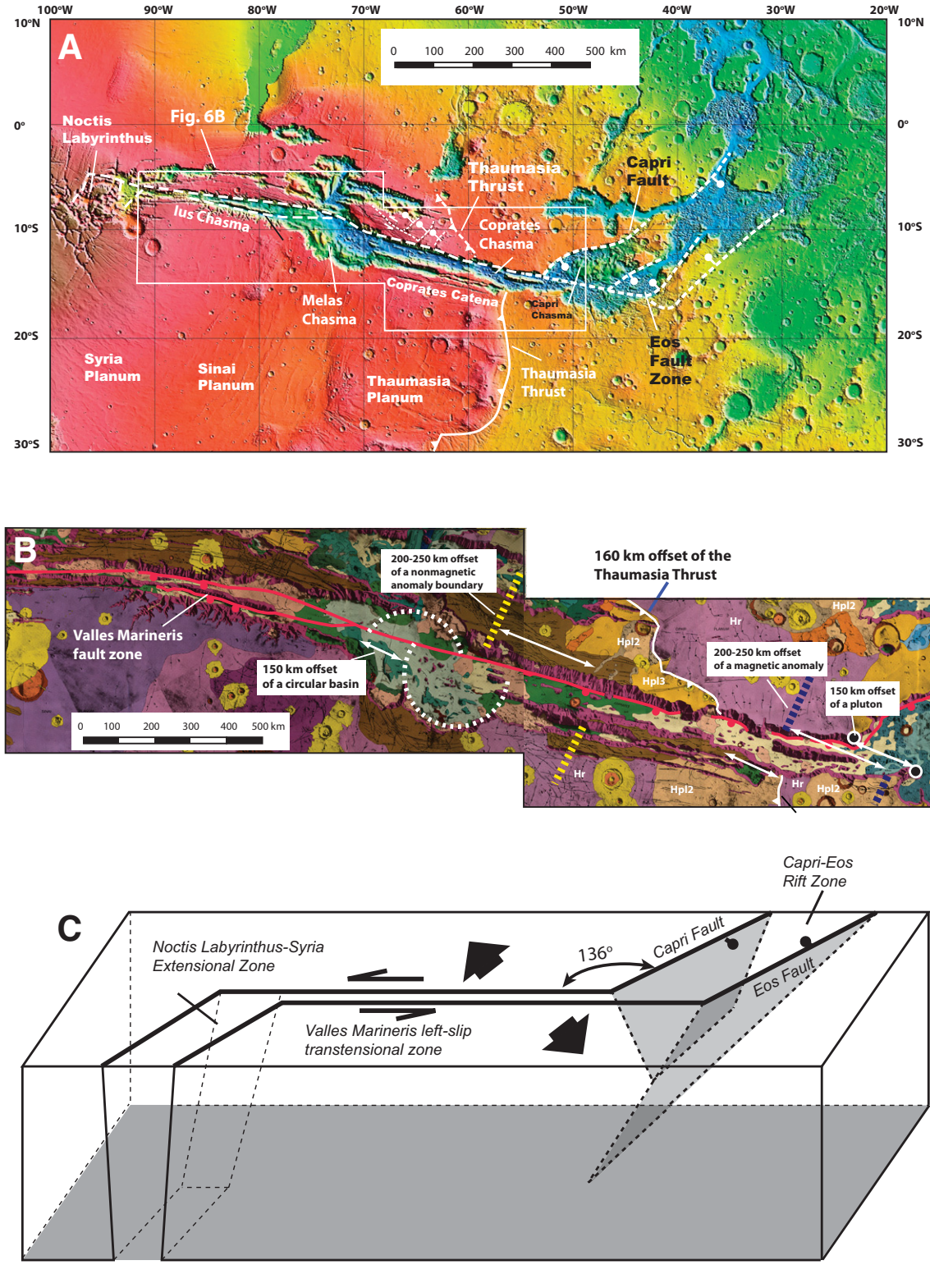

Figure 6. (A) Mars Orbiter Laser Altimetry (MOLA) topographic map of Valles Marineris and major faults in the trough system. (B) Geologic map of southern Valles Marineris from Witbeck et al. (1991). Units Hpl2 and Hpl3 are Hesperian plain deposits, and Hr is an Early Hesperian volcanic flow. Offset markers are also shown. Nonmagnetic-magnetic boundary is from Lillis et al. (2009), and offset magnetic anomaly is from Purucker et al. (2000). (C) Relationship between the Valles Marineris transtensional fault and rift zones at its two ends. (*Continued on following page.*)

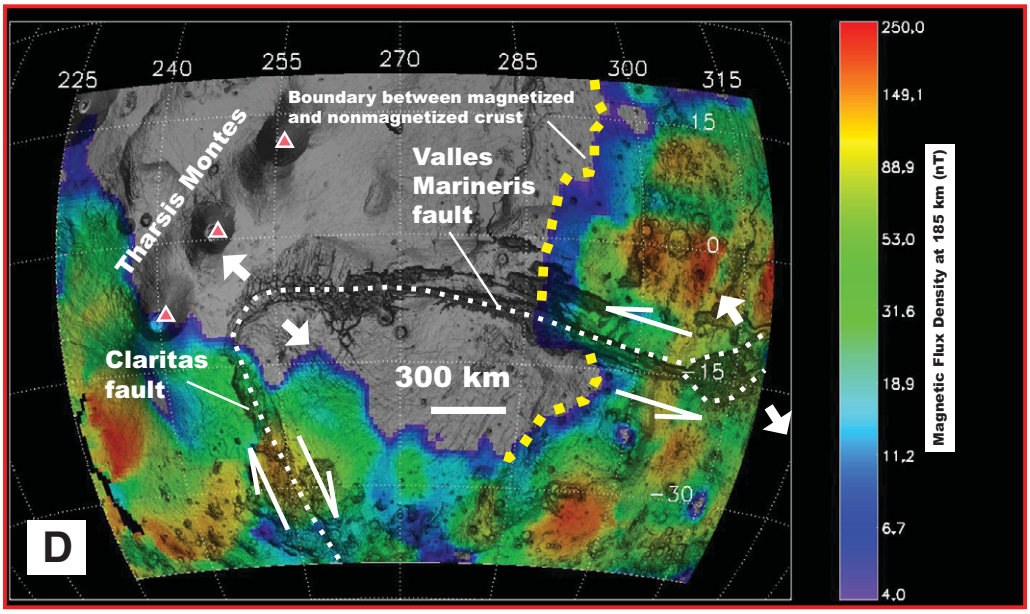

Figure 6 (*continued*). (D) Transitional zone between magnetized and nonmagnetized Tharsis crust is offset left laterally by the Valles Marineris fault zone, after Lillis et al. (2008). As the spatial resolution of the transition zone is ~200 km (Lillis et al., 2009), the exact magnitude of offset is not well resolved, but the sense of shear is well established.

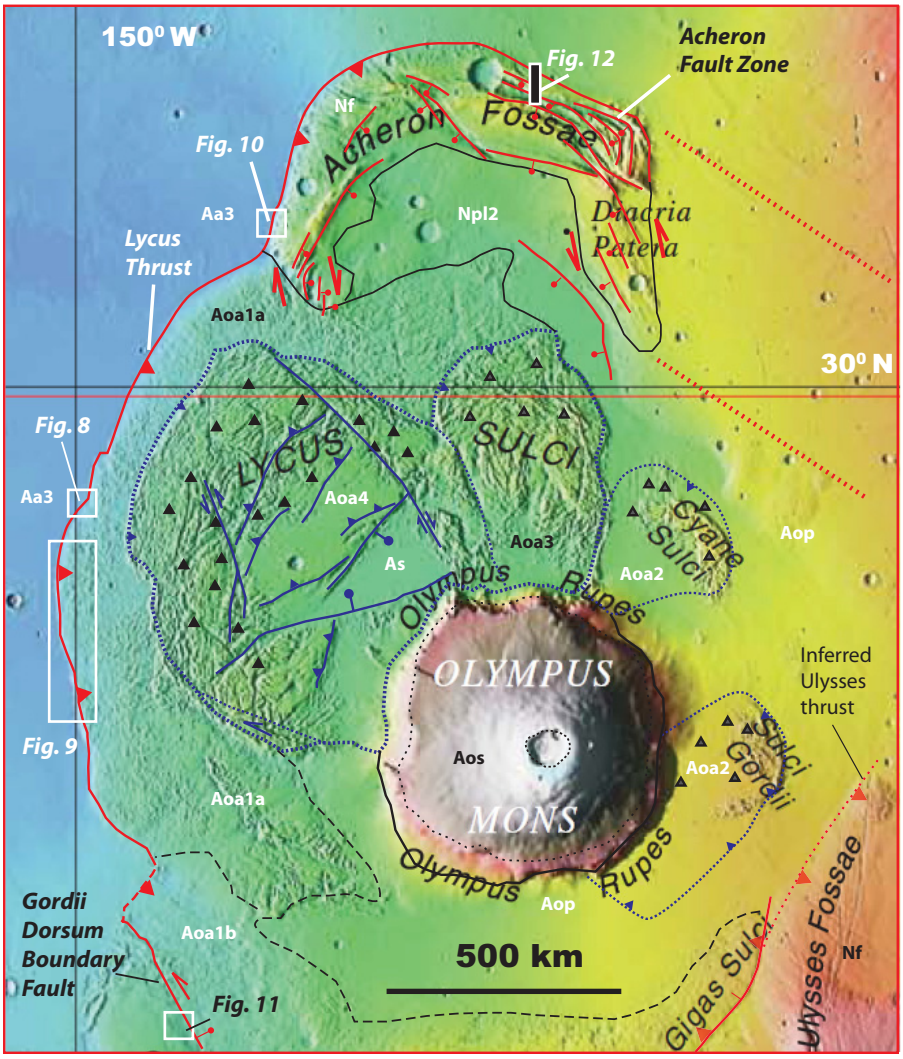

Figure 7. Structural map of the Lycus thrust system. See Figure 2A for location. Units are adopted from Scott and Tanaka (1986) with modified interpretations from this study: Aa3—the Late Amazonian plain deposits; Aoa1—protolith derived from unit Aa3 that was incorporated by thrusting into the hanging wall of the Lycus thrust; Aoa2, Aoa3, and Aoa 4—landslide or pyroclastic sheets derived from the base of Olympus Mons; Nf—Noachian basement.

includes (1) uplifted fluvial terraces in the thrust hanging wall with their risers truncated by the proposed thrust trace (Fig. 8), (2) an anticline deflecting a stream, which is a common feature resulting from laterally growing folds in thrust belts on Earth (e.g., Burbank and Anderson, 2001) (Fig. 8), and (3) sharp fault scarps (Figs. 9A and 9B). The interpreted scarps truncate curvilinear ridges that may represent layers of original lithology (Fig. 9). Minor back thrusts are also present in the proposed thrust zone (Figs. 9C and 9D). Tight and isoclinal folds can also be inferred from the shape and distribution of ridges, which appear to represent resistant layered rocks (Fig. 9). The limbs of the inferred folds are truncated sharply by the fault scarps (Fig. 9).

The Lycus thrust continues northeastward and follows the northwestern edge of Acheron Fossae, a regional uplift involving Noachian basement (Figs. 3 and 7; Scott and Tanaka, 1986; Skinner et al., 2006). The existence of the thrust there is indicated by the presence of curvilinear fault scarps (Figs. 10A and 10B). Locally, small streams appear to be offset left laterally for ~80–120 m (Figs. 10C–10F), suggesting that the Lycus fault zone bounding the Acheron Fossae uplift may be a left-slip transpressional fault system. The image shown in Figure 10 also displays scarps on the margins of promontories, interpreted to be several regressive shorelines that mark the edges of the northern lowlands (e.g., Baker et al., 1991; Scott et al., 1995; Head et al., 1999). These features can be distinguished from the fault scarps facing both north and south versus the shoreline-related scarps, which face only to the south. In addition, the regressive shoreline scarps are long (>5–10 km) and laterally continuous, whereas the fault scarps are short (<2–3 km) and discontinuous.

Gordii Dorsum Fault Zone

The 500-km-long Gordii Dorsum fault zone was interpreted as a normal fault (Scott and Tanaka, 1986) or a left-slip fault (Forsythe and Zimbelman, 1988). Analysis of high-resolution Thermal Emission Imaging System (THEMIS) images in this study suggests that the fault zone is a left-slip transtensional structure. This is indicated by oroclinal bending of fractures, the oblique orientation of joints to the main fault zone, and the presence of fault scarps (Fig. 11; THEMIS image V27687034). The southern end of the Gordii Dorsum fault zone is buried by young volcanic flows of the Tharsis Montes, whereas its northern tip approaches the Lycus thrust and may have been kinematically linked with this structure, as shown in Figure 7.

Acheron Fault Zone

The arcuate-shaped Acheron Fossae uplift is dominated by east-striking normal faults (Figs. 7 and 12; Kronberg et al., 2007). Two sets of en echelon normal faults at the western and eastern limbs of the arc indicate broad shear accommodating overall north-south extension.

Ulysses Thrust

Ulysses Fossae is an arc-shaped topographic high northwest of the Tharsis Montes and southeast of Olympus Mons (Fig. 7). Its morphology mimics the Olympus aureole zone, also

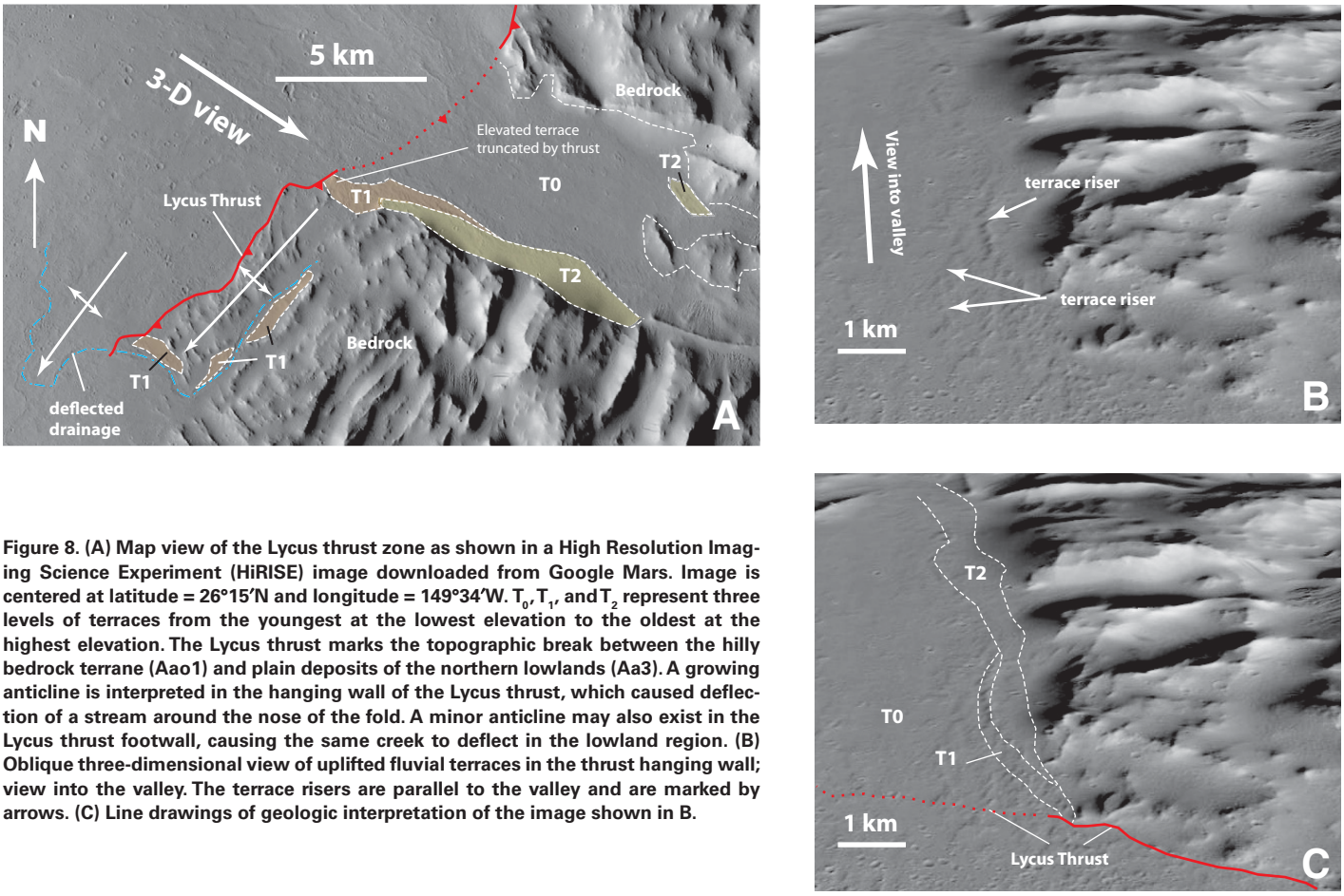

Figure 8. (A) Map view of the Lycus thrust zone as shown in a High Resolution Imaging Science Experiment (HiRISE) image downloaded from Google Mars. Image is centered at latitude = 26°15′N and longitude = 149°34′W. T_0, T_1, and T_2 represent three levels of terraces from the youngest at the lowest elevation to the oldest at the highest elevation. The Lycus thrust marks the topographic break between the hilly bedrock terrane (Aao1) and plain deposits of the northern lowlands (Aa3). A growing anticline is interpreted in the hanging wall of the Lycus thrust, which caused deflection of a stream around the nose of the fold. A minor anticline may also exist in the Lycus thrust footwall, causing the same creek to deflect in the lowland region. (B) Oblique three-dimensional view of uplifted fluvial terraces in the thrust hanging wall; view into the valley. The terrace risers are parallel to the valley and are marked by arrows. (C) Line drawings of geologic interpretation of the image shown in B.

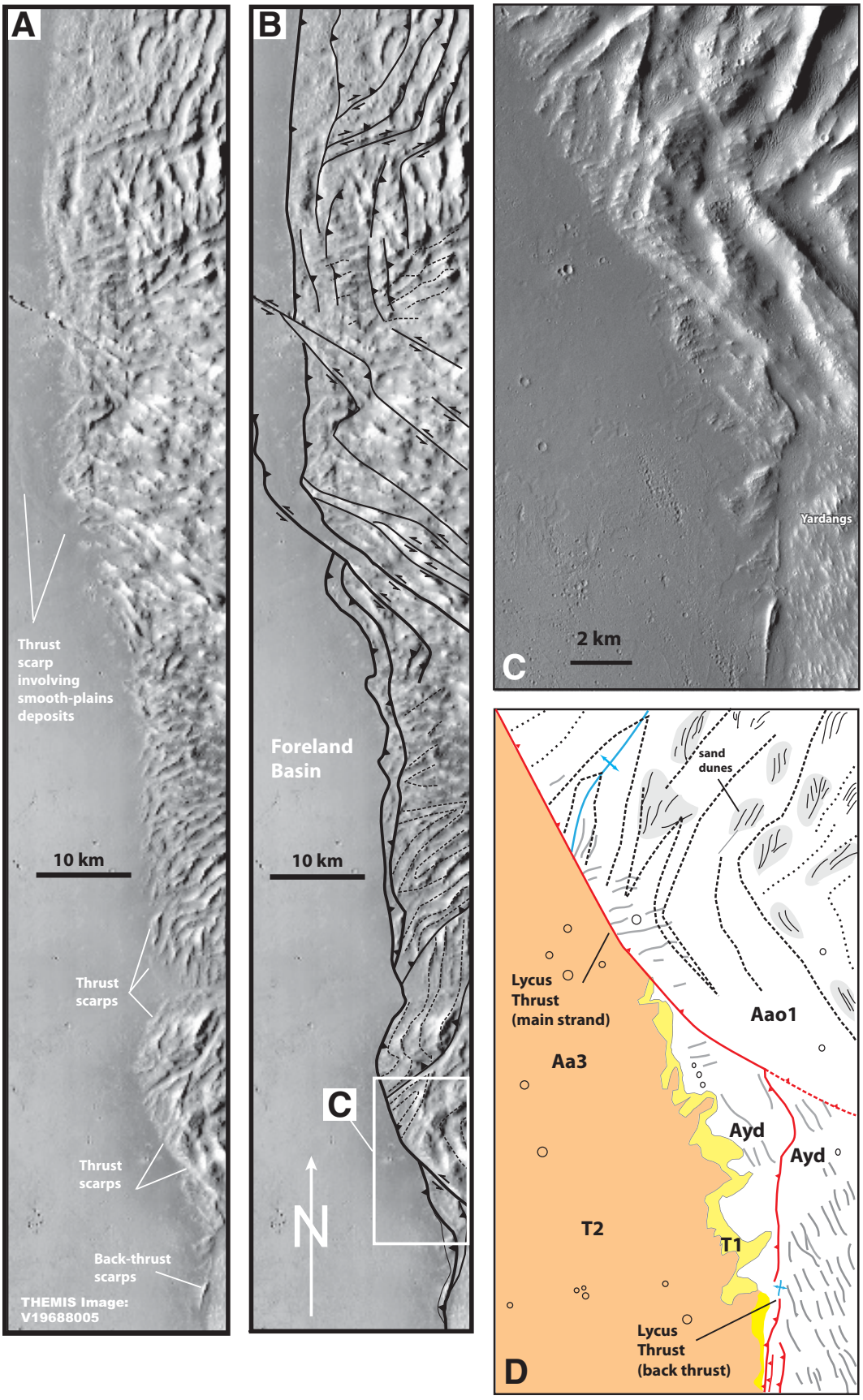

Figure 9. (A) Interpreted trace of the Lycus thrust defined by prominent fault scarps from THEMIS image (V19688005). (B) Uninterpreted image. (C) Close-up view of Thermal Emission Imaging System (THEMIS) image (V19688005) that shows a sharp scarp. (D) Interpreted geologic map from image in (C). T_1 and T_2 are older and younger members of unit Aa3 in Figure 7. T_1 below T_2 is tilted westward due to motion on the back thrust. The ridges in unit Aao1 appear to define a series of folds that are parallel to the trend of the fault scarp.

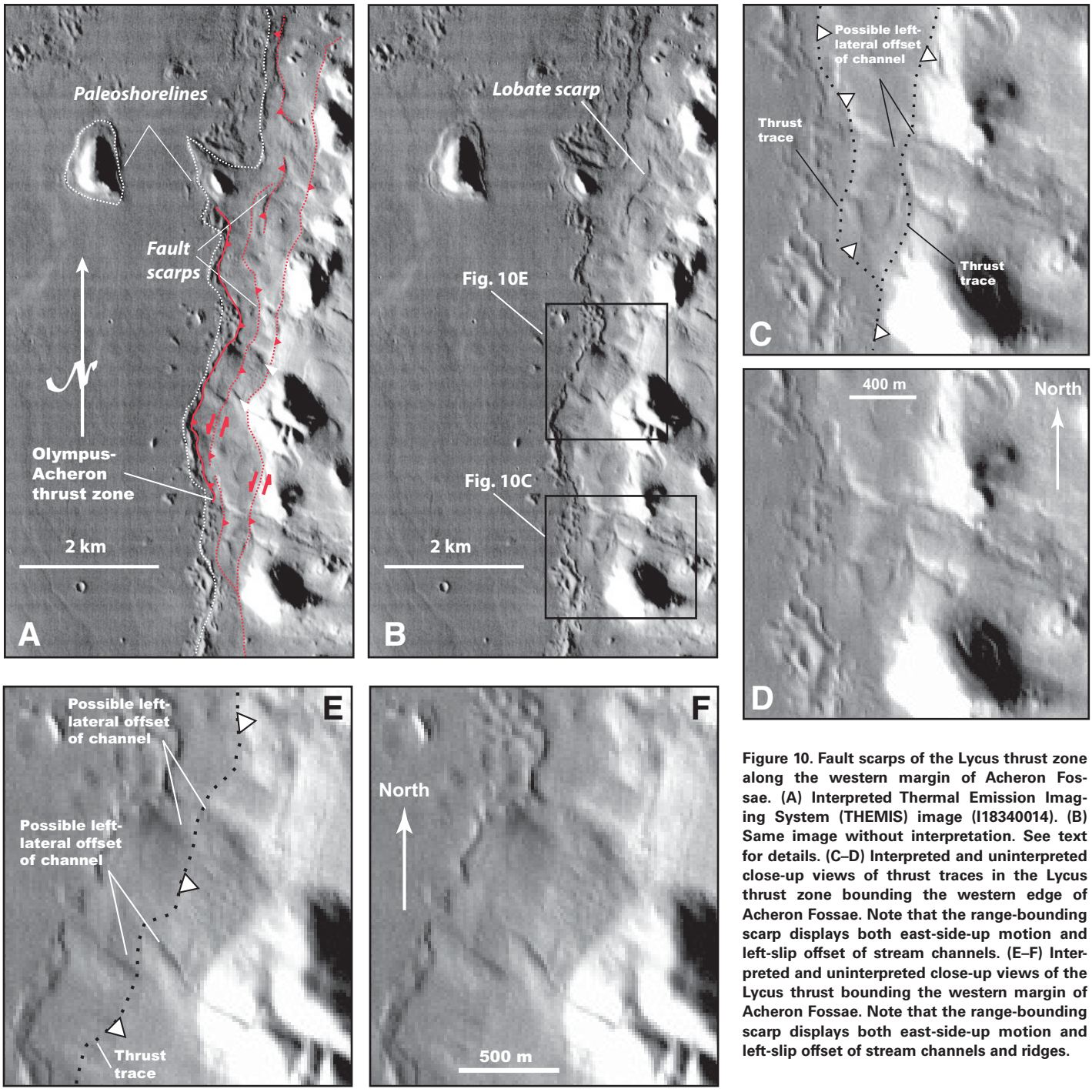

Figure 10. Fault scarps of the Lycus thrust zone along the western margin of Acheron Fossae. (A) Interpreted Thermal Emission Imaging System (THEMIS) image (I18340014). (B) Same image without interpretation. See text for details. (C–D) Interpreted and uninterpreted close-up views of thrust traces in the Lycus thrust zone bounding the western edge of Acheron Fossae. Note that the range-bounding scarp displays both east-side-up motion and left-slip offset of stream channels. (E–F) Interpreted and uninterpreted close-up views of the Lycus thrust bounding the western margin of Acheron Fossae. Note that the range-bounding scarp displays both east-side-up motion and left-slip offset of stream channels and ridges.

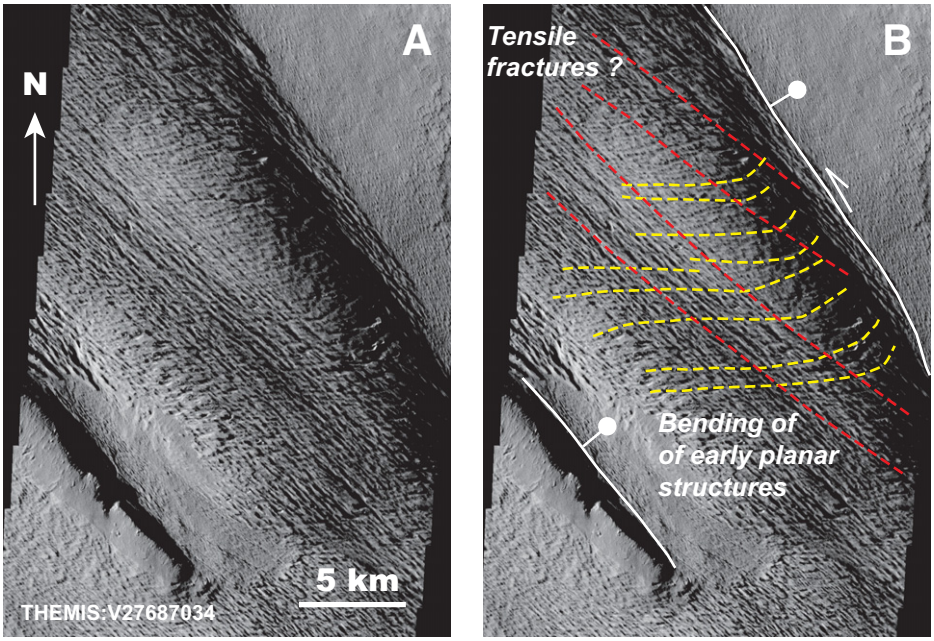

Figure 11. Thermal Emission Imaging System (THEMIS) image (V27687034) showing normal faults in Gordii Dorsum area. The faults are part of the southwestern lateral boundary fault zone of the subducted slab below the Olympus Mons. See Figure 7 for location. (A) Image without interpretations. (B) Image with interpretations. The Gordii Dorsum fault may have a left-slip component as indicated bending of east-trending fractures toward the range-bounding fault. It is also indicated by the oblique alignment of northwest-trending fractures interpreted as joints.

suggesting origin through west-directed thrusting. This thrust truncates grabens in the hanging wall and places the Noachian basement (unit Nf) over plains deposits surrounding Olympus Mons (unit Aop; Fig. 3). The thrust is buried in the west by the oldest aureole deposits of Olympus Mons (unit Aoa1) and by a volcanic flow from the Tharsis Montes (unit AHt3; Fig. 3). This relationship implies that the Ulysses thrust is an Amazonian structure, and its development was coeval with the early phase of volcanism in the Tharsis Montes but probably postdates the main phase of Olympus Mons development.

Summary of Tharsis Structural Geology

The Tharsis rise exhibits four sets of fault systems (Fig. 4). The first set includes the Noachian Thaumasia thrust and Early Hesperian wrinkle ridges across Solis Planum south of the Valles Marineris and Lunae Planum north of Valles Marineris. The second set is expressed by the development of the cryptic Ulysses thrust along the western margin of the Tharsis Montes volcanic zone. This fault was probably active during the early stage of Tharsis Montes volcanism and predated the main phase of the younger Olympus volcanism to the west. The third set of fault systems is the kinematically linked Lycus thrust, Gordii Dorsum left-lateral transtensional fault zone, and Acheron extensional fault system bounding the northwestern edge of the Tharsis rise. The fourth set of structures includes the Main Tharsis graben zone in the center and a V-shaped conjugate strike-slip fault system in the southeastern part of Tharsis rise. The Main Tharsis graben zone consists of two northeast-trending segments in the north and south, which are linked by a north-trending, right-slip transfer-fault system in between (e.g., Ceraunius fault zone) (Fig. 4).

The V-shaped strike-slip system consists of the left-slip Valles Marineris fault zone and the right-slip Claritas fault zone (Fig. 4). Both faults link with NE-trending extensional zones (possibly dominated by coeval volcanism; see Yin, 2012) at their western terminations in Syria Planum; this extensional zone may be part of the Main Tharsis graben zone. The V-shaped conjugate faults are referred to as the "SE Tharsis conjugate system" in this study (Fig. 4), with its geometry remarkably similar to V-shaped conjugate strike-slip systems on Earth (Taylor et al., 2003; Taylor and Yin, 2009; Yin, 2010c). According the mechanical model of Yin and Taylor (2011), a V-shaped conjugate strike-slip fault system is most likely generated by basal shear due to flow in the mantle and/or by gravitational spreading of a thickened lithosphere. Based on the orientations and kinematics of the SE Tharsis conjugate system, it may be inferred that the development of the Main Tharsis graben zone and the SE Tharsis conjugate system was induced by overall NW-SE extension across the central and southeastern Tharsis rise during the latest stage of its tectonic development.

In the context of the slab rollback model discussed in detail later herein, the Noachian contractional deformation along the southern margin of the Tharsis rise was generated by the Argyre impact (i.e., Thaumasia thrust) and retro-arc contraction (Solis-Lunae fold belt). The linked and rectangular-shaped Lycus–Gordii Dorsum–Acheron fault system is interpreted in the slab rollback model as the most recent trench zone accommodating downward motion of a strip of southeast-dipping subduction slab. The Ulysses thrust is interpreted to be a relic of an early trench zone when zone 3 volcanism was active. Finally, the development of the Main Tharsis graben zone and the eastern Tharsis conjugate strike-slip fault system was a result of backarc extension.

CRUSTAL MAGNETIZATION ACROSS THE THARSIS RISE

Crustal Magnetization of the Tharsis Rise and Surrounding Regions

Most of the Tharsis rise lacks detectable crustal magnetization except along its margins or in regions where small patches of ancient Noachian crust are exposed (Acuña et al., 1999; Connerney et al., 1999, 2001; Lillis et al., 2009; Dohm et al., 2009a). Regions that do display crustal magnetization include the Thaumasia highlands and Claritas Fossae along the southeastern and southwestern rims of the Tharsis rise (Lillis et al., 2009). The correspondence between the Noachian basement, the oldest rocks in the Tharsis rise, and crustal magnetization led many workers to suggest that their emplacement occurred during the operation of the Martian dynamo (Johnson and Phillips, 2005; Whaler and Purucker, 2005; Mitchell et al., 2007; Lillis et al., 2008, 2009; Dohm et al., 2009a).

Demagnetization of Tharsis Crust and Generation of Juvenile Crust

The lack of crustal magnetization across most of the Tharsis rise may have been caused by later thermal demagnetization related to either impact-induced crustal remelting (e.g., Acuña et al., 1999; Connerney et al., 1999; Reese et al., 2004) or magmatic accretion as a result of plume activities (Johnson and Phillips, 2005; Lillis et al., 2009). Impact-induced demagnetization implies that the Tharsis crust

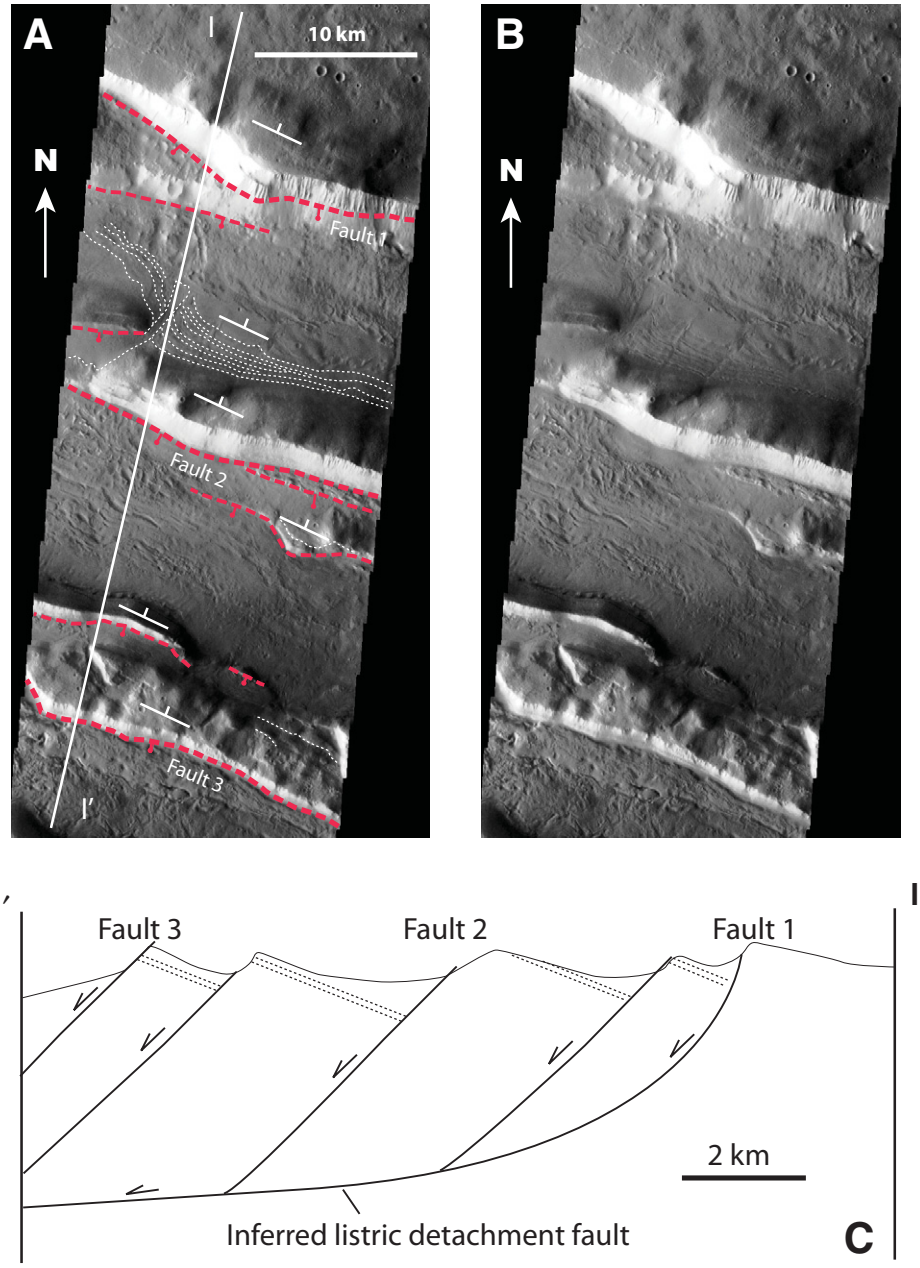

Figure 12. Thermal Emission Imaging System (THEMIS) image (V14446004) showing a series of south-dipping normal faults spaced ~2.5 km in northern Acheron Fossae. Note that layered rocks in the footwall of fault 2 are tilted to the north, consistent with a domino style of faulting during extension.

is mostly an old crust formed prior to the shutdown of the Martian dynamo; it subsequently went through remelting and thermal heating during major impact in the Tharsis region when the dynamo had stopped operation. In contrast, the magmatic accretion model of Lillis et al. (2009) requires that the Tharsis crust is a mixture of preexisting crust formed prior to the shutdown of the Martian dynamo and juvenile rocks emplaced after the termination of the dynamo. An end-member model of Tharsis demagnetization is that its entire crust was created by juvenile materials derived from upwelling mantle after the termination of the Martian dynamo (i.e., GEOMARS theory of Baker et al., 2007).

For the process of thermal demagnetization to be effective in the magmatic accretion model, a great amount of juvenile materials (see discussion later herein) must have been emplaced into the older Tharsis crust (Lillis et al., 2009). This in turn requires horizontal crustal extension and vertical crustal thickening within the Tharsis rise and horizontal shortening around the rims of the Tharsis rise in order to accommodate the extra crustal volume due to magmatic accretion. For example, matching the observed crustal magnetization in the southwestern Tharsis rise requires 33% of horizontal extension and 67% vertical crustal thickening (Lillis et al., 2009). If such extension had occurred uniformly across the interior of the 3500-km-wide and 6000-km-long Tharsis rise, it would have required some 1000 km and 1800 km of crustal shortening along the NE/SW and NW/SE edges of the Tharsis rise. Such required shortening seems highly unlikely unless some form of plate subduction or large-scale underthrusting had occurred coeval with magmatic accretion. This problem is addressed in the context of a slab rollback model proposed later herein.

It is possible that magmatic intrusion occurred entirely in the form of horizontal sills below the Tharsis rise. This would have required no horizontal extension, and magmatic emplacement would have been accommodated completely by crustal thickening. This demagnetization process could be effective for removing crustal magnetization of the Tharsis rise if the originally magnetized upper crust was nearly completely replaced by plutons (up to 90%; see Lillis et al., 2009). Although this is theoretically possible in thermal modeling, in reality, basaltic melts derived from the mantle on Mars most likely have been accumulated in the middle crust at neutral-buoyancy depths, as commonly observed in oceanic arcs on Earth (e.g., Yoshino et al., 1998). As shown by Jellinek et al. (2008), lower-crustal magmatic addition alone would not be enough to thermally demagnetize the upper crust, and thus detectable crustal magnetization would have been preserved in the Tharsis crust.

ARGYRE IMPACT AND ITS RELATIONSHIP TO THE THARSIS RISE

With a diameter of ~1500 km and located ~400 km southeast of the Tharsis rise, the multiringed Early Noachian (ca. 4.0 Ga) Argyre impact basin has a maximum topographic relief of ~10 km and a crustal thickness of ~25 km, which is significantly thinner than the 55–65 km crust surrounding the basin (Fig. 1; Scott and Tanaka, 1986; Dohm and Tanaka, 1999; Hartmann and Neukum, 2001; Hiesinger and Head, 2002; Neumann et al., 2004; Frey, 2008; Robbins and Hynek, 2012). The thin crust indicates that some 30 km of the crust must have been displaced by excavation and lateral flow during the Argyre impact (e.g., Pierazzo and Melosh,

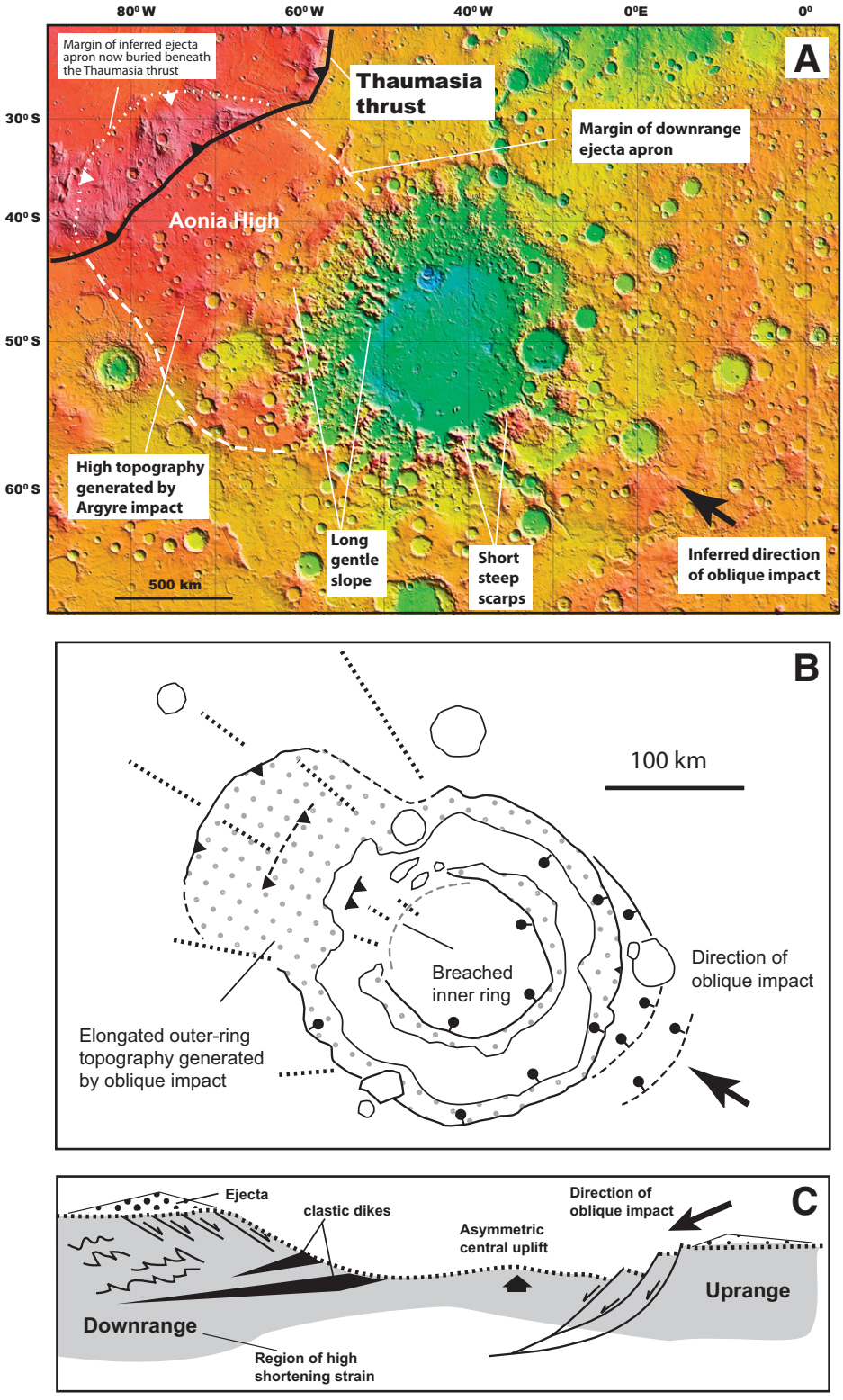

Figure 13. (A) Mars Orbiter Laser Altimetry (MOLA) topographic map of Argyre impact structures. See Figure 2 for location. (B) Bach Basin on Mercury, a classic oblique impact basin (redrawn from Schultz and D'Hondt, 1996). Note its remarkable similarity to the Argyre impact structure. (C) A typical topographic profile and associated internal structures across an impact basin generated by an oblique impact, modified from Schultz and Anderson (1996) and Melosh (1989).

1999). The rectangular Aonia Highland northwest of Argyre Basin may have been the product of ejecta deposition and crustal thickening during oblique impact (Fig. 13A). This inferred oblique direction of impact is supported by the morphologic similarity between the Argyre Basin and the Bach impact basin on Mercury (Fig. 13A; Schultz and Anderson, 1996). In particular, the tongue-shaped topographic high in the downrange direction of the Bach impact is similar in shape and relative size to the Aonia Highland in the inferred downrange direction of the Argyre impact. Following Melosh (1989), a possible cross section with a steep rim on the southeast side and a gentle rim on the northwest side for the Argyre impact basin is shown in Figure 13B.

The Aonia Highland predates the Tharsis rise, since its topography is truncated by the linear Thaumasia Highlands (Fig. 14A). This topographic feature must postdate the hemispheric dichotomy because it cuts across the northeast-trending regional slope that marks the transitional boundary between the northern lowlands and southern highlands (Fig. 14A). Note that the edge of the northern lowlands starts at the base of this long and gentle slope. The excess of topography generated by the proposed oblique Argyre impact can be estimated by projecting a topographic profile across the region between the Argyre impact basin and the southeastern edge of the Tharsis rise (i.e., Thaumasia Highlands) onto a topographic profile across a portion of the dichotomy boundary that has not been disturbed by the Argyre impact and tectonic development of the Tharsis rise. This reveals that more than 6 km of topography was generated from the formation of the Aonia Highland above the original transitional zone between the northern lowlands and southern highlands (Figs. 14B and 14C). The estimate is based on the assumption that the Aonia Highland was built on top of the dichotomy transition zone that had exactly the same form as the one shown in Figure 14C.

HEMISPHERIC DICHOTOMY

The hemispheric dichotomy between the northern lowlands and southern highlands lies at the base of a topographic slope with various widths and steepness (Fig. 15). The original position of the dichotomy boundary below the Tharsis rise passes through Syria Planum (Andrews-Hanna et al., 2008a; cf., Sleep, 1994; Zuber et al., 2000) (Fig. 15). This interpretation implies that the upper boundary of the marginal slope of the southern highlands at Arabia Terra must pass through the region that includes the southeastern margin of the Tharsis rise and the northwest side of Argyre Basin (Fig. 15). The

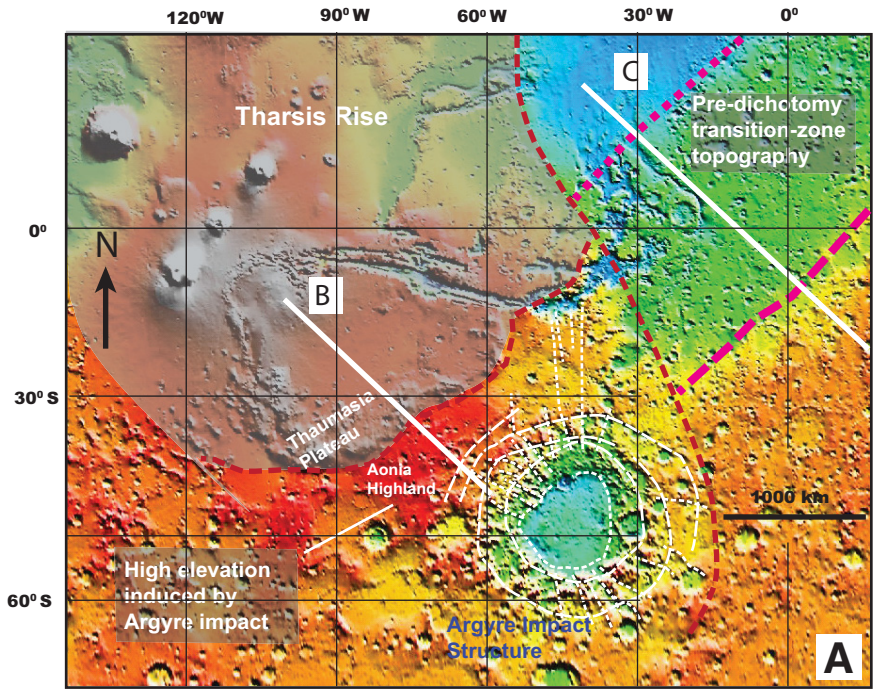

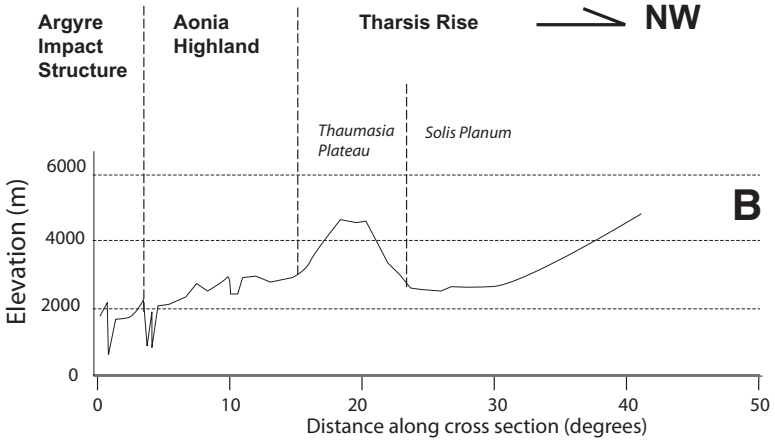

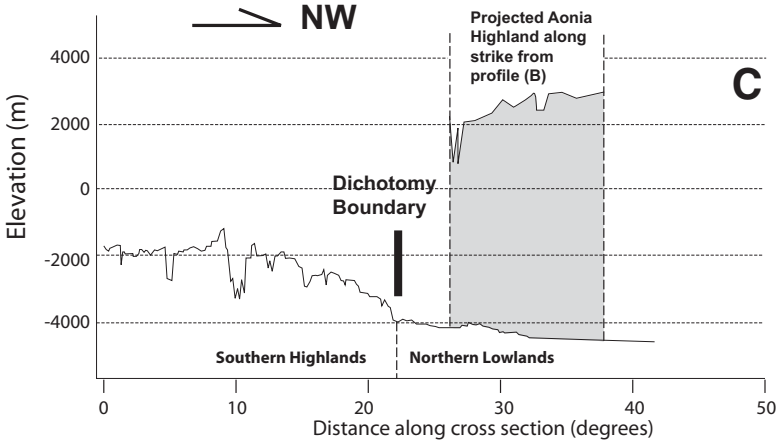

Figure 14. (A) Detailed topographic relationship between the exposed dichotomy boundary and the Tharsis rise. The gray area was created by combined effect of the Argyre impact and Tharsis uplift that truncates the older topography as represented by the exposed segment of the transition zone between the plateau region of the southern highlands and the floor of the northern lowland basin. Note that the area between the Thaumasia Plateau and the Argyre impact structure is much higher that the transitional zone, which was probably created by the oblique (northwestward) Argyre impact. See text for details. (B) Topographic profile from northern edge of the Argyre impact basin to the southeastern part of Syria Planum. (C) Topographic profile across the transition zone between the southern highlands and the northern lowlands. Note that the dichotomy boundary lies at the break of slope between the north-sloping southern highlands and the flat northern lowlands. Also note that the region between the Thaumasia Plateau and Argyre impact basin has an elevation that is ~6.5 km above the average elevation of the northern lowlands. As no obvious structures or deposition of volcanic rocks from the Tharsis rise can be used to explain this topographic high, its formation must be related to the Argyre impact, postdating the formation of the dichotomy boundary.

high topography generated by the Argyre impact must have exerted a vertical load at the topographic slope marking the transition between the northern lowlands and southern highlands.

DISCUSSION

Geologic Evolution of the Tharsis Rise

Based on the existing literature and newly conducted structural analysis of high-resolution satellite images presented here, the following tectonic history of the Tharsis rise can be deduced (Fig. 16). In the Noachian, the Argyre impact created the Argyre Basin on the east side of the future Tharsis rise (Fig. 16A). The Argyre impact event may have created the Noachian Thaumasia thrust system and caused initiation of effusive volcanism across the Thaumasia Mountains and Coprates rise along the southeastern margin of the Tharsis rise (i.e., zone 1 volcanic centers; Fig. 16B). In the Early Hesperian, widespread effusive volcanism occurred (Fig. 16C). The source of the volcanic flow is unclear but could have been originated from zone 1 volcanic centers. Immediately after the emplacement of Hesperian volcanic flows, wrinkle ridges began to develop in the Solis-Lunae fold belt (Fig. 16C). During the Middle Hesperian, eruptions centers migrated across Solis Planum

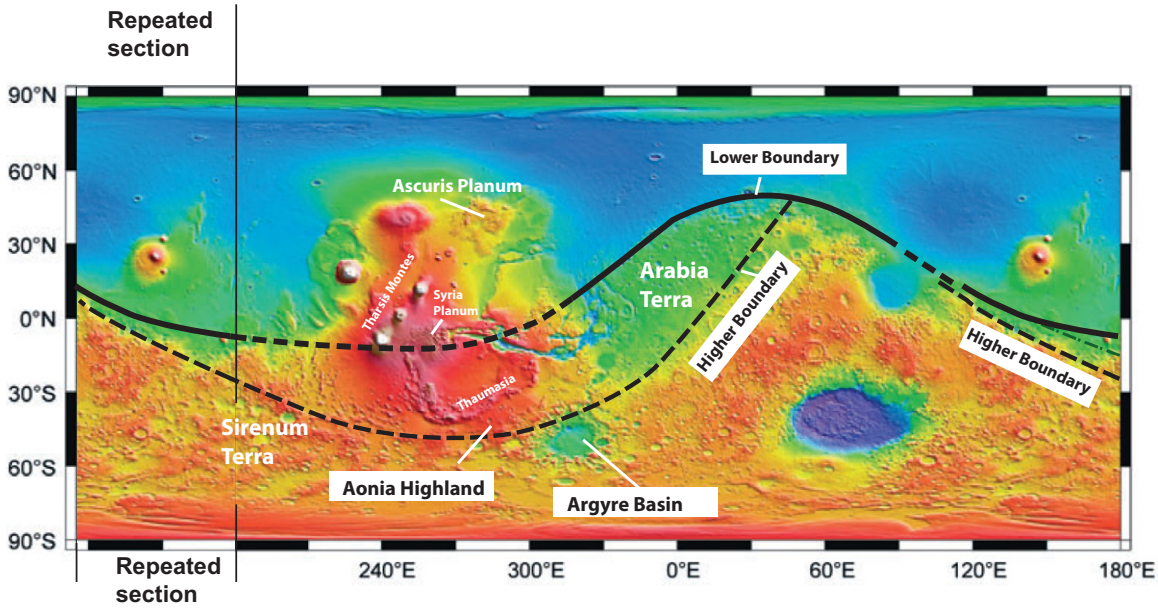

Figure 15. Topographic relationship between Tharsis rise and hemispheric dichotomy. Note that boundary between the northern lowlands and southern highlands is a gentle slope on the west side of Tharsis rise across Arabia Terra. Its lower boundary correlates with the dichotomy boundary designated by Andrews-Hanna et al. (2008a); its upper boundary can be projected between the southern edge of Tharsis rise and Argyre Basin. This relationship indicates that the southeastern part of Tharsis rise and Aonia Highland sits on top of this transition. The broad slope across Arabia Terra is remarkably similar to a continental slope at a passive margin. On Earth, accumulation of sediments at this position has often led to the development of active Andean-type continental margins (e.g., Kemp and Stevenson, 1996).

and Claritas Fossae (units Ht and Hsl in Fig. 3), superposing on top of unit Hr (not shown for clarity; Fig. 16D). In the Late Hesperian, zone 2 volcanism was initiated across Syria Planum (Fig. 16E), and the style of volcanism changed from effusive fissure eruption in zone 1 to central volcano eruption in zone 2. In the Late Hesperian and Early Amazonian, central volcanoes were developed across the Tharsis Montes along the zone 3 volcanic belt (Fig. 16F). In the Early Amazonian, volcanic centers at Olympus Mons and Alba Patera began to develop (Fig. 16G). Development of the Main Tharsis graben zone was active at this time across the Tharsis rise and its neighboring lowland regions to the north and south. The initiation of some of the graben structures in the Main Tharsis graben zone may have occurred earlier, as they are partially overlain by Hesperian volcanic flows in the Syria Planum region (Scott and Tanaka, 1986). On the other hand, extensional structures in the graben zone cut Late Amazonian volcanic flows and volcanic constructs as seen in the Tharsis Tholus region (Platz et al., 2011). The trend of the highly curved graben zone may have been controlled by the thermally weakened and recently ceased volcanic centers, as it passed through Alba Patera, the Tharsis Montes, and Syria Planum (Figs. 4 and 16G). In the Late Amazonian, zone 4 volcanic centers became fully developed. NW-SE extension across the Tharsis rise has been mainly accommodated by the Main Tharsis graben zone and its kinematically linked eastern Tharsis conjugate strike-slip system (Fig. 16H).

The geologic history as summarized in Figure 16 is inconsistent with the stationary hotspot model of Carr (1974). As pointed out by Tanaka et al. (1991) and Banerdt et al. (1992), a rising plume from below the Tharsis rise would require coeval radial extension in the central Tharsis rise and contraction along the rims of the Tharsis rise. With the new revelation that the north-trending segment of the Main Tharsis graben zone is a right-slip structure and the Valles Marineris fault zone is a major left-slip structure, the early inferred radial-extension pattern by Carr (1974) (also see Anderson et al., 2001) across the Tharsis rise no longer holds. Lack of thrusting along the entire rim of the Tharsis rise and the extension of Tharsis grabens into the neighboring lowlands are both inconsistent with the plume models (Banerdt et al., 1992).

The geologic history of the Tharsis rise derived from this study is inconsistent with the notion that the formation of the Tharsis rise was largely accomplished in the Early Noachian (Phillips et al., 2001). Phillips et al. (2001) used gravity and topographic data to determine the effect of the mass load of Tharsis on the shape and gravity field of the rest of the planet. They found that the Tharsis-induced topography matches the observed strain accommodated by Noachian structures and predicts the orientation of the outwash flows around the Tharsis rise (see their Fig. 3A based on the work of Carr, 1996). A major problem with their inference is that many of their inferred Noachian outwash channels in fact flow over Hesperian and Amazonian units or have upper stream channels that can be traced to the younger rock units. The best examples are the Maja Valles and Kasei Valles along the rim of the Tharsis rise, both of which flow over Hesperian units (Figs. 2 and 3). The second problem with the Noachian formation of Tharsis mass is that the Tharsis rise is dominated by giant Hesperian and Amazonian volcanoes (Olympus Mons and Tharsis Montes; Fig. 2). The region is also covered by volcanic rocks over more than 80% of its surface areas (Fig. 3). On the deep-cut walls of Valles Marineris, the surface exposure of Hesperian volcanic flows can be traced downward as conformable layered successions that are >6–8 km thick (e.g., Witbeck et al., 1991; McEwen et al., 1999; Williams et al., 2003).

The suggestion that Tharsis mass was emplaced largely in the Noachian by Phillips et al. (2001) was based critically on the structural work of Anderson et al. (2001) and the

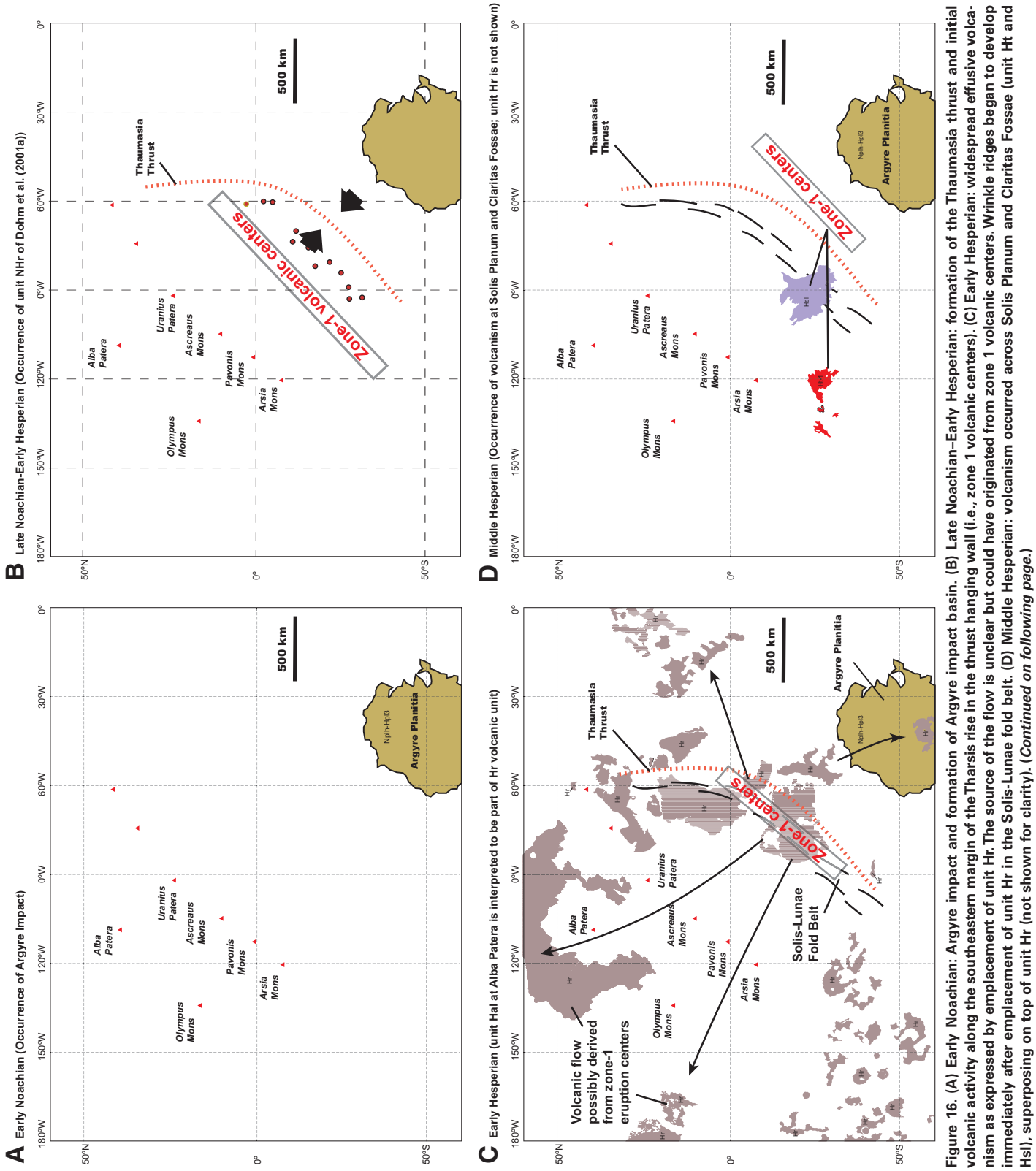

Figure 16. (A) Early Noachian: Argyre impact and formation of Argyre impact basin. (B) Late Noachian–Early Hesperian: formation of the Thaumasia thrust and initial volcanic activity along the southeastern margin of the Tharsis rise in the thrust hanging wall (i.e., zone 1 volcanic centers). (C) Early Hesperian: widespread effusive volcanism as expressed by emplacement of unit Hr. The source of the flow is unclear but could have originated from zone 1 volcanic centers. Wrinkle ridges began to develop immediately after emplacement of unit Hr in the Solis-Lunae fold belt. (D) Middle Hesperian: volcanism occurred across Solis Planum and Claritas Fossae (unit Ht and Hsl), superposing on top of unit Hr (not shown for clarity). ***(Continued on following page.)***

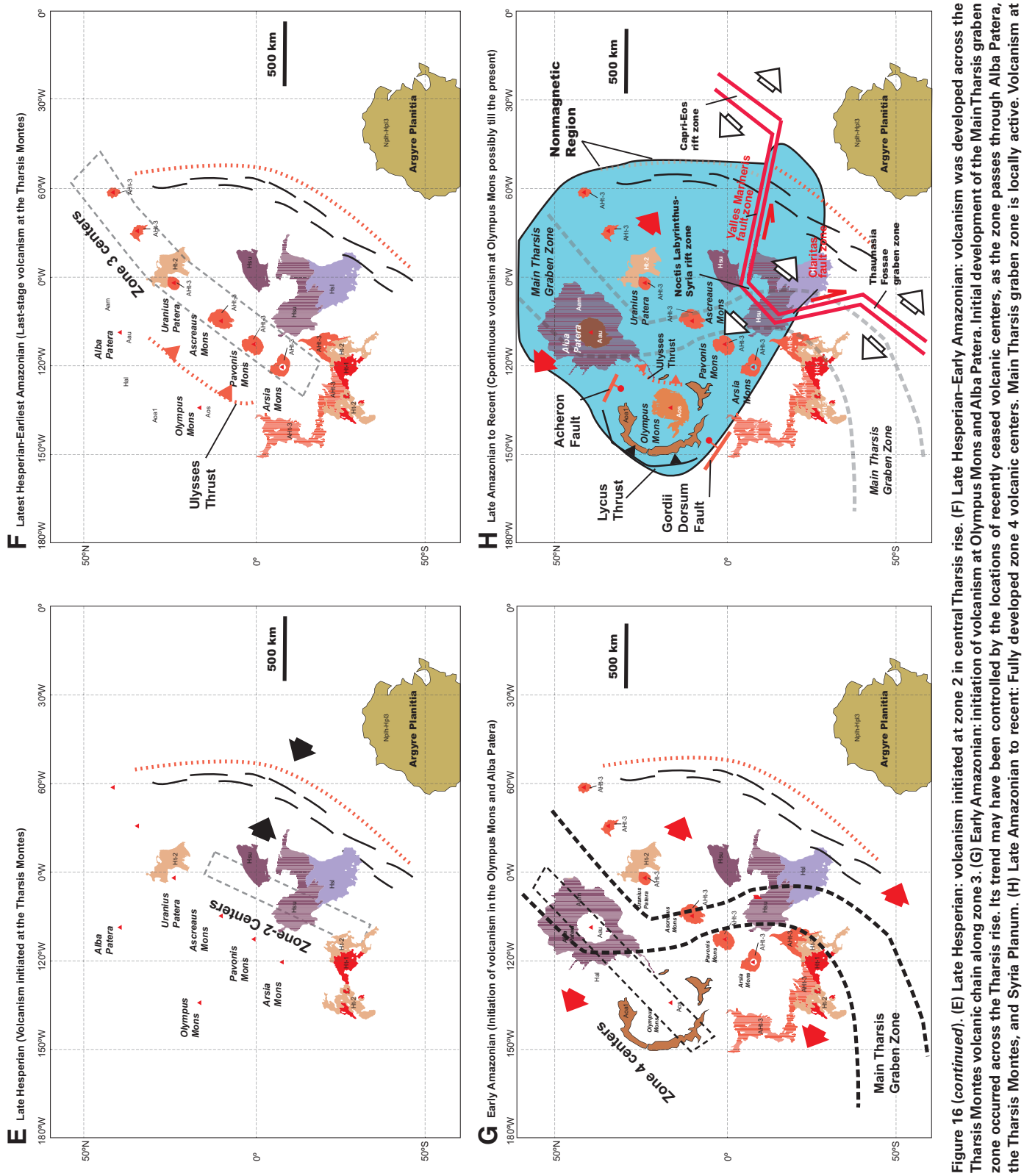

Figure 16 (*continued*). (E) Late Hesperian: volcanism initiated at zone 2 in central Tharsis rise. (F) Late Hesperian–Early Amazonian: volcanism was developed across the Tharsis Montes volcanic chain along zone 3. (G) Early Amazonian: initiation of volcanism at Olympus Mons and Alba Patera. Initial development of the MainTharsis graben zone occurred across the Tharsis rise. Its trend may have been controlled by the locations of recently ceased volcanic centers, as the zone passes through Alba Patera, the Tharsis Montes, and Syria Planum. (H) Late Amazonian to recent: Fully developed zone 4 volcanic centers. Main Tharsis graben zone is locally active. Volcanism at Olympus Mons may still be active. Initiation and full development of the Valles Marineris fault zone and its linked rifts at the two ends.

paleodrainage study of Hynek and Phillips (2001). Anderson et al. (2001) argued that the majority of the Tharsis structures formed in the Noachian, because they cut and are exposed in Noachian terranes. As stated by these authors, this estimate only places a lower age bound, because, in many cases, there are no younger overlapping units to place an upper age bound. For example, the Main Tharsis graben zone and Valles Marineris fault zone, the most dominant structures in the Tharsis rise, are both younger than Noachian, as they cut Hesperian and even Amazonian units (Fig. 3).

The work of Hynek and Phillips (2001) established the existence of an ancient Noachian drainage system on the northwestern slope of the Arabia Terra, which flowed to the northwest from the southern highlands to the northern lowlands. Their studied drainage system has no topographic relationships to the Tharsis rise farther to the west. The most important piece of geologic observations that is against the construction of the Tharsis rise by the Noachian is the dominance of volcanic rocks in the region, occupying more than 80% of the surface area of Tharsis (Fig. 3).

Hynek et al. (2011) listed four pieces of evidence in support of the migrating plume model of Zhong (2009): (1) a track of concentrated plain units between the southern polar region and the southeastern edge of the Tharsis rise, (2) the lack of crustal magnetization along the proposed hotspot track based on the work of Whaler and Purucker (2005) *Mars Global Surveyor* (MGS) magnetometer data, (3) the presence of a strip of thickened crust along the inferred track based on the modeling work of Cheung and King (2011), and (4) the presence of graben structures on the proposed track. Although this is an admirable effort, the evidence presented by Hynek et al. (2011) remains ambiguous. First, the concentrated strip of plain deposits may simply be explained by surficial deposits related to the development of a fluvial system linking the southern polar source regions with the northern lowlands where the fluvial sediments were deposited.

Second, the track of nonmagnetization along their proposed path based on the early work of Whaler and Purucker's (2005) disappears completely in the later model of Lillis et al. (2008) (see their Fig. 4), which was constructed from data from both the magnetometer and electron reflectometer carried by the *Mars Global Surveyor*. As a result, the model has considerably higher sensitivity to crustal fields, and its spatial resolution is a factor of two higher than global maps of magnetic-field components produced with magnetometer data alone (Lillis et al., 2008). Even assuming that a strip of nonmagnetized crust exists along the proposed migrating plume path, complete removal of preexisting magnetization requires emplacement of at least 30-km-thick magmatic crust in the upper crust (Lillis et al., 2009), which would require the presence of a prominent ridge several kilometers high and hundreds of kilometers along the track, which is not obvious in the Mars Orbiter Laser Altimeter (MOLA) topographic map of Mars (Smith et al., 1999).

Third, the inferred strip of thickened crust by Cheung and King (2011) used as evidence in support of the hotspot migration model is based on inversion of gravity data under many untestable assumptions (e.g., uniform crustal density) with nonunique results.

Fourth, the graben structures mentioned by the authors are only present at the northernmost segment of their proposed hotspot track, although their model predicts their presence along the whole track. It is important to note that the grabens shown in the study of Hynek et al. (2011) are the southeastern extension of the Main Tharsis graben zone, which extends far beyond the northern limb of the Tharsis rise and cannot be related to a migrating hotspot track leading to the current site of the Tharsis rise. Like the stationary hotspot model, the migrating plume model of Zhong (2009) predicts central radial extension and peripheral shortening around the plume heads, which are not observed in the Tharsis rise or their proposed hotspot track.

An Episodic Slab Rollback Model for the Origin of the Tharsis Rise

Based on the synthesis of existing literature, new structural analysis presented in this study, and the required geologic history for the evolution of the Tharsis rise (Fig. 16), the following first-order observations must be considered for any tectonic models for the origin of the Tharsis rise:

(1) Initial development of the Tharsis rise started in its southeast part after the occurrence of the nearby Argyre impact.

(2) Zonal volcanism also started in the southeastern margin of the Tharsis rise and migrated from southeast to northwest.

(3) Across the generally northeast-trending volcanic zones, effusive volcanism occurred first in southeastern Tharsis (in zones 3 and 4 in Fig. 3), followed by explosive volcanism in zone 3 (i.e., Tharsis Montes) and possibly in zone 4 (i.e., Olympus Mons) in northwestern Tharsis.

(4) Within volcanic zones 3 and 4, an along-strike change in morphology of central volcanoes occurs: Tall and thin volcanoes (i.e., Tharsis Montes and Olympus Mons) occur in the southwest, whereas short and flat volcanoes (i.e., Alba Patera and Uranius Patera) occur in the northeast. The northeastern segment of volcanic zone 3 may include Tempe Terra igneous plateau that was built on top of Noachian basement (Scott and Tanaka, 1986).

(5) Olympus Mons is bounded in the northwest by a thick-skinned thrust (i.e., Lycus thrust) and two transtensional fault zones along its northeast and southwest edges (i.e., Gordii Dorsum and Acheron fault zones).

(6) Internal deformation of the Tharsis rise was dominated by NW-SW extension.

(7) The bulk of the Tharsis rise lacks crustal magnetization (Acuña et al., 1999; Connerney et al., 1999, 2001; Mitchell et al., 2007; Lillis et al., 2008, 2009). Where crustal magnetization is preserved, such as in the Thaumasia Mountains and Coprates rise along the southeastern edge of the Tharsis rise and parts of Claritas Fossae, the exposed rocks have a Noachian age, and their emplacement predates Tharsis volcanism and construction of the Tharsis rise (Baker et al., 2007; Dohm et al., 2009a).

(8) The distance between zone 3 and zone 4 Tharsis volcanism is spaced ~1550 km (Fig. 2), which is similar to the depth to the core-mantle boundary of Mars. The spacing between zone 3 and zone 2 and between zone 2 and zone 1 Tharsis volcanism is in the range of 1100–1600 km (Fig. 2). Thus, a successive tectonic model must explain this rather peculiar spacing of volcanic zonation.

These observations may be explained by a tectonic model invoking initiation of subduction by Argyre impact in the Early Noachian and episodic slab rollback from the Late Noachian to the Late Amazonian (Fig. 17). The difference in color for the crust of the southern highlands and the northern lowlands in Figure 17 does not imply that the crustal composition of the two regions is different. The proposed slab rollback process is required to produce explosive volcanism, as the subducted slab must have carried hydrated sulfates and hydrated phyllosilicates from the surface of the Noachian crust into the deep mantle. This inference is consistent with the current knowledge that early Mars in the Noachian was hot and wet, producing abundant hydrous minerals at the surface of Mars (e.g., Squyres et al., 2004; also see a recent review by Ehlmann et al., 2011). As detailed in the following, the proposed model requires episodic cessation of plate subduction induced by slab rollback once the slab touches the core-mantle boundary at a depth of ~1580 km. Slab rollback–induced subduction does not restart until the stalled slab become buckled, allowing the upper segment of the subducting slab to resume subduction. This scheme provides a simple mechanism for intermittent operation of plate tectonics on a planet

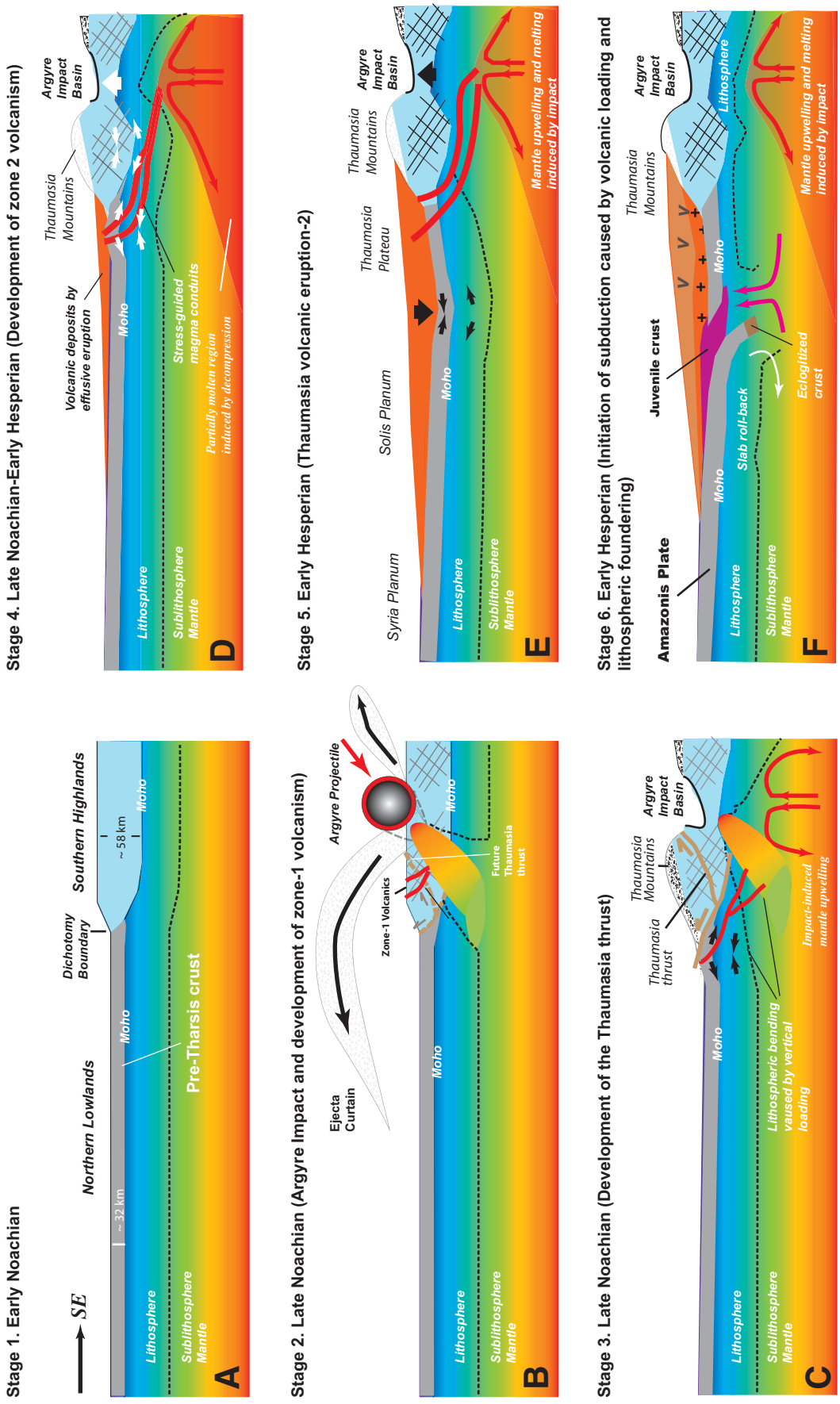

Figure 17. (A) In the Early Noachian, oblique Argyre impact generated ejecta deposits and crustal thickening on the northwestern rim of the impact basin. (B) Melts concentrated in the downrange region were induced by oblique impact. (C) Loading of thickened crust caused lithospheric bending and concentration of tensile stress at the outer rise. (D) Accumulation of volcanic deposits caused downward bending and tensile stress below the volcanic load. (E) Positive feedback between volcanic loading and melt migration further enhanced lithospheric bending. (F) The volcanic load eventually broke the underlying lithosphere, causing it to plunge into the mantle. As the slab moved down, its space was replaced by juvenile crust generated by mantle upwelling to fill the gap. (*Continued on following page.*)

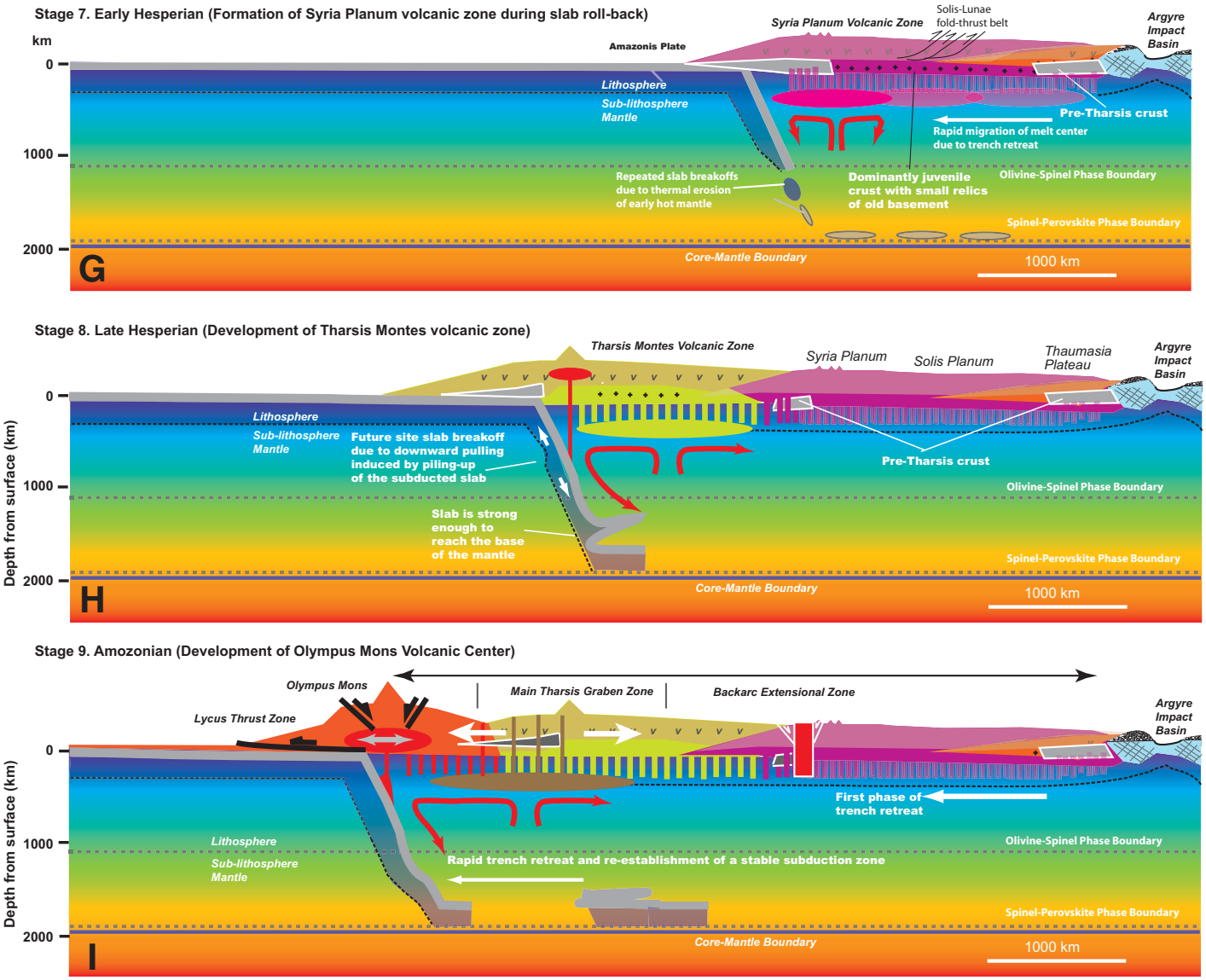

Figure 17 (continued). (G) The presence of water in the subducted slab ensured rapid transformation of mafic crust to eclogite. Eclogitized thick mafic crust provided additional driving force for subduction. Rapid slab rollback is expected to have occurred, which again created voluminous melts from mantle upwelling, leading to volcanic eruption at the surface and creation of juvenile crust below, all of which occurred after shutdown of the Mars dynamo, and thus the newly created Tharsis crust through arc magmatism does not carry any magnetic signatures. Rapid emplacement of plutons may have caused lateral push of country rocks, creating the Thaumasia thrust first and then the Solis-Lunae fold belt. (H) The cooler Late Hesperian and Early Amazonian mantle permitted the subducting slab to reach the core-mantle boundary. The strong and cold slab may have been stalled to form a stationary subduction system during which large volcanoes in zone 3 and zone 4 were built. Note that the subducted slab may have experienced dehydration reaction, leading to explosive eruption first. As the water was carried out by volcanic eruption, the subsequent volcanic flows would have erupted via effusion due to continuous mantle upwelling in the subduction wedge. (I) Continuous thermal weakening of the transient stationary subduction slab would eventually snap and new, eclogitized mafic crust would again drive the subduction. The lack of major volcanic centers between zone 3 and zone 4 suggests that this process occurred rapidly until a new stationary subducting system was established below Olympus Mons and Alba Patera. This proposed process is consistent with the observation that the northwest-southeast distance between the axis of volcanic centers in zone 3 and zone 4 is ~2000 km, similar to the depth to the core-mantle boundary of the Mars.

purely from a kinematic perspective. However, arc volcanism indicating the existence of plate tectonics may continue above a stalled subducting slab, even though there is no actual relative motion of plates.

In the Noachian at ca. 4 Ga (see Robbins and Hynek, 2012), the oblique Argyre impact generated ejecta deposits and crustal thickening on the northwestern rim of the impact basin (i.e., the future Thaumasia Mountains and Coprates rise; Fig. 17A). Melts concentrated in the downrange region, possibly induced by the directivity of the oblique impact (Fig. 17B; e.g., Pierazzo and Melosh, 1999; Reese et al., 2004). Note that the elliptical shape of Hellas Basin was clearly created by an oblique impact (e.g., Melosh, 1989). This impact event did not initiate plate subduction because it occurred in the thick-crust southern highlands (see more detailed discussion on this issue in the following; also, other major impact basins and their relationships to possible initiation of plate subduction are also discussed later in detail).

Loading of thickened crust caused lithospheric bending and concentration of tensile stress at the outer rise (Fig. 17C; ten Brink, 1991; Hieronymus and Bercovici, 2001), and accumulation of volcanic deposits may have enhanced downward bending, creating tensile stress at the base of the lithosphere below the Thaumasia Mountains and Coprates rise (Figs. 17D and 17E). Cracks created by the tensile stress formed conduits along which impact-generated melts migrated upward to the surface along fissure cracks. Positive feedback between volcanic loading and melt migration eventually broke the thin northern lowlands lithosphere adjacent to the dichotomy boundary. Subsequently, the southern tip of the northern lowlands lithosphere, here referred to as the Amozonis plate, started plunging into the mantle (Fig. 17F). The presence of water in the subducting slab ensured rapid transformation of the subducted mafic crust of the Amazonis plate to eclogite (Arhens and Schubert, 1975). The eclogitized thick mafic crust of Martian lithosphere would drive subsequent plate subduction and slab rollback (Fig. 17F). Rapid slab rollback may have induced mantle upwelling, massive dike injections, and eruption of voluminous volcanic rocks and creation of new crust in the southeastern Tharsis rise (Fig. 17G). Rapid emplacement of plutons may have also led to the development of the Solis-Lunae fold belt as a retro-arc fold-and-thrust belt (Fig. 17G).

Because the spinel-perovskite phase boundary and the core-mantle boundary are located near one another at a depth of ~2000 km for Mars (Bertka and Fei, 1997; Fei and Berka, 2005), the tip of the subducting slab would have touched the base of the mantle and terminated at the phase transition or core-mantle boundary. The lack of large central volcanoes in zone 1 and zone 2 may be a result of a hot mantle that thermally weakened the subducting slab enough so as to impede its penetration into the whole mantle (e.g., see numerical simulations of van Hunen and van den Berg, 2008). The cooler Late Hesperian and Early Amazonian mantle permitted the subducting slab to reach the core-mantle boundary. The strong and cold slab may have been stalled *during which slab rollback–induced subduction ceased to operate.* Although *no plate tectonics mechanism was operating at the subduction stoppage*, the presence of a subducted slab with a hydrated crust in the mantle would have caused continued dehydration and thus arc volcanism above (Fig. 17H). A prediction of this stationary source due to the presence of a stalled subducting slab is that its early phase of volcanism should be characterized by explosive eruption due to the presence of a large amount of volatiles in the upper mantle. Subsequent volcanism would become less eruptive due to a progressive decrease of volatiles in the mantle. This proposed scenario also implies that the operation of plate tectonics during the growth of the Tharsis rise was episodic, which was likely characterized by a long period of arc volcanism without plate tectonics and a short period of rapid slab rollback with a flare-up of volcanism over a broad region. Thus, it was the long duration above stationary sources of mantle melts that allowed the formation of the exceptionally large volcanoes in size and volume in zone 3 and zone 4 of Tharsis volcanism.

Continuous thermal weakening may eventually have caused the stalled slab to be buckled, with its lower part detached from the upper part (Fig. 17H). The removal of the slab support by slab buckling and the continued eclogitization of the mafic crust would have propelled the upper segment of the subducted slab to resume slab rollback–induced subduction. The lack of major volcanic centers between zone 3 and zone 4 suggests that the slab rollback process occurred rapidly until the subducting slab was installed again below Olympus Mons and Alba Patera (Fig. 17I). This proposal, that the core-mantle boundary was a major barrier for continued slab rollback and subduction, is consistent with the observation that the northwest-southeast distance between the axial traces of volcanic centers in zone 3 and zone 4 is 1550 km (Fig. 2), similar to the depth to the core-mantle boundary for Mars (Bertka and Fei, 1997; Fei and Berka, 2005). The general spacing of 1100–1600 km between other volcanic zones in the Tharsis rise (Fig. 2) could be attributed also to the retardation effect of the core-mantle boundary and episodic buckling of the stalled subducting slab. As a result of slab rollback, the axis of arc magmatism shifted from Tharsis Montes in zone 3 to Olympus Mons and Alba Patera in zone 4 (Figs. 17H and 17I). A feature related to arc migration is the occurrence of backarc extension, which was expressed by the development of the NE-trending Main Tharsis graben zone and motion on the SE Tharsis conjugate strike-slip system (Fig. 17I; also see Figs. 4 and 6C).

In the proposed model (Fig. 17), the pre-Tharsis crust was extremely stretched, and its fragments were scattered across the Tharsis rise, as shown on the geologic map of the region (Fig. 3). The space between the stretched crustal fragments was filled by feeder dikes that were connected with the eruption centers at the top (Fig. 17). The proposed extension occurred within an active magmatic arc accommodated by dike injection. This large-magnitude extension should not be confused with minor late-stage backarc extension as expressed by the Main Tharsis graben zone.

It is also important to note that eclogitization of the Martian mafic crust is not required to drive the subduction, as the thick lithosphere of Mars, possibly greater than 250 km (e.g., Phillips et al., 2008; also see inferred lithospheric thickness based on interpreted position of a foreland basin and its related forebulge later herein), is itself sufficiently dense to maintain the proposed subduction. As the gravitational acceleration on the surface of Mars is about a factor of 2.5 smaller than that on Earth, the depth to which the eclogitization occurred is ~2.5 times deeper, likely in the range of 100 and 150 km (e.g., Babeyko and Zharkov, 2000). One should also note that eclogitization is not induced by crustal thickening of the Tharsis rise but by the subduction of the northern lowlands lithosphere below the Tharsis rise in the context of the proposed impact-induced slab rollback model here.

Mantle Delamination during Slab Rollback

The along-strike variation of tall and thin to wide and short and flat volcanoes in zone 3 and zone 4 may have resulted from the difference between wholesale lithospheric subduction and delamination of the lower crust and mantle lithosphere (Fig. 18). The boundary between the two styles of volcanism trends southeast parallel to the inferred slab rollback direction (Fig. 19). Scott and Wilson (2003) had also proposed that the uplift of Alba Patera was induced by convective removal of the mantle lithosphere. It is possible that delamination of the mantle lithosphere may have also occurred southwest of the Tharsis rise across the southern Claritas Fossae,

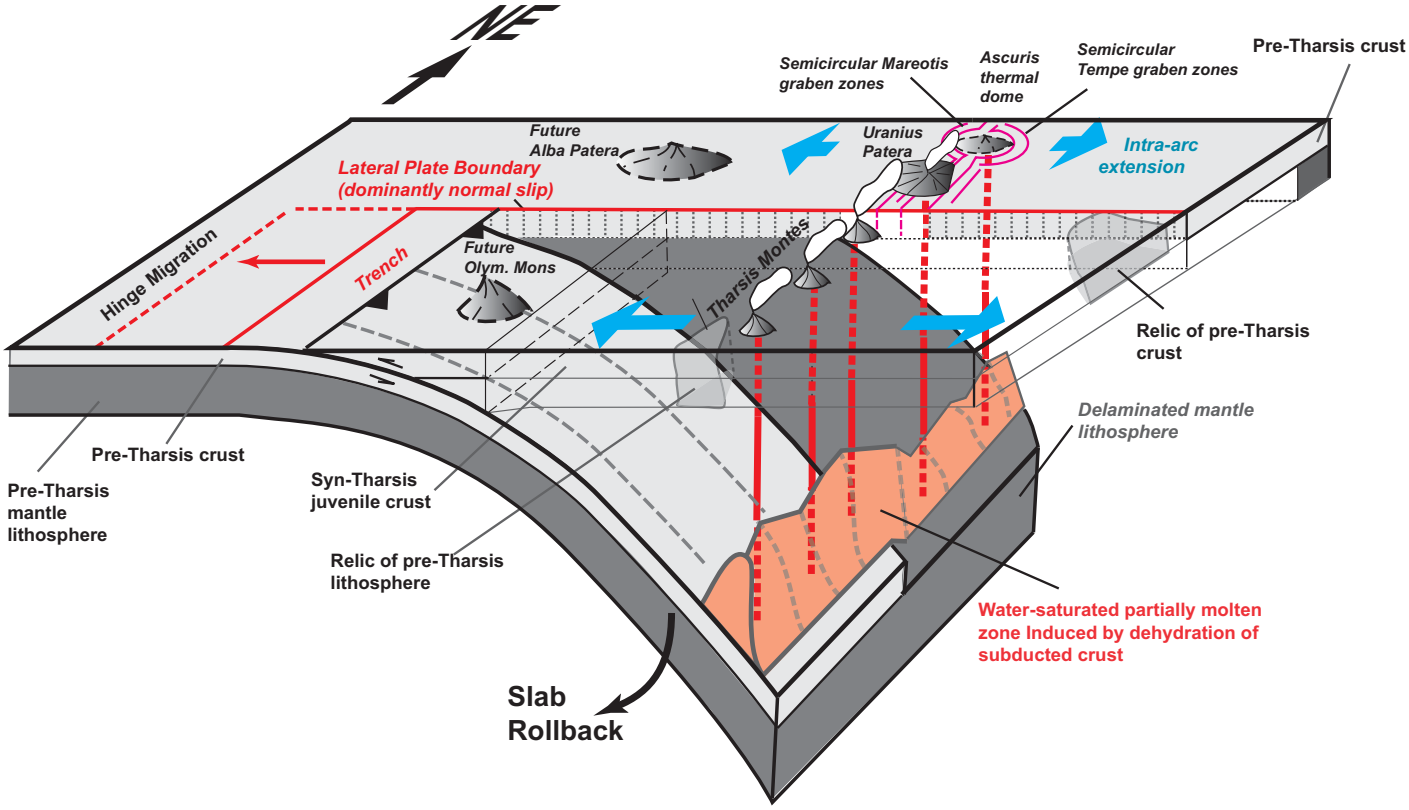

Figure 18. A three-dimensional (3-D) block diagram illustrating a possible configuration of the subduction system across the Tharsis rise. The key feature of the diagram is the along-strike variation of subduction style below the Tharsis Montes–Uranius and Olympus Mons–Alba Patera volcanic chains. Wholesale subduction of the northern lowlands lithosphere occurred below Tharsis Montes and Olympus Mons. Meanwhile, subduction of delaminated mantle lithosphere occurred below the Alba Patera and Uranius Patera volcanic centers. Delamination of the mantle lithosphere allowed preservation of ancient Noachian crust, but it was demagnetized during magmatic accretion from below. The 3-D configuration of the subduction model requires that the Olympus Mons and Tharsis Montes were generated by melting with a significant addition of volatiles in the mantle, while melting below the Alba and Uranius Patera was probably induced by pressure release during rapid migration and re-establishment of the volcanic chains. See text for details. Note that although the Tharsis rise is dominated by juvenile crust created by arc and backarc magmatism during rapid trench retreats, there are fragments of pre-Tharsis basement trapped in the tectonic province, which may have been highly stretched, intensely intruded by syn-Tharsis plutons, and thus demagnetized.

Thaumasia Fossae, Icaria Fossae, and Sirenum Terra. This may explain the scattered occurrence of volcanic centers and the occurrence of the southern Main Tharsis graben zone in the region (Fig. 19).

Oblique Impacts, Volcanism, and Initiation of Global Plate Subduction

An obvious question for the proposed model in Figure 17 is why the Hellas, Isidis, and Utopia impacts did not initiate plate subduction and thus the formation of large highlands like the Tharsis rise. Three factors may decide whether a major impact event could initiate plate subduction: (1) the ability of the lithosphere to subduct at the time of the impact, which depends on the density and thickness of the crust and the mantle lithosphere, (2) the oblique-impact direction and position of the impact basin in relation to the preexisting lithospheric structure on the planet, (3) the distributions of the impact-induced volcanic piles and ejecta, and (4) the polarity of subduction with respect to the impact basin. These factors are discussed next.

Volcanic Loading Induced by Impact

As the proposed model for the formation of the Tharsis rise requires volcanic loading on lithosphere with a thin crust that is able to subduct, it is critical to examine the temporal and spatial relationships between major impact basins and their related volcanism. The close association of major impact basins and volcanic fields on Mars has long been noted (Fig. 19; Meyer and Grolier, 1977; Greeley and Spudis, 1978, 1981): (1) Argyre Basin correlates with the Thaumasia volcanic field across the southeastern edge of the Tharsis rise, (2) Hellas Basin correlates with the combined Malea and Hesperian volcanic fields, (3) Isidis Basin correlates with the Syrtis Major volcanic field, and (4) Utopia Basin correlates with the Elysium volcanic province. Based on crater statistics, eruption in these volcanic fields typically began 200–400 m.y. after the formation of the nearby impact basins (Fig. 20; Scott and Tanaka, 1986; Leonard and Tanaka, 2001; Dohm et al., 2001a; Frey, 2008; Werner, 2009; Robbins and Hynek, 2012). It is also interesting to note that the volcanic fields are located on one or two sides of the nearby impact basins but never surrounding the impact basins completely (Fig. 19). The physical meaning of this time delay for impact-related volcanism is unclear, which could have been related to melt transport processes controlled by mantle and crustal permeability, melt-production rates, and melt viscosity. Also, note that the time duration shown in Figure 20 should be regarded as rough estimates, because

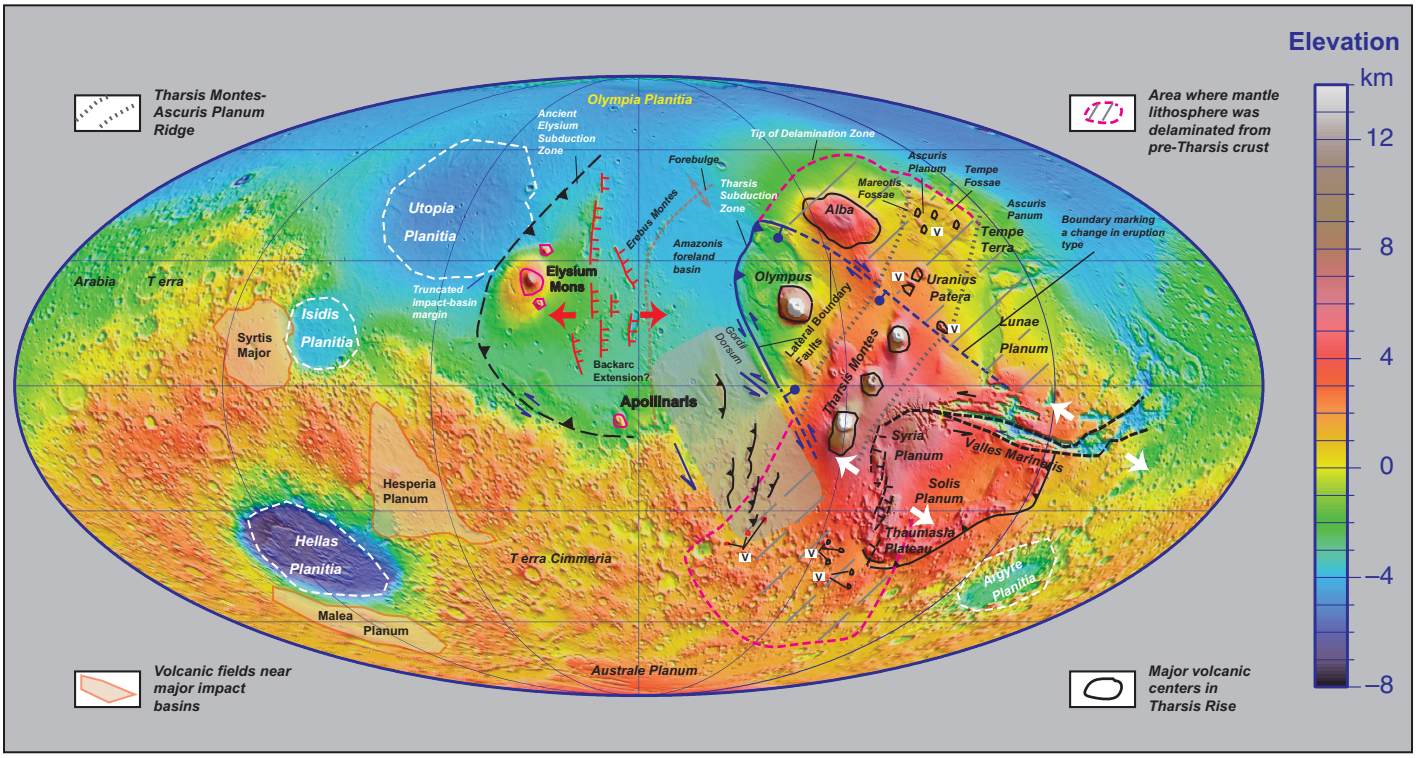

Figure 19. Tectonic map of Mars with emphasis on local subduction zones. Two subduction systems are proposed: (1) the inactive Elysium system and (2) the possibly active Tharsis system. The Elysium system accommodates subduction of Utopia Planitia, whereas the Tharsis system accommodates subduction of Amazonis Planitia. The region between Elysium province and the Olympus Mons is marked by a series of north-trending linear scarps possibly representing normal faults (Scott and Tanaka, 1986; Dohm et al., 2008; Anderson et al., 2008). These structures may be induced by downward bending of the northern lowlands lithosphere. There is also a group of northeast-trending, curvilinear scarps aligned in an en echelon pattern on the southwest side of the Tharsis rise. These structures are interpreted as parts of a broad left-slip shear zone accommodating northwestward sinking and retreat of a strip of the subducting northern lowland slab.

many assumptions are involved in establishing the relationship between crater counts and the absolute time scale on Mars (e.g., Hartmann and Neukum, 2001). The asymmetric distribution of volcanic fields near large impact basins may be induced by oblique impacts, with melts preferentially generated in the downrange regions.

Relationships between Major Impact Basins and Preexisting Lithospheric Structures

The northern lowlands crust (32 km thick) is much thinner than the southern highlands crust (52 km thick; Neumann et al., 2004). As a result, the northern lowlands lithosphere is more readily subducted than the southern highlands lithosphere. Thus, for a large meteorite hitting the thick-crust southern highlands, it is unlikely to initiate plate subduction. This may be the reason that the larger Hellas impact did not cause subduction, as it is located entirely within the southern highlands.

The Isidis impact basin is located on the dichotomy boundary close to the thin-crust northern lowlands. Its position is thus quite similar to that of the Argyre Basin and thus should have been an excellent candidate for initiating plate subduction. The key ingredient of the proposed model in this study (Fig. 17) is the site of volcanic loading; thus, if the position of volcanic loading induced by a major impact is on the southern highlands, the resulting broken lithosphere is not subductable due to the excessive thickness of the crust. The volcanic field associated with the Isidis impact basin is located on the southern highlands side (i.e., the Syrtis Major field in Fig. 19), and thus it could not initiate plate subduction. This observation also applies to the two volcanic fields associated with the Hellas impact, the Hesperian and Malea volcanic fields, which are both located within the southern highlands.

Subduction of Hot versus Cold Sides of a Broken Plate with Respect to Impact Basins

The volcanic field associated with the Utopia impact basin lies entirely in the northern lowlands (i.e., the Elysium volcanic chain in Fig. 19). Thus, impact-induced plate subduction is expected. The MOLA topographic map of the region (Fig. 19) shows that the nearly circular Utopia Basin is truncated along its eastern margin by the Elysium volcanic chain. I interpret this truncation as a result of a limited plate subduction of the Utopia Basin below the Elysium volcanic arc. This subduction was probably terminated shortly after its initiation because of the polarity of the subduction. This inference is based on the results of numerical modeling on the thermal effects of large impacts, which show that the region below and surrounding an impact basin is hotter than regions away from the impact site (e.g., Reese et al., 2004). This thermal structure dictates whether an impact-induced subduction is sustainable or not. The broken lithosphere caused by impact-induced volcanic loading may be divided into the hot and cold sides (Figs. 21A and 21B). The hot side is closer to the impact basin, whereas the cold side is away from the impact basin. As the subduction of the hot side would eventually bring the hot impact basin to the trench zone, the buoyancy of its lithosphere

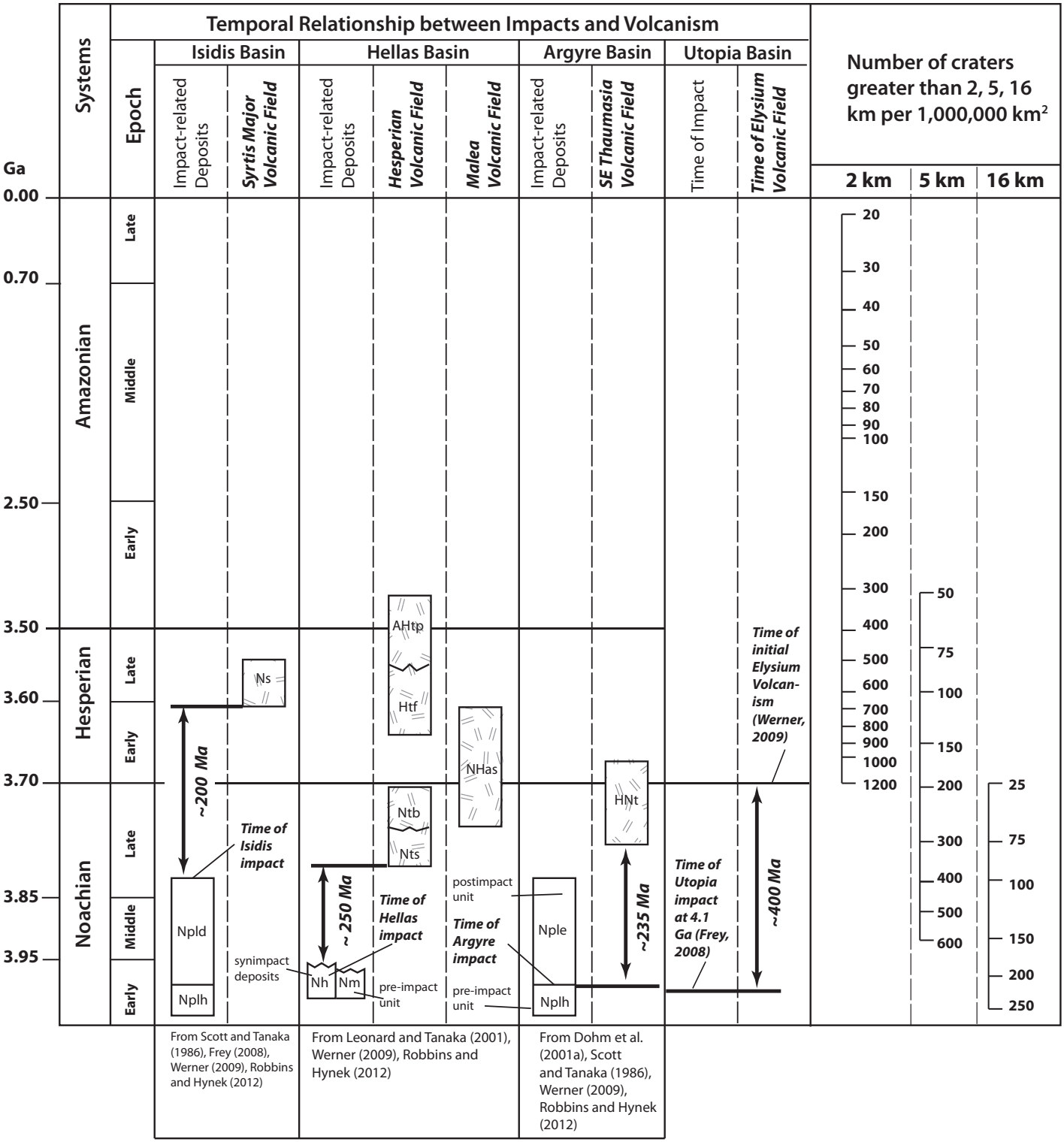

Figure 20. Temporal relationship between major impact events on Mars and the initiation of nearby volcanism. Units Npld and Nplh predate Isidis impact event, while unit Ns postdates Isidis impact, bracketing the event to have occurred within ~200 m.y., which would be the maximum delay time between impact and nearby volcanic eruption. Unit Nh is the synimpact deposits that date the timing of the Hellas impact event, while Nts is the oldest volcanic unit from the nearby volcanic province. This constrains the delay time of volcanism after the Hellas impact to be ~250 m.y. The Argyre impact event occurred between the deposition of units Nplh and Nple, while the oldest volcanic unit in the nearby volcanic field is represented by unit HNt. This yields a delay time of volcanism after impact to be ~230 m.y. The impact age of Utopia is from Frey (2008), and the initiation of Elysium volcanism is from Werner (2009).

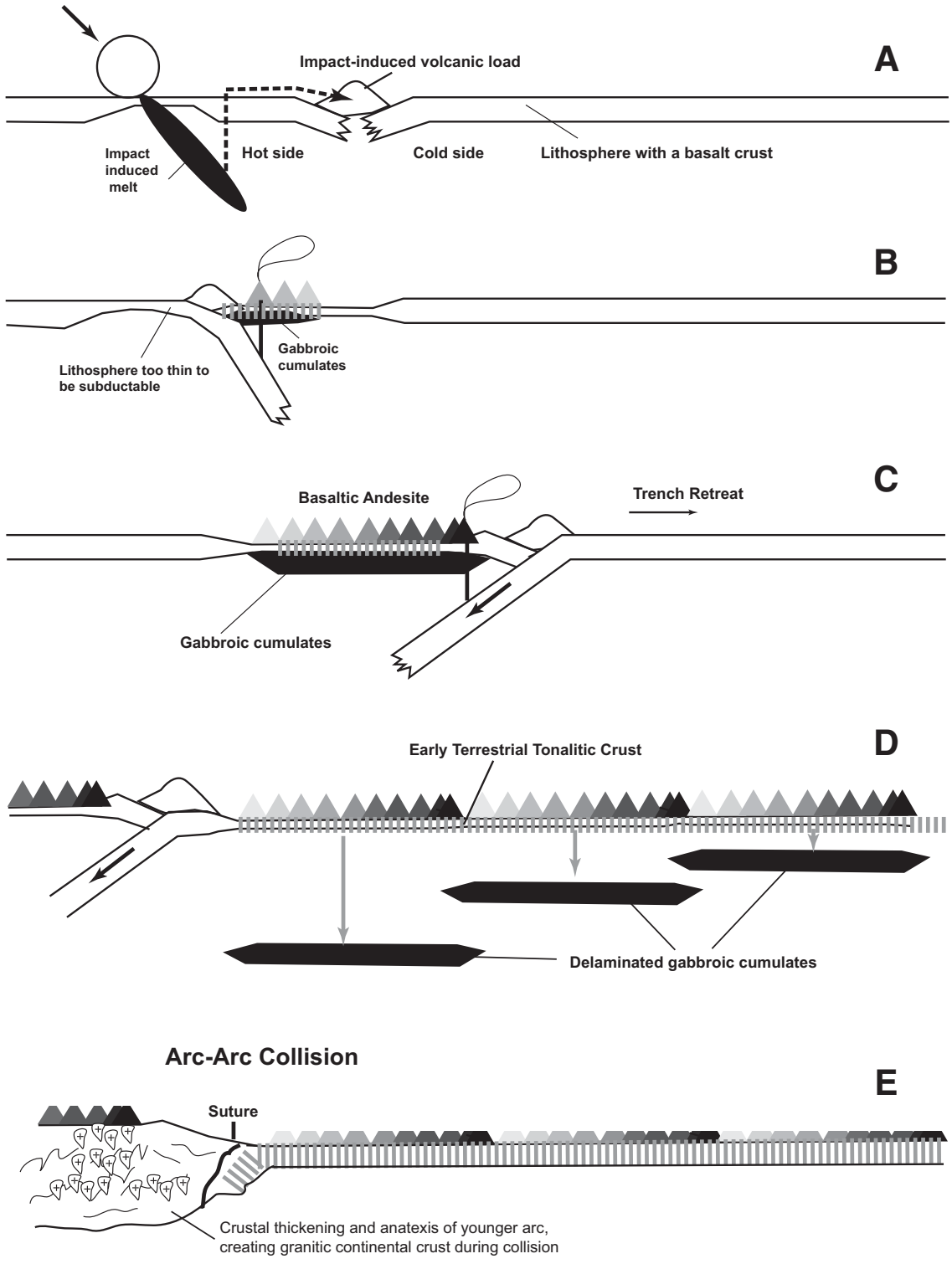

Figure 21. Possible processes for initiation of plate subduction and generation of continental crust during Hadean time on Earth. (A) Impact-generated vertical load leads to rupturing of lithosphere. Due to oblique impact, mantle below the broken plate closer to the impact basin is hotter than mantle below the broken plate farther away from the impact basin. (B) If the hotter side of the broken plate starts to subduct, the process is not sustainable as the thermally thinned lithosphere is too buoyant to subduct. This may explain why subduction induced by Utopia impact was terminated with little subduction of the lithosphere from the Utopia Basin side of the lithosphere. (C) If the colder side of the broken plate starts to subduct, the process is sustainable. This situation may represent the processes associated with the Argyre impact and the later development of the Tharsis rise. Subduction of basaltic crust produces andesite in an oceanic-island arc. (D) Gabbroic cumulates below the arc delaminate into the mantle, leaving the crust to be dominantly andesitic/dioritic in composition. Continuous subduction may lead to collision of a young arc with old arcs created by the subduction system on the sphere of the planet. (E) Arc-arc collision may cause crustal thickening of the younger arc, leading to anatexis of the andesitic arc crust and generation of granites. These processes lead to the eventual creation of continental crust on Earth.

due to a hot temperature below would stall the subduction process. As a result, the subduction process is a short lived. On the hand, if the cold side was subducted after the lithosphere was broken by volcanic loading, the negative buoyancy of the lithosphere could sustain the subduction over a long period of time. The Argyre-induced subduction event belongs to this class.

Foreland Basin and the Effective Elastic Thickness of the Subducting Slab

The proposed slab rollback model requires the existence of a foreland basin. Amazonis Planitia against the northwestern edge of the Tharsis rise displays the largest contrast in gravity anomalies (>300 mGal) on Mars (e.g., Phillips et al., 2001; Zhong and Roberts, 2003, 2004; Solomon et al., 2005), and its position is consistent with the foreland basin of the Lycus thrust; its negative gravity anomaly is similar to those observed at trenches of oceanic subduction zones and foreland basins of continental collision zones on Earth (e.g., McKenzie and Fairhead, 1997; Sandwell and Smith, 2009).

The Erebus Montes may represent the forebulge, and its distance from the location of the load is ~2000 km. This observation may be used to estimate the effective elastic thickness of the subducting plate using the following relationship (e.g., Turcotte and Schubert, 2002):

$$T_e = \left[\left(\frac{2x_0}{\pi}\right)\frac{(\rho_m - \rho_{basalt})(1-\upsilon^2)}{E}\right], \qquad (1)$$

where T_e is the effective thickness of the subducting plate, x_0 is the distance between the crest of the forebulge and the load, ρ_m is mantle density, and ρ_{basalt} is the density of basin fill over the Amazonis foreland basin, which is presumably basaltic flows from the Olympus Mons and Alba Patera, E is Young's modulus, and υ is Poisson's ratio. Assuming a distance of 2000 km between the load at the center of Olympus Mons and the proposed forebulge, 100 GPa for Young's modulus, 0.25 for Poisson's ratio, and 300 kg/m^3 for the density difference between mantle and crust, an effective elastic thickness of ~280 km can be obtained. This is significantly thicker than the effective elastic thickness of the Tharsis rise at 20–100 km (Comer et al., 1985; McKenzie et al., 2002; McGovern et al., 2004; Kronberg et al., 2007; Williams et al., 2008; Dohm et al., 2009a).

Comparison of Arc Construction on Mars and Earth

The following differences can be immediately noticed between oceanic-island arcs in a slab rollback system on Earth and those proposed on Mars in this study (Figs. 2 and 4): (1) the highly elevated arcs and backarc regions on Mars compared to the generally low-lying island arcs and oceanic backarcs on Earth, (2) much straighter traces of volcanic chains on Mars than oceanic arcs on Earth, (3) much larger individual central volcanoes in peak elevations and volumes on Mars than those on Earth, and (4) much greater spacing of volcanoes in general on Mars than those on Earth. Next, I address these issues by analyzing the role of the time scale of arc construction, depth to the core-mantle boundary, the effective elastic thickness of the subducting lithosphere, and the mantle viscosity of underlying arcs on Mars and Earth.

High Elevation of Magmatic Arcs on Mars

I would have thought that the best potential terrestrial analogue for the proposed slab rollback system on Mars is the arc and backarc systems in the western and southwestern Pacific Ocean. For example, the Tonga arc-trench system has evolved since 80 Ma with its vast arc and backarc regions that lie 2–5 km above the surrounding oceanic floors (Schellart et al., 2006). However, this elevation difference is much smaller than the elevation difference between the Tharsis rise (average elevation of ~11 km) and its surrounding regions (below the mean elevation of Mars). There are two key differences between arc construction on Mars and the development of island arcs in a slab rollback system on Earth. First, on Mars, individual volcanic chains were developed above stationary sources over a time scale of >0.5–1 b.y. (e.g., Werner, 2009); this is more than 10–20 times longer than the longest duration of terrestrial arc construction in a slab rollback system on Earth (<20–40 m.y.) (e.g., Schellart et al., 2006). Second, the short duration of island-arc construction on Earth is a result of constant shifting of the trench positions (advances and retreats), while the source regions of Mars arcs, as envisioned in this study, were stationary relative to the overlying plate. Thus, the situation of arc construction on Mars is more like the development of continental arcs rather than oceanic arcs on Earth, where long-term subduction over 100–200 m.y. could have generated large highland regions similar in size to the Tharsis rise, such as the Mesozoic Huabei Plateau of Yin and Nie (1996), the Mesozoic-Cenozoic South American Cordillera (Allmendinger et al., 1997), and the Mesozoic North American Cordillera (Coney and Harms, 1984; DeCelles, 2004). In all these cases, the subducting slabs were moving toward the overriding plates, creating long-term stationary sources of melts in the upper mantle relative to the overriding plates. This situation is similar to the stationary sources of melts created by stalled subducting slabs on Mars as envisioned in this study.

Note that although the 660 km phase boundary on Earth may alternate the speed of subduction, it is incapable of preventing a subducting slab from sinking into the lower mantle (e.g., van Hunen and van den Berg, 2008). A much thinner lithosphere (i.e., about one third of the 300-km-thick Martian lithosphere) (Phillips et al., 2008; also see the result of this study presented earlier herein) and a much longer distance to the core-mantle boundary on Earth at a depth of ~2900 km imply that it is difficult to maintain a coherent slab and become stalled on Earth, as envisioned for Mars in this study.

Another important factor that made it easier to stabilize a stalled subducting slab on Mars is its much higher mantle viscosity below continental arcs, our best terrestrial analogues. This inference is based on the observation that the volcano size on the Tharsis rise increases with volcano spacing through time: (1) Small (diameter <40 km and peak elevation <600 m above surrounding areas) central volcanoes at Syria Planum spaced at 25 ± 5 km were emplaced in the Late Noachian and Early Hesperian (Figs. 2 and 22A; e.g., Baptista et al., 2008), (2) moderately sized central volcanoes (peak elevation <5000 m) on the northwestern flank (i.e., Biblis Patera and Ulysses Patera) and the northeastern flank (i.e., Ceraunius Tolus and Uranius Tolus) of the Tharsis Montes are spaced at ~138 ± 12 km (Figs. 2 and 22A) and were emplaced in the Late Hesperian and Late Amazonian (Werner, 2009), (3) the triplets of the Tharsis Montes, spaced at an average distance of ~860 ± 135 km (Figs. 2 and 22A), were emplaced between the latest Hesperian and early Late Amazonian (Werner, 2009), and (4) the Olympus Mons and Alba Patera are spaced at 1850 km (Figs. 2 and 22A) and were emplaced in the Amazonian (Werner, 2009).

The *dominant* spacing of concurrently initiated volcanoes on Earth has been explained by Rayleigh-Taylor instability, which relates the distance between nearby volcanoes (d) to the viscosity ratio of melt (μ_1) and the surrounding mantle (μ_2), and the thickness of the melt layer (h_2) in the following form (Marsh, 1979):

$$d = \frac{2\pi h_2}{2.15}\left(\frac{\mu_1}{\mu_2}\right)^{1/3}. \qquad (2)$$

The most important implication of this relationship is that the volcano spacing is proportional to the ambient mantle viscosity. If Rayleigh-Taylor instability had controlled the location and spacing of Tharsis volcanoes, then the temporal variation of volcano spacing can be used to infer the viscosity evolution of the Tharsis

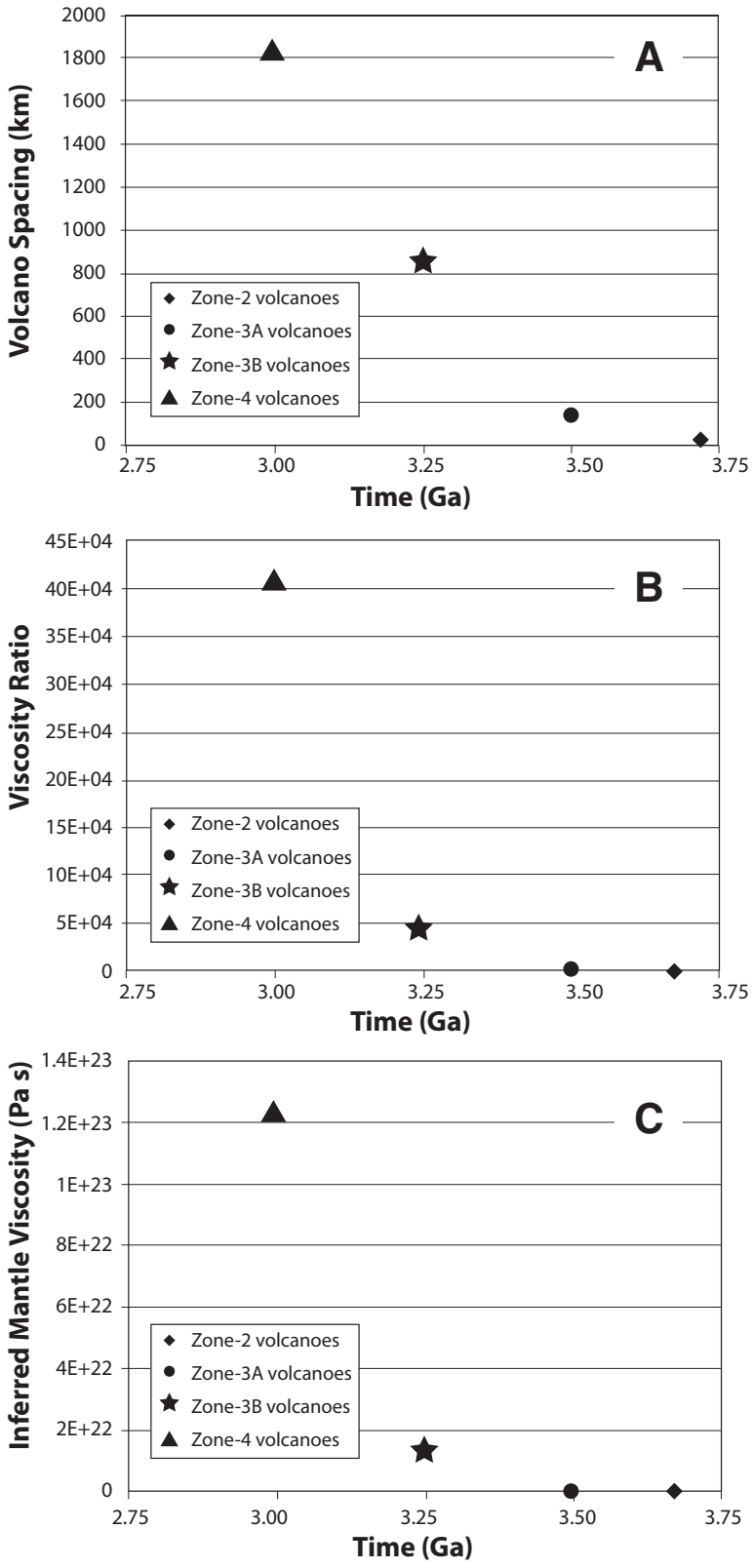

Figure 22. (A) Spacing of Tharsis volcanoes as a function of time. (B) Inferred temporal variation of mantle viscosity during the initiation of zone 2, zone 3, and zone 4 volcanism relative to mantle viscosity below zone 1 volcanism during its initiation. (C) Possible temporal variation of absolute mantle viscosity below Tharsis rise relative to an upper-mantle viscosity of 10 × 10^{18} Pa s below a continental arc.

mantle. To do this requires the assumption that the thickness of the melt layer and the viscosity of the melt remained constant with time. This assumption probably provides a lower bound of the estimated mantle viscosity discussed next. This is because as the planet cools, melt layers in the Tharsis region may have also decreased with time. Using Equation 1, the following simple relationship can be obtained:

$$\frac{\mu_{mantle}^{Stage(i+1)}}{\mu_{mantle}^{Stage\ i}} = \left(\frac{d^{Stage\ (i+1)}}{d^{Stage\ i}}\right)^3. \quad (3)$$

Using this equation and volcano spacing in the four volcanic zones, the following conclusions can be reached: (1) The ambient mantle viscosity during stage 2 volcanism was ~168 times higher than that in stage 1, (2) the ambient mantle viscosity during stage 3 volcanism was 4.1 × 10^4 times higher than that in stage 1, and (3) the ambient mantle viscosity during stage 3 volcanism was 4.1 × 10^5 times higher than that in stage 1 (Fig. 22B).

The absolute value of Tharsis mantle viscosity may be obtained if the melt viscosity and melt-layer thickness are assumed to be the same as those on Earth in continental arc settings, where the dominant spacing between major volcanoes or volcano clusters/groups is ~70–90 km (Vogt, 1974; Marsh, 1979; Savant and de Silva, 2005). Assuming 10^{18} Pa s for terrestrial mantle viscosity, Tharsis mantle viscosity at stage 1, 2, 3, and 4 would have been 3.1 × 10^{17} Pa s, 5.1 × 10^{19} Pa s, 1.2 × 10^{22} Pa s, and 1.2 × 10^{23} Pa s, respectively, at the time of volcano-zone or volcano-group initiation (Fig. 22C). This implies that the Tharsis mantle had cooled rapidly from ca. 3.7 Ga in the Late Noachian to ca. 3.0 Ga at the onset of the Amazonian, causing its viscosity to increase over five orders of magnitude (Fig. 22C). Regardless of the reference viscosity assumed for a continental-arc mantle on Earth, the difference in volcano spacing from an average value of 80 km on Earth to the large distance of 1850 km for the zone 4 Tharsis volcanic chain requires the Tharsis mantle viscosity to be four orders of magnitude higher than that on Earth! This much higher value of Martian mantle viscosity, starting as early as ca. 3 Ga, has important implications for the time scale of chemical mixing in Martian mantle.

Straight Traces of Volcanic Chains on Mars

Styles and curvatures of islands arcs on Earth have been noted to correlate with slab geometry and subduction kinematics (e.g., Schellart, 2008; Di Giuseppe et al., 2008). Stegman et al. (2010) investigated subduction dynamics using three-dimensional (3-D) numerical experiments

simulations. They found that the key physical parameters that control the curvature of an arc are Stokes buoyancy and the effective flexural stiffness of the subducting slab. In their very-strong-slab model (i.e., viscous beam mode), Stegman et al. (2010) showed that subduction in this mode begins with an initially vertical sinking trajectory of the slab tip with the final linear configuration of the trench. As trenches and arcs are parallel to one another, the work of Stegman et al. (2010) implies that a strong subducting plate would have produced a linear arc, which is consistent with our estimated elastic thickness of 280 km for the subducting slab beneath the Tharsis rise.

Large Tharsis Volcanoes

The exceptionally large size of Tharsis volcanoes was interpreted as a result of prolonged volcanism above a stationary hotspot (e.g., Carr, 1974). Although the longevity is clearly a contributing factor, as discussed already, the large spacing of Tharsis volcanoes may have also played a role. Assuming simple cone geometry, the volume (V) of a volcano can be obtained from

$$V = \frac{1}{3}\pi R^2 h, \tag{4}$$

where R is the radius of the base, and h is the peak height. The volume ratio of two volcanoes with the same flank slope (α), or h/R ratio (tan α), can be expressed by

$$\frac{V_1}{V_2} = \left(\frac{h_1}{h_2}\right)^3. \tag{5}$$

For the Tharsis Montes, the average elevation of the three central volcanoes is ~17.6 km, and the total length of the volcanic chain along strike is ~2500 km. The highest arc volcano on Earth is located in the Andes, at an elevation of 6893 m (the Ojos del Salado volcano) along the Argentina-Chile border. As an example of comparison, it is assumed that the Tharsis Montes volcanoes were initially built from the mean elevation of Mars and the Andean volcanoes from sea level. If the Martian and terrestrial volcano geometry is similar and the effect of isostasy is neglected, the volume ratio between a single Tharsis Montes–type volcano and a single large Andean-type volcano would be ~16.5. That is, the total volume of the three Tharsis Montes volcanoes is equivalent to the total volume of ~50 (i.e., 3 × 16.5 = 49.5) of the largest volcanoes in the Andes. Using 80 km for the average volcano spacing in the Andes (Savant and de Silva, 2005), the 2800-km-long Tharsis Montes belt could have hosted 35 of the largest Andean volcanoes. This rough comparison, though with uncertainties about the initial elevation of volcano constructions, the role of erosion, details in volcano shapes, and the effect of isostasy, implies that the large size of Marian volcanoes can be partially accounted for by their large spacing in addition to the longevity of stationary melt sources from below.

Shape of Tharsis Volcanoes

The shape of major volcanoes in the Tharsis rise is often described as shield volcanoes, as they display similar geometry to those on Earth (e.g., Carr, 2006). Because of this similarity, the origin of the volcanoes has been exclusively attributed to hotspot activities since the early work of Carr (1974). However, one must keep in mind that the shape of volcanoes, according to the simplest model of Lacey et al. (1981), is controlled by the viscosity of lava, the flux rate, and the gravity. Because the volcano shape is gravity-dependent, similar geometry of volcanoes on Earth and Mars does not mean that they share the same physical properties. Indeed, when the viscosity and flux rate are held the same, the lower gravity on Mars would create a volcano with a gentler slope according to the formulation by Lacey et al. (1981).

Initiation of Plate Subduction on Rocky Planets in the Solar System

If plate tectonics have operated on Mars and Earth, what made the two planets so special? A possible insight may come from considering two possible governing factors: (1) ability of the crust to subduct and (2) a mechanism by which to initiate the subduction. If large impact was the mechanism of breaking the lithosphere, then the question of initiating plate tectonism becomes whether the crust of a rocky planet was able to subduct at the time of impact.

Due to differences in the concentration of incompatible elements and rigor of mantle convection, various planets may have generated different thicknesses of the crust during pressure-released melting. For the most conservative consideration—that the mantle lithosphere below the newly generated crust cools via conductive cooling—the earliest possible time that the overlying crust becomes subductable can be represented by a half-space cooling problem, as outlined by Davies (1992). Assuming that the lithosphere of a rocky planet formed by conductive cooling and the crust formed by partially melting of an upwelling mantle, the time when the lithosphere reaches the neutral buoyancy state can be determined by the following relationship (Davies, 1992),

$$\tau = \left[\frac{(\rho_L - \rho_C) + (\rho_D - \rho_L)\delta}{(\rho_L - \rho_M)\gamma}\right] h^2, \tag{6}$$

where ρ_L is the average density of the lithosphere, ρ_C is the average density of the crust, ρ_M is the average density of the depleted mantle layer immediately below the crust, δ is a lithospheric thickening constant due to conductive cooling, ρ_M is the average density of the mantle, γ is the thickness of the depleted mantle layer from which the crust was extracted, and h is the thickness of the crust. Assuming that Mars crust and mantle have the same composition as the oceanic lithosphere on Earth and its underlying mantle, the following values are assigned: ρ_L = 3400 kg/m^3, ρ_m = 3300 kg/m^3, ρ_c = 2900 kg/m^3 and 3000 kg/m^3, and γ = 0. I assigned the thickness of the depleted mantle layer to be zero because its effect cannot be differentiated from the presence of the lighter crust above. Because of this assumption, one may think that the parameter h in Equation 3 should be regarded as the thickness of combined depleted mantle and the overlying crust. The most uncertain parameter to assign is the thickening rate of the lithosphere, which depends on the heat flux, mantle temperature, and the thermal conductivity of the lithosphere (Davies, 1992). The average plate/lithospheric thickening rate on Earth is estimated to be ~10 km/m.y. (Davies, 1992). If this rate applies to early evolution of all rocky planets, we can display the relationship of the ability of a planet's lithosphere to subduct as a function (Fig. 23). Although this is a very crude analysis, two parameters emerge as the most important controlling factors for whether a rocky planet would have impact-induced plate subduction during the Late Heavy Bombardment: (1) the initial crustal thickness immediately after consolidation of the outer shell of the planet, and (2) the cooling and thus lithospheric thickening rate. These two factors decide whether the lithosphere of a rocky planet was ready for subduction when outside perturbation such as large impacts was enforced.

For Earth, with an initial crustal thickness at 6 km or less (Davies, 2006), Mars at 32 km for its northern lowlands (Zuber, 2001), and Venus at either 20 km or 60 km (e.g., Hoogenboom et al., 2004, and references therein), the likelihood of initiating plate subduction by large impacts on Earth and Mars during the first 500 m.y. history of the inner solar system is high, as their crust was thin, assuming both share the same thickening rate of lithosphere due to conductive cooling. It is, however, unlikely for Venus to have initiated plate tectonics by large impact if its crust was thick, at ~60 km, during the Late Heavy Bombardment. Even if Venus had a thin crust, the lack of water means that the phase transition of basalt to eclogite would have been too sluggish to allow a broken lithosphere to sink rapidly into the mantle.

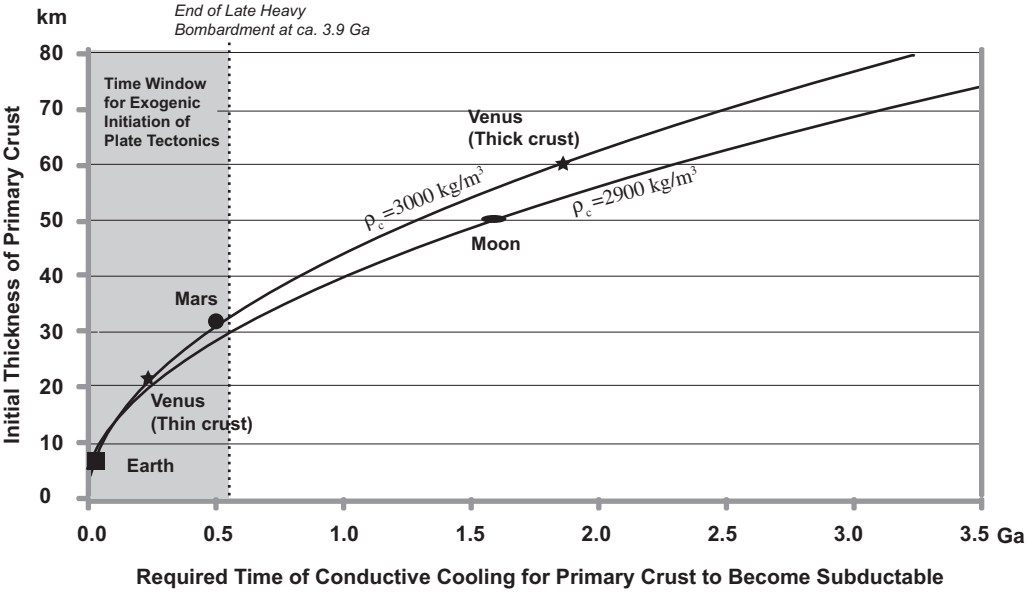

Figure 23. Relationship between initial crustal thickness and the required time for the lithosphere hosting the crust to become subductable via conductive cooling. As no consideration is given to heating in the mantle from radioactive decay and possible small-scale convection below the cooling lithosphere, the time shown here represents a minimum time for crust to become subductable since its hot start from a molten magma ocean. Two average densities of the crust are given. The density of mantle lithosphere is assumed to be 3300 kg/m^3, and mantle below the lithosphere is assumed to be 3250 kg/m^3. The gray area represents the time window during which the inner solar system was experiencing frequent large impacts, which were capable of initiating plate subduction of the lithosphere near the impact sites where the lithosphere was subductable.

Implications for Early Earth

Davies (2006) argued that the Hadean oceanic crust may have been significantly thinner due to depletion of the mantle by vigorous convection of a hotter Earth. Although this mechanism provides a necessary condition for plate subduction, it does not offer a cause for initiation of plate subduction on Hadean Earth (Korenaga, 2008; van Hunen et al., 2008; van Hunen and van den Berg, 2008). Terrestrial planets experienced intense bombardments peaking (i.e., Late Heavy Bombardment) at 4.2–4.0 Ga in the early history of the solar system (e.g., Frey, 2008). Thus, it is conceivable that large impacts repeatedly triggered plate subduction on the Hadean Earth (Hansen, 2007), forming strip-like subduction systems (Fig. 24A). Slab rollback would have caused trench migration and merging of the subduction systems (Fig. 24B). Arc-arc collision could in turn lead to the creation of a new subduction zone, which was much longer and bounded a larger plate (Fig. 24C). Collision between a slab rollback–induced arc and a basaltic plateau generated by a plume could lead to termination of an impacted-induced subduction zone (Fig. 24D).

The processes proposed in Figure 24 would have eventually created a coalesced and kinematically linked global network of plate tectonics on Earth. The time scale from initiation of local subduction to the establishment of a unified plate tectonic network on Earth may have taken up to 1 b.y. or longer throughout the Hadean and Archean. This inference is based on the view that the modern style of plate tectonics was not established until the early Proterozoic (Condie, 1998, 2005; Stern, 2005, 2008; Dewey, 2007; Brown, 2008; Ernst, 2009). An important prediction of the local plate-subduction model proposed here is that plate-tectonic and non-plate-tectonic processes could have occurred simultaneously on Earth in the Hadean and Archean. This may resolve the paradox that low-temperature Hadean zircons require the existence of plate subduction or large-scale underthrusting (Watson and Harrison, 2005; Harrison et al., 2005, 2007; Harrison and Schmitt, 2007; Harrison, 2009) while the commonly observed structural styles and petrologic assemblages of the Early Archean from certain geographic locations on Earth contradict the notion that the process of plate tectonics was operating at that time (e.g., Hamilton, 2007; Stern, 2008).

Another prediction of the model shown in Figure 24 is that the mode of plate tectonics in the Hadean and Archean should have been dominated by slab rollback processes, which are generally associated with voluminous volcanic eruption and magmatic underplating (e.g., Schellart et al., 2006). Perhaps it was this process coupled with frequent arc-arc collisions causing remelting of the andesitic-basalt crust (Fig. 21) that contributed to the rapid creation of continental crust on early Earth.

SUMMARY AND CONCLUSIONS

Based on a review of existing literature, reinterpretation of geologic relationships, and new photogeologic mapping from this study, the following inferences can be made for volcanism during construction of the Tharsis rise. (1) Volcanism was zonal, trending dominantly in the northeast direction, with initiation ages of zonal volcanism becoming younger from southeast to northwest. (2) Early volcanism was dominated by effusive eruption, followed by the development of closely spaced (20–30 km) central volcanoes in an intermediate stage, with final formation of linear chains of giant volcanoes that are spaced at 750–800 km and 1800 km, respectively.

Based on structural analysis of satellite images conducted in this study and the early work of others, four sets of fault systems can be established across the Tharsis rise: (1) the Noachian Thaumasia thrust and Early Hesperian Solis-Lunae fold belt in southeastern Tharsis, (2) the cryptic Early Amazonian Ulysses thrust along the western margin of the Tharsis Montes, (3) the kinematically linked Amazonian Lycus thrust, Gordii Dorsum left-lateral transtensional fault zone, and Acheron extensional fault system, and (4) the Late Hesperian (?) and Amazonian Main Tharsis graben zone and the eastern Tharsis conjugate strike-slip system.

In order to explain the spatial and temporal evolution of the Tharsis volcanism and the Tharsis deformation history, a new tectonic model is proposed that invokes (1) initiation of plate subduction on Mars by large impact and (2) generation of Tharsis volcanism by slab rollback. The new model explains the temporal evolution, dominant NW-SW extension in the interior, and the lack of crustal magnetization of the bulk of the Tharsis rise. The model also explains (1) the formation of thrust systems as a result of impact-generated crustal thickening (i.e., Thaumasia thrust), retro-arc contraction (i.e., Solis-Lunae fold belt), and plate subduction (Lycus and Ulysses thrusts), (2) the development of dominantly NE-trending

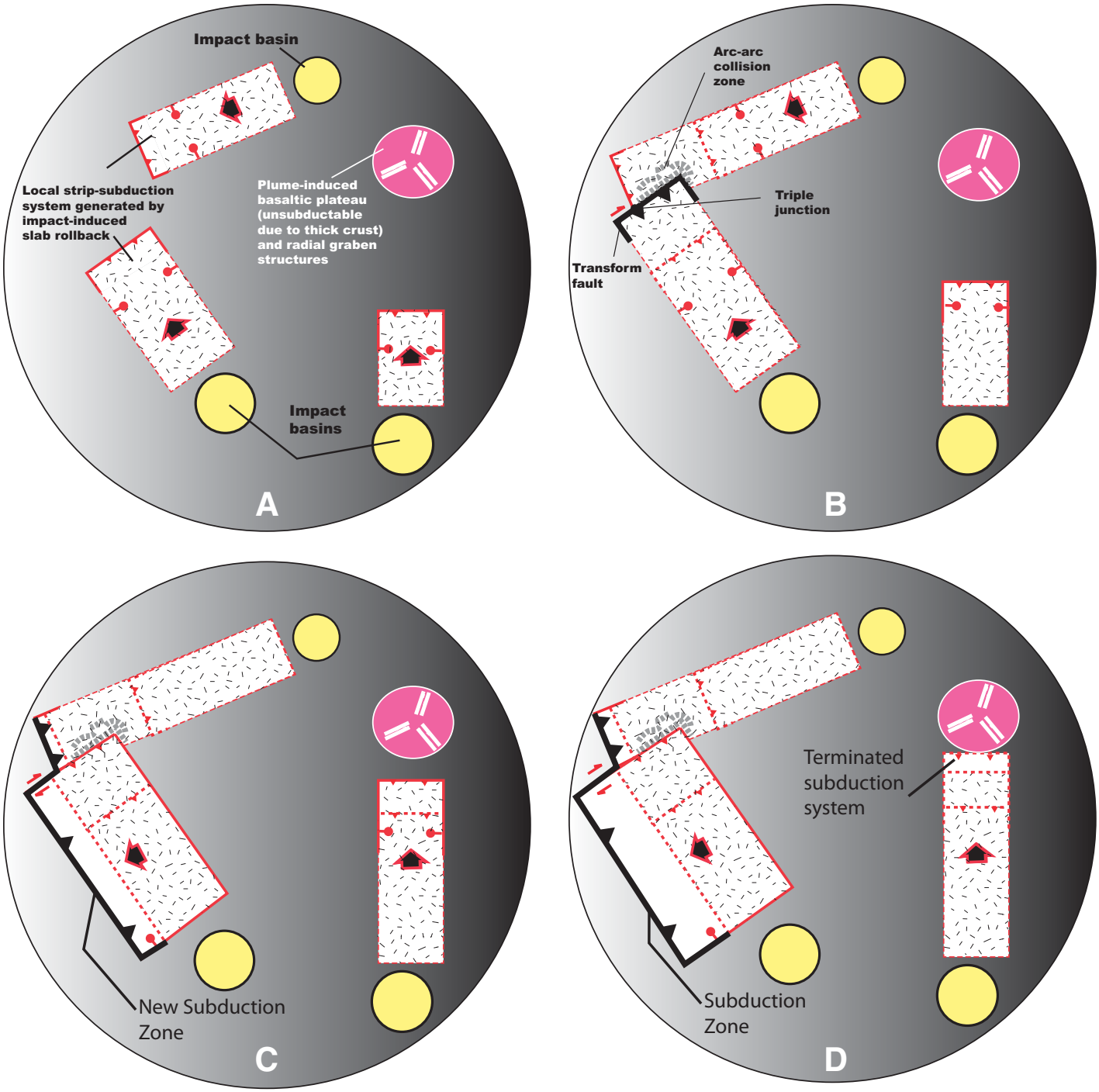

Figure 24. Schematic diagram for initiation of plate subduction and possible evolution of a global network of plate tectonics on early Earth. (A) Impacts during the Late Heavy Bombardment may have created strips of isolated subduction systems induced by slab rollback. Regions outside the strip subduction systems may be affected by plumes and plume-generated basaltic plateaus and related graben structures schematically shown in the pink regions. (B) Lengthening of subduction zones eventually leads to arc-arc collision and formation of a larger plate. Note that a transform fault and a triple junction can be produced by this process. (C) Arc-arc collision may lead to the creation of a new subduction zone, which bounds a larger plate in its hanging wall. (D) Collision between slab rollback–induced arc and a basaltic plateau terminated an impact-induced subduction zone on the right side of diagram. Meanwhile, the long subduction zone on the left side of the diagram continues to develop.

grabens and a major east-facing V-shaped conjugate strike-slip system across the Tharsis rise as a result of backarc extension, and (3) crustal thickening of the Tharsis rise as a result of magmatic accretion during intra-arc extension.

The proposed model has important implications for processes that may have been initiated on Earth in the first 500 m.y., during which large impacts were common and frequent. First, impact-induced plate subduction is highly localized and associated only with trench retreat and slab rollback. Localization of plate subduction in conjunction with uneven thickness and composition of the crust mean that multiple modes of tectonic processes (e.g., plate tectonics, crustal sagging, plume activity, etc.) could have occurred simultaneously on early Earth. Second, the presence of water at the surface of Earth is a prerequisite for plate subduction on the Hadean Earth, as it allows rapid transformation of basaltic crust to eclogite and thus sustainable subduction of lithosphere into deep mantle once it was broken and pushed down deep enough by large impact. It is proposed here that Earth in the Hadean and most of the Archean had only localized plate-subduction systems, all characterized by slab rollback and trench retreat. Trench advance and related shallow plate subduction did not occur until the beginning of the Proterozoic, when a single global network was established by coalescing formerly independent subduction systems. It was perhaps through the incorporation of trench-advance processes (possibly induced by interactions of multiple subduction systems in a single global network) that crustal structures and petrologic assemblages resembling those seen on modern Earth began to emerge.

The difference in style between Martian plate tectonics and modern plate tectonics on Earth provides an important lesson that has parallels to the processes of searching for life on Mars. Since the form of organisms evolves with time, no serious scientist expects to find highly evolved species such as *Homo sapiens* on Mars. Likewise, the mode of plate tectonics may have also evolved with time. The primitive form of plate tectonics documented in this study on Mars and the highly evolved style of modern plate tectonics on Earth are just two of many possible modes of tectonics for which their operation follows the basic kinematic rule of rigid-block motion. Thus, it should not be surprising when plate tectonics with styles that differ from those on Mars and Earth are found in other rocky planets in and outside our solar system in the future.

ACKNOWLEDGMENTS

This research would not have been possible without the extraordinary efforts toward releasing data to the public domains from several National Aeronautics and Space Administration (NASA)–supported missions to Mars. I acknowledge especially the use of data collected by the Mars Orbiter Laser Altimeter (MOLA) research team, the Thermal Emission Imaging System (THEMIS) research team, and the research team in charge of processing and releasing the data collected by the Context Camera and High Resolution Imaging Science Experiment instrument carried on the *Mars Reconnaissance Orbiter* spacecraft. I would also like to thank Greg Neumann for providing the base map for Figure 1 in this study. The scientific content of this study has benefited greatly from discussion with Mark Harrison and Gary Ernst on early Earth, Dave Paige on Mars, Rob Lillis, and Dave Stegman on the dynamics of slab rollback subduction systems. Rob Lillis provided Figure 6D, while Dave Stegment pointed out the correlation between straight arcs and strong subducting lithosphere in a slab rollback system. Review of an early draft by Norm Sleep made the paper more concise, although it is still quite long. I thank John Wakabayashi for inviting me to submit this paper and his encouragement during the entire revision processes. His comments on comparing the proposed arc volcanism on Mars and that observed on Earth led to significant revision of the original Discussion section in the paper. I would also like to acknowledge the thorough, critical, and highly stimulating reviews by James Dohm and an anonymous *Lithosphere* referee. Their comments greatly improve the science and presentation of the paper. I thank Jessica Watkins for her detailed comments that helped to improve the final writing of the paper. Studies on the V-shaped conjugate strike-slip system in the SE Tharsis rise were supported by a grant from the National Science Foundation Tectonics Program.

REFERENCES CITED

Acuña, M.H., Connerney, J.E., Ness, N.F., Lin, R.P., Mitchell, D., Carlson, C.W., McFadden, J., Anderson, K.A., Rème, H., Mazelle, C., Vignes, D., Wasilewski, P., and Cloutier, P., 1999, Global distribution of crustal magnetization discovered by the *Mars Global Surveyor* MAG/ER experiment: Science, v. 284, p. 790–793, doi:10.1126/science.284.5415.790.

Adams, J.B., Gillespie, A.R., Jackson, M.P.A., Montgomery, D.R., Dooley, T.P., Combe, J.-P., and Schreiber, B.C., 2009, Salt tectonics and collapse of Hebes Chasma, Valles Marineris, Mars: Geology, v. 37, p. 691–694, doi:10.1130/G30024A.1.

Allmendinger, R.W., Jordan, T.E., Kay, S.M., and Isacks, B.L., 1997, The evolution of the Altiplano-Puna plateau of the Central Andes: Annual Review of Earth and Planetary Sciences, v. 25, p. 13–174, doi:10.1146/annurev.earth.25.1.139.

Anderson, R.C., Dohm, J.M., Golombek, M.P., Haldemann, A.F.C., and Franklin, B.J., 2001, Primary centers and secondary concentrations of tectonic activity through time in the western hemisphere of Mars: Journal of Geophysical Research, v. 106, no. E9, p. 20,563–20,585, doi:10.1029/2000JE001278.

Anderson, R.C., Dohm, J.M., Haldemann, A.F.C., Hare, T.M., and Baker, V.R., 2004, Tectonic histories between Alba Patera and Syria Planum, Mars: Icarus, v. 171, p. 31–38, doi:10.1016/j.icarus.2004.04.018.

Anderson, R.C., Dohm, J.M., Haldemann, A.F.C., Pounders, E., Golombek, M., and Castanoa, A., 2008, Centers of tectonic activity in the eastern hemisphere of Mars: Icarus, v. 195, p. 537–546, doi:10.1016/j.icarus.2007.12.027.

Anderson, R.C., Dohm, J.M., Robbins, S., Hynek, B., and Andrews-Hanna, J., 2012, Terra Sirenum: Window into pre-Tharsis and Tharsis phases of Mars evolution, *in* Lunar Planetary Science Conference XLIII: Houston, Texas, Lunar and Planetary Institute, abstract 2803 (CD-ROM).

Andrews-Hanna, J.C., Zuber, M.T., and Banerdt, W.B., 2008a, The Borealis Basin and the origin of the Martian crustal dichotomy: Nature, v. 453, p. 1212–1215, doi:10.1038/nature07011.

Andrews-Hanna, J.C., Zuber, M.T., and Hauck, S.A., II, 2008b, Strike-slip faults on Mars: Observations and implications for global tectonics and geodynamics: Journal of Geophysical Research, v. 113, E08002, doi:10.1029/2007JE002980.

Anguita, F., Farelo, A.-F., Lopez, V., Mas, C., Munoz-Espadas, M.-J., Marquez, A., and Ruiz, J., 2001, Tharsis dome, Mars: New evidence for Noachian–Hesperian thick-skin and Amazonian thin-skin tectonics: Journal of Geophysical Research, v. 106, p. 7577–7589, doi:10.1029/2000JE001246.

Anguita, F., Fernandez, C., Cordero, G., Carrasquilla, S., Anguita, J., Nunez, A., Rodriguez, S., and Garcia, J., 2006, Evidences for a Noachian–Hesperian orogeny in Mars: Icarus, v. 185, p. 331–357, doi:10.1016/j.icarus.2006.07.026.

Arhens, T.J., and Schubert, G., 1975, Gabbro-eclogite reaction rate and its geophysical significance: Reviews of Geophysics and Space Physics, v. 13, p. 383–400, doi:10.1029/RG013i002p00383.

Babeyko, A.Y., and Zharkov, V.N., 2000, Martian crust: A modeling approach: Physics of the Earth and Planetary Interiors, v. 117, p. 421–435, doi:10.1016/S0031-9201(99)00111-9.

Baker, V.A., Strom, R.G., Gulick, V.C., Kargel, J.S., Kamatsu, G., and Kale, V.S., 1991, Ancient oceans, ice sheets and hydrological cycle on Mars: Nature, v. 352, p. 589–594, doi:10.1038/352589a0.

Baker, V.R., Maruyama, S., and Dohm, J.M., 2007, Tharsis superplume and the geologic evolution of early Mars, *in* Yuen, D.A., Maruyama, S., Karato, S.-i., and Windley, B.F., eds., Superplumes: Beyond Plate Tectonics: New York, Springer, p. 507–522.

Banerdt, W.B., Golombek, M.P., and Tanaka, K.L., 1992, Stress and tectonics on Mars, *in* Kieffer, H.H., Jakosky, B.M., Snyder, C.W., and Matthews, M.S., eds., Mars: Tucson, Arizona, University of Arizona Press, p. 249–297.

Baptista, A.R., Mangold, N., Ansan, V., Baratoux, D., Lognonne, P., Alves, E.I., Williams, D.A., Bleacher, J.E., Masson, P., and Neukum, G., 2008, A swarm of small shield volcanoes on Syria Planum, Mars: Journal of Geophysical Research, v. 113, E09010, doi:10.1029/2007JE002945.

Bertka, C.M., and Fei, Y.W., 1997, Mineralogy of the Martian interior up to core-mantle boundary pressures: Journal of Geophysical Research–Solid Earth, v. 102, p. 5251–5264, doi:10.1029/96JB03270.

Bistacchi, N., Massironi, M., and Baggio, P., 2004, Large-scale fault kinematic analysis in Noctis Labyrinthus (Mars): Planetary and Space Science, v. 52, p. 215–222, doi:10.1016/j.pss.2003.08.015.

Blasio, F.V., 2011, The aureole of Olympus Mons (Mars) as the compound deposit of submarine landslides: Earth and Planetary Science Letters, v. 312, p. 126–139.

Blasius, K.R., Cutts, J.A., Guest, J.E., and Masursky, H., 1977, Geology of Valles Marineris: First analysis of imaging from the *Viking 1 Orbiter* primary mission: Journal of Geophysical Research, v. 82, p. 4067–4091, doi:10.1029/JS082i028p04067.

Bleacher, J.E., Greeley, R., Williams, D.A., Cave, S.R., and Neukum, G., 2007, Trends in effusive style at the Tharsis Montes, Mars, and implications for the development of the Tharsis province: Journal of Geophysical Research, v. 112, E09005, doi:10.1029/2006JE002873.

Bleacher, J.E., Glaze, L.S., Greeley, R., Hauber, E., Baloga, S.M., Sakimoto, S.E.H., Williams, D.A., and Glotch, T.D., 2009, Spatial and alignment analyses for a field of small volcanic vents south of Pavonis Mons and implications for the Tharsis province, Mars: Journal of Volcanology and Geothermal Research, v. 185, p. 96–102, doi:10.1016/j.jvolgeores.2009.04.008.

Borgia, A., Burr, J., Montero, W., Morales, L.D., and Alvarado, G.E., 1990, Fault-propagation folds induced by gravitational failure and slumping of the Central Costa Rica volcanic range: Implications for large terrestrial and Martian volcanic edifices: Journal of Geophysical Research, v. 95, p. 14,357–14,382, doi:10.1029/JB095iB09p14357.

Borraccini, F., Lanci, L., Wezel, F.C., and Baioni, D., 2005, Crustal extension in the Ceraunius Fossae, northern Tharsis region, Mars: Journal of Geophysical Research, v. 110, E06006, 10 p., doi:10.1029/2004JE002373.

Borraccini, F., Di Achille, G., Ori, G.G., and Wezel, F.C., 2007, Tectonic evolution of the eastern margin of the Thaumasia Plateau (Mars) as inferred from detailed structural mapping and analysis: Journal of Geophysical Research, v. 112, E05005, doi:10.1029/2006JE002866.

Brown, M., 2008, Characteristic thermal regimes of plate tectonics and their metamorphic imprint throughout Earth history: When did Earth first adopt a plate tectonics mode of behavior?, *in* Condie, K.C., and Pease, V., eds., When Did Plate Tectonics Begin on Planet Earth?: Geological Society of America Special Paper 440, p. 97–128.

Brož, P., and Hauber, E., 2012, A unique volcanic field in Tharsis, Mars: Pyroclastic cones as evidence for explosive eruptions: Icarus, v. 218, p. 88–99, doi:10.1016/j.icarus.2011.11.030.

Burbank, D.W., and Anderson, R.S., 2001, Tectonic Geomorphology: Oxford, UK, Blackwell, 274 p.

Cailleau, B., Walter, T.R., Janle, P., and Hauber, E., 2003, Modeling volcanic deformation in a regional stress field: Implications for the formation of graben structures on Alba Patera, Mars: Journal of Geophysical Research, v. 108, no. E12, 5141, doi:10.1029/2003JE002135.

Carr, M.H., 1973, Volcanism on Mars: Journal of Geophysical Research, v. 78, p. 4049–4062, doi:10.1029/JB078i020p04049.

Carr, M.H., 1974, Tectonism and volcanism of the Tharsis region of Mars: Journal of Geophysical Research, v. 79, p. 3943–3949, doi:10.1029/JB079i026p03943.

Carr, M.H., 1996, Water on Mars: New York, Oxford University Press, 265 p.

Carr, M.H., 2006, The Surface of Mars: New York, Cambridge University Press, 307 p.

Carr, M.H., and Head, J.W., III, 2010, Geologic history of Mars: Earth and Planetary Science Letters, v. 294, p. 185–203, doi:10.1016/j.epsl.2009.06.042.

Carr, M.H., Greeley, R., Blasius, K.R., Guest, J.E., and Murray, J.B., 1977, Some Martian volcanic features as viewed from the *Viking Orbiters*: Journal of Geophysical Research, v. 82, p. 3985–4015, doi:10.1029/JS082i028p03985.

Cheung, K.K., and King, S.D., 2011, Using crustal thickness modeling to study Mars' crustal/mantle structures: 42nd Lunar Planet. Sci. Conf. Abstract, p. 1534.

Comer, R.P., Solomon, S.C., and Head, J.W., III, 1985, Thickness of lithosphere from the tectonic response to volcanic loads: Journal of Geophysical Research, v. 23, p. 61–92.

Condie, K.C., 1998, Episodic continental growth and supercontinents: A mantle avalanche connection?: Earth and Planetary Science Letters, v. 163, p. 97–108, doi:10.1016/S0012-821X(98)00178-2.

Condie, K.C., 2005, Earth as an Evolving Planetary System: Amsterdam, Netherlands, Academic Press, 447 p.

Coney, P.J., and Harms, T.A., Cordilleran metamorphic core complexes—Cenozoic extensional relics of Mesozoic compression: Geology, v. 12, p. 550–554, doi:10.1130/0091-7613(1984)12<550:CMCCCE>2.0.CO;2.

Connerney, J.E.P., Acuña, M.H., Wasilewski, P., Ness, N.F., Rème, H., Mazelle, C., Vignes, D., Lin, R.P., Mitchell, D.L., and Cloutier, P.A., 1999, Magnetic lineations in the ancient crust of Mars: Science, v. 284, p. 794–798, doi:10.1126/science.284.5415.794.

Connerney, J.E.P., Acuña, M.H., Wasilewski, P.J., and Kletetschka, G., 2001, The global magnetic field of Mars and implications for crustal evolution: Geophysical Research Letters, v. 28, p. 4015–4018, doi:10.1029/2001GL013619.

Courtillot, V.E., Allegre, C.J., and Mattauer, M., 1975, On the existence of relative lateral motions on Mars: Earth and Planetary Science Letters, v. 25, p. 279–285, doi:10.1016/0012-821X(75)90242-3.

Crumpler, L.S., and Aubele, J.C., 1978, Structural evolution of Arsia Mons, Pavonis Mons, an Ascraeus Mons: Tharsis region of Mars: Icarus, v. 34, p. 496–511, doi:10.1016/0019-1035(78)90041-6.

Davies, G.F., 1992, On the emergence of plate tectonics: Geology, v. 20, p. 963–966, doi:10.1130/0091-7613(1992)020<0963:OTEOPT>2.3.CO;2.

Davies, G.F., 2006, Gravitational depletion of the early Earth's upper mantle and the viability of early plate tectonics: Earth and Planetary Science Letters, v. 243, p. 376–382, doi:10.1016/j.epsl.2006.01.053.

DeCelles, P.G., 2004, Late Jurassic to eocene evolution of the Cordilleran thrust belt and foreland basin system, western USA: American Journal of Science, v. 304. p. 105–168, doi:10.2475/ajs.304.2.105.

Dewey, J.F., 2007, The secular evolution of plate tectonics and the continental crust: An outline, *in* Hatcher, R.D., Jr., Carlson, M.P., McBride, J.H., and Martínez Catalán, J.R., eds., 4-D Framework of Continental Crust: Geological Society of America Memoir 200, p. 1–7.

Di Giuseppe, E., van Hunen, J., Funiciello, F., Faccenna, C., and Giardini, D., 2008, Slab stiffness control of trench motion: Insights from numerical models: Geochemistry Geophysics Geosystems, v. 9, Q02014, doi:10.1029/2007GC001776.

Dohm, J.M., and Tanaka, K.L., 1999, Geology of the Thaumasia region, Mars: Plateau development, valley origins, and magmatic evolution: Planetary and Space Science, v. 47, p. 411–431, doi:10.1016/S0032-0633(98)00141-X.

Dohm, J.M., Tanaka, K.L., and Hare, T.M., 2001a, Geologic Map of the Thaumasia Region of Mars: U.S. Geological Survey Map I-2650.

Dohm, J.M., Ferris, J.C., Baker, V.R., Anderson, R.C., Hare, T.M., Strom, R.G., Barlow, N.G., Tanaka, K.L., Klemaszewski, J.E., and Scott, D.H., 2001b, Ancient drainage basin of the Tharsis region, Mars: Potential source for outflow channel systems and putative oceans or paleolakes: Journal of Geophysical Research, v. 106, p. 32,943–32,958.

Dohm, J.M., Anderson, R.C., Baker, V.R., Ferris, J.C., Rudd, L.P., Hare, T.M., Rice, J.W., Casavant, R.R., Strom, R.G., Zimbelman, J.R., and Scott, D.H., 2001c, Latent outflow activity for western Tharsis, Mars: Significant flood record exposed: Journal of Geophysical Research-Planets, v. 106. p. 12,301–12,314, doi:10.1029/2000JE001352.

Dohm, J.M., Maruyama, S., Baker, V.R., and Anderson, R.C., 2007, Traits and evolution of the Tharsis superplume, Mars, *in* Yuen, D.A., Maruyama, S., Karato, S.-i., and Windley, B.F., eds., Superplumes: Beyond Plate Tectonics: New York, Springer, p. 523–537.

Dohm, J.M., Anderson, R.C., Barlow, N.G., Miyamoto, H., Davies, A.G., Taylor, G.J., Baker, V.R., Boynton, W.V., Keller, J., Kerry, K., Janes, D., Fairén, A.G., Schulze-Makuch, D., Glamoclija, M., Marinangeli, L., Ori, G.G., Strom, R.G., Williams, J.-P., Ferris, J.C., Rodríguez, J.A.P., de Pablo, M.A., and Karunatillake, S., 2008, Recent geological and hydrological activity on Mars: The Tharsis/Elysium corridor: Planetary and Space Science, v. 56, p. 985–1013, doi:10.1016/j.pss.2008.01.001.

Dohm, J.M., Williams, J.P., Anderson, B.C., Ruiz, J., McGuire, P.C., Komatsu, G., Davila, A.F., Ferris, J.C., Schulze-Makuch, D., Baker, V.R., Boynton, W.V., Fairen, A.G., Hare, T.M., Miyamoto, H., Tanaka, K.L., and Wheelock, S.J., 2009a, New evidence for a magmatic influence on the origin of Valles Marineris, Mars: Journal of Volcanology and Geothermal Research, v. 185, p. 12–27, doi:10.1016/j.jvolgeores.2008.11.029.

Dohm, J.M., Anderson, R.C., Williams, J.-P., Ruiz, J., McGuire, P.C., Buczkowski, D.L., Wang, R., Scharenbroich, L., Hare, T.M., Connerney, J.E.P., Baker, V.R., Wheelock, S.J., Ferris, J.C., and Miyamoto, H., 2009b, Claritas rise, Mars: Pre-Tharsis magmatism?: Journal of Volcanology and Geothermal Research, v. 185, p. 139–156, doi:10.1016/j.jvolgeores.2009.03.012.

Ehlmann, B.L., Mustard, J.F., Murchie, S.L., Bibring, J.-P., Meunier, A., Fraeman, A.A., and Langevin, Y., 2011, Subsurface water and clay mineral formation during the early history of Mars: Nature, v. 7371, p. 53–60.

Ernst, W.G., 2009, Archean plate tectonics, rise of Proterozoic supercontinentality and onset of regional, episodic stagnant-lid behavior: Gondwana Research, v. 15, p. 243–253, doi:10.1016/j.gr.2008.06.010.

Fei, Y.W., and Berka, C., 2005, The interior of Mars: Science, v. 308, p. 1120–1121, doi:10.1126/science.1110531.

Forsythe, R.D., and Zimbelman, J.R., 1988, Is the Gordii Dorsum escarpment on Mars an exhumed transcurrent fault?: Nature, v. 336, p. 143–146, doi:10.1038/336143a0.

Frey, H., 1979, Martian canyons and African rifts: Structural comparisons and implications: Icarus, v. 37, p. 142–155, doi:10.1016/0019-1035(79)90122-2.

Frey, H. 2008, Ages of very large impact basins on Mars: Implications for the Late Heavy Bombardment in the inner solar system: Geophysical Research Letters, v. 35, L13203, doi:10.1029/2008GL033515.

Golabek, G.J., Keller, T., Gerya, T.V., Zhu, G., Tackley, P.J., and Connolly, J.A.D., 2011, Origin of the Martian dichotomy and Tharsis from a giant impact causing massive magmatism: Icarus, v. 215, p. 346–357, doi:10.1016/j.icarus.2011.06.012.

Golombek, M.P., and Phillips, R.J., 2010, Mars tectonics, *in* Watters, T.R., and Schultz, R.A., eds., Planetary Tectonics: New York, Cambridge University Press, p. 183–232.

Greeley, R., and Spudis, P.D., 1978, Volcanism in cratered terrain hemisphere of Mars: Geophysical Research Letter, v. 5, p. 453–455, doi:10.1029/GL005i006p00453.

Greeley, R., and Spudis, P.D., 1981, Volcanism on Mars: Reviews of Geophysics, v. 19, p. 13–41, doi:10.1029/RG019i001p00013.

Hamilton, W.B., 2007, Earth's first two billion years—The era of internally mobile crust, *in* Hatcher, R.D., Jr., Carlson, M.P., McBride, J.H., and Martínez Catalán, J.R., eds., 4-D Framework of Continental Crust: Geological Society of America Memoir 200, p. 233–296.

Hansen, V.L., 2007, Subduction origin on early Earth: A hypothesis: Geology, v. 35, p. 1059–1062, doi:10.1130/G24202A.1.

Harder, H., and Christensen, U.R.A., 1996, A one-plume model of Martian mantle convection: Nature, v. 380, p. 507–509.

Harris, S.A., 1977, The aureole of Olympus Mons, Mars: Journal of Geophysical Research, v. 82, p. 3099–3107, doi:10.1029/JB082i020p03099.

Harrison, T.M., 2009, The Hadean crust: Evidence from >4 Ga zircons: Annual Review of Earth and Planetary Sciences, v. 37, p. 479–505, doi:10.1146/annurev.earth.031208.100151.

Harrison, T.M., and Schmitt, A.K., 2007, High sensitivity mapping of Ti distributions in Hadean zircons: Earth and Planetary Science Letters, v. 261, p. 9–19, doi:10.1016/j.epsl.2007.05.016.

Harrison, T.M., Blichert-Toft, J., Müller, W., Albarede, F., Holden, P., and Mojzsis, S.J., 2005, Heterogeneous Hadean hafnium: Evidence of continental crust at 4.4 to 4.5 Ga: Science, v. 310, no. 5756, p. 1947–1950.

Harrison, T.M., Watson, E.B., and Aikman, A.K., 2007, Temperature spectra of zircon crystallization in plutonic rocks: Geology, v. 35, p. 635–638, doi:10.1130/G23505A.1.

Hartmann, W.K., and Neukum, G., 2001, Cratering chronology and evolution of Mars: Space Science Reviews, v. 96, p. 165–194, doi:10.1023/A:1011945222010.

Hauber, E., and Kronberg, P., 2001, Tempe Fossae, Mars: A planetary analog to a terrestrial continental rift?: Journal of Geophysical Research, v. 106, p. 20,587–20,602, doi:10.1029/2000JE001346.

Hauber, E., and Kronberg, R., 2005, The large Thaumasia graben on Mars: Is it a rift?: Journal of Geophysical Research, v. 110, E07003, doi:10.1029/2005JE002407.

Hauber, E., Bleacher, J.E., Gwinner, K., Williams, D., and Greeley, R., 2009, The topography and morphology of low volcanic shields and associated landforms of plains volcanism in the Tharsis region on Mars: Journal of Volcanology and Geothermal Research, v. 185, p. 69–95, doi:10.1016/j.jvolgeores.2009.04.015.

Head, J.W., III, and Wilson, L., 1998a, Tharsis Montes as composite volcanoes?: The role of explosive volcanism in edifice construction and implications for the volatile contents of edifice-forming magmas, *in* Lunar and Planetary Science Conference XXIX: Houston, Texas, Lunar and Planetary Institute, abstract 1127 (CD-ROM).

Head, J.W., III, and Wilson, L., 1998b, Tharsis Montes as composite volcanoes?: 3. Lines of evidence for explosive volcanism in edifice construction, *in* Lunar and

Planetary Science Conference XXIX: Houston, Texas, Lunar and Planetary Institute, abstract 1124 (CD-ROM).
Head, J.W., III, Hiesinger, H., Ivanov, M.A., Kreslavsky, M.A., Pratt, S., and Thomson, B.J., 1999, Possible ancient oceans on Mars: Evidence from Mars Orbiter Laser Altimeter Data: Science, v. 286, p. 2134–2137, doi:10.1126/science.286.5447.2134.
Hieronymus, C.F., and Bercovici, D., 2001, Focusing of eruptions by fracture wall erosion: Journal of Geophysical Research, v. 28, p. 1823–1826, doi:10.1029/2000GL011885.
Hiesinger, H., and Head, J.W., III, 2002, Topography and morphology of the Argyre Basin, Mars: Implications for its geologic and hydrologic history: Planetary and Space Science, v. 50, p. 939–981, doi:10.1016/S0032-0633(02)00054-5.
Hiesinger, H., Head, J.W., III, and Neukum, G., 2007, Young lava flows on the eastern flank of Ascraeus Mons: Rheological properties derived from High Resolution Stereo Camera (HRSC) images and Mars Orbiter Laser Altimeter (MOLA) data: Journal of Geophysical Research, v. 112, E05011, doi:10.1029/2006JE002717.
Hodges, C.A., and Moore, H.J., 1979, Subglacial birth of Olympus Mons and its aureoles: Journal of Geophysical Research, v. 84, p. 8061–8074.
Hoogenboom, T., Smrekar, S.E., Anderson, F.S., and Houseman, G., 2004, Admittance survey of type 1 coronae on Venus: Journal of Geophysical Research, v. 109, E03002, doi:10.1029/2003JE002171.
Hynek, B.M., and Phillips, R.J., 2001, Evidence for extensive denudation of the Martian highlands: Geology, v. 29, p. 407–410, doi:10.1130/0091-7613(2001)029<0407:EFEDOT>2.0.CO;2.
Hynek, B.M., Phillips, R.J., and Arvidson, R.E., 2003, Explosive volcanism in the Tharsis region: Global evidence in the Martian geologic record: Journal of Geophysical Research, v. 108, no. E9, 5111, doi:10.1029/2003JE002062.
Hynek, B.M., Robbins, S.J., Sramek, O., and Zhong, S.J., 2011, Geological evidence for a migrating plume on early Mars: Earth and Planetary Science Letters, v. 310, p. 327–333, doi:10.1016/j.epsl.2011.08.020.
Ivanov, M.A., and Head, J.W., III, 2006, Alba Patera, Mars: Topography, structure, and evolution of a unique Late Hesperian–Early Amazonian shield volcano: Journal of Geophysical Research, v. 111, E09003, doi:10.1029/2005JE002469.
Jellinek, A.M., Johnson, C.L., and Schubert, G., 2008, Constraints on the elastic thickness, heat flow, and melt production at early Tharsis from topography and magnetic field observations: Journal of Geophysical Research, v. 113, E09004, doi:10.1029/2007JE003005.
Johnson, C.L., and Phillips, R.J., 2005, Evolution of the Tharsis regions of Mars: Insights from magnetic field observations: Earth and Planetary Science Letters, v. 230, p. 241–254, doi:10.1016/j.epsl.2004.10.038.
Karasozen, E., Andrews-Hanna, J.C., Dohm, J.M., and Anderson, R.C., 2012, The formation mechanism of the south Tharsis ridge belt, Mars, *in* Lunar and Planetary Science Conference XLIII: Houston, Texas, Lunar and Planetary Institute, abstract 2592 (CD-ROM).
Kemp, D.V., and Stevenson, D.J., 1996, A tensile, flexural model for the initiation of subduction: Geophysical Journal International, v. 125, p. 73–93, doi:10.1111/j.1365-246X.1996.tb06535.x.
Korenaga, J., 2008, Plate tectonics, flood basalts and the evolution of Earth's oceans: Terra Nova, v. 20, p. 419–439, doi:10.1111/j.1365-3121.2008.00843.x.
Kronberg, P., Hauber, E., Grott, M., Werner, S.C., Schäfer, T., Gwinner, K., Giese, B., Masson, P., and Neukum, G., 2007, Acheron Fossae, Mars: Tectonic rifting, volcanism, and implications for lithospheric thickness: Journal of Geophysical Research, v. 112, E04005, doi:10.1029/2006JE002780.
Lacey, A., Ockendon, J.R., and Turcott, D.L., 1981, On the geometrical form of volcanoes: Earth and Planetary Science Letters, v. 54, no. 1, p. 139–143, doi:10.1016/0012-821X(81)90074-1.
Leonard, G.J., and Tanaka, K.L., 2001, Geologic Map of the Hellas Region of Mars: U.S. Geological Survey Geologic Investigations Series I-2694.
Lillis, R.J., Frey, H.V., Manga, M., Mitchell, D.L., Lin, R.P., Acuña, M.H., and Bougher, S.W., 2008, An improved crustal magnetic field map of Mars from electron reflectometry: Highland volcano magmatic history and the end of the Martian dynamo: Icarus, v. 194, p. 575–596, doi:10.1016/j.icarus.2007.09.032.
Lillis, R.J., Dufek, J., Bleacher, J.E., and Manga, M., 2009, Demagnetization of crust by magmatic intrusion near the Arsia Mons volcano: Magnetic and thermal implications for the development of the Tharsis province, Mars: Journal of Volcanology and Geothermal Research, v. 185, p. 123–138, doi:10.1016/j.jvolgeores.2008.12.007.
Lopes, R.M.C., Guest, J.E., and Wilson, C.J.N., 1980, Origin of the Olympus Mons aureole and perimeter scarp: The Moon and the Planets, v. 22, p. 221–234, doi:10.1007/BF00898433.
Lopes, R.M.C., Guest, J.E., Hiller, K., and Neukum, G., 1982, Further evidence for a mass movement origin for the Olympus Mons aureole: Journal of Geophysical Research, v. 87, p. 9917–9928, doi:10.1029/JB087iB12p09917.
Lucchitta, B.K., McEwen, A.S., Clow, G.D., Geissler, P.E., Singer, R.B., Schultz, R.A., and Squyres, S.W., 1992, The canyon system of Mars, *in* Kieffer, H.H., Jakosky, B.M., Snyder, C.W., and Matthews, M.S., eds., Mars: Tucson, Arizona, University of Arizona Press, p. 453–492.
Lucchitta, B.K., Isbell, N.K., and Howington-Kraus, A., 1994, Topography of Valles Marineris: Implications for erosional and structural history: Journal of Geophysical Research, v. 99, p. 3783–3798, doi:10.1029/93JE03095.
Mangold, N., Allemand, P., and Thomas, P.G., 1998, Wrinkle ridges of Mars: Structural analysis and evidence for shallow deformation controlled by ice-rich décollements: Planetary and Space Science, v. 46, p. 345–356, doi:10.1016/S0032-0633(97)00195-5.
Mangold, N., Allemand, P., Thomas, P.G., and Vidal, G., 2000, Chronology of compressional deformation on Mars: Evidence for a single and global origin: Planetary and Space Science, v. 48, p. 1201–1211, doi:10.1016/S0032-0633(00)00104-5.
Márquez, A., Fernández, C., Anguita, F., Farelo, A., Anguita, J., and de la Casa, M.-Á., 2004, New evidence for a volcanically, tectonically, and climatically active Mars: Icarus, v. 172, p. 573–581, doi:10.1016/j.icarus.2004.07.015.
Marsh, B.D., 1979, Island arc development: Some observations, experiments, and speculations: The Journal of Geology, v. 87, p. 687–713, doi:10.1086/628460.
Masson, P., 1977, Structure pattern analysis of the Noctis Labyrinthus–Valles Marineris regions of Mars: Icarus, v. 30, p. 49–62, doi:10.1016/0019-1035(77)90120-8.
Masson, P., 1980, Contribution to the structural interpretation of the Valles Marineris–Noctis Labyrinthus–Claritas Fossae regions of Mars: The Moon and the Planets, v. 22, p. 211–219, doi:10.1007/BF00898432.
Masson, P., 1985, Origin and evolution of the Valles Marineris region of Mars: Advanced Space Research, v. 50, p. 83–92.
McEwen, A.S., Malin, M.C., Carr, M.H., and Hartmann, W.K., 1999, Voluminous volcanism on early Mars revealed in Valles Marineris: Nature, v. 397, p. 584–586, doi:10.1038/17539.
McGovern, P.J., and Morgan, J.K., 2009, Volcanic spreading and lateral variations in the structure of Olympus Mons: Marine Geology, v. 37, p. 139–142.
McGovern, P.J., and Solomon, S.C., 1993, State of stress, faulting, and eruption characteristics of large volcanoes on Mars: Journal of Geophysical Research, v. 98, p. 23,553–23,579, doi:10.1029/93JE03093.
McGovern, P.J., Smith, J.R., Morgan, J.K., and Bulmer, M.H., 2004, The Olympus Mons aureole deposits: New evidence for a flank failure origin: Journal of Geophysical Research, v. 109, E08008, doi:10.1029/2004JE002258.
McKenzie, D., and Fairhead, D., 1997, Estimates of the effective elastic thickness of the continental lithosphere from Bouguer and free air gravity anomalies: Journal of Geophysical Research, v. 102, p. 27,523–27,552, doi:10.1029/97JB02481.
McKenzie, D., and Nimmo, F., 1999, The generation of Martian floods by the melting of ground ice above dykes: Nature, v. 397, p. 231–233, doi:10.1038/16649.
McKenzie, D., Barnett, D.N., and Yuan, D.-N., 2002, The relationship between Martian gravity and topography: Earth and Planetary Science Letters, v. 195, p. 1–16, doi:10.1016/S0012-821X(01)00555-6.
Mège, D., and Masson, P., 1996a, Stress models for Tharsis formation, Mars: Planetary and Space Science, v. 44, p. 1471–1497, doi:10.1016/S0032-0633(96)00112-2.
Mège, D., and Masson, P., 1996b, A plume tectonics model for the Tharsis Province, Mars: Planetary and Space Science, v. 44, p. 1499–1546, doi:10.1016/S0032-0633(96)00113-4.
Melosh, H.J., 1989, Impact Cratering: A Geological Process: New York, Oxford University Press, 245 p.
Meyer, J.D., and Grolier, M.J., 1977, Geologic Map of the Syrtis Major Quadrangle of Mars: U.S. Geological Survey Map I-995(MC-13).
Mitchell, D.L., Lillis, R.J., Lin, R.P., Connerney, J.E.P., and Acuña, M.H., 2007, A global map of Mars' crustal magnetic field based on electron reflectometry: Journal of Geophysical Research, v. 112, no.E1, doi:10.1029/2005JE002564.
Montgomery, D.R., and Gillespie, A., 2005, Formation of Martian outflow channels by catastrophic dewatering of evaporite deposits: Geology, v. 33, p. 625–628, doi:10.1130/G21270.1.
Montgomery, D.R., Som, S.M., Jackson, M.P.A., Schreiber, B.C., Gillespie, A.R., and Adams, J.B., 2009, Continental-scale salt tectonics on Mars and the origin of Valles Marineris and associated outflow channels: Geological Society of America Bulletin, v. 121, p. 117–133.
Morris, E.C., 1982, Aureole deposits of the Martian volcano Olympus Mons: Journal of Geophysical Research, v. 87, p. 1164–1178, doi:10.1029/JB087iB02p01164.
Morris, E.C., and Tanaka, K.L., 1994, Geologic Maps of the Olympus Mons Region of Mars: U.S. Geological Survey Miscellaneous Investigation Series I-2327.
Mouginis-Mark, P.J., 2002, Prodigious ash deposits near the summit of Arsia Mons volcano, Mars: Geophysical Research Letters, v. 29, doi:10.1029/2002GL015296.
Mouginis-Mark, P.J., Wilson, L. and, Zimbelman, 1988, Polygenic eruptions on Alba Patera, Mars: Bulletin of Volcanology, v. 50, p. 361–379.
Mueller, K., and Golombek, M., 2004, Compressional structures on Mars: Annual Review of Earth and Planetary Sciences, v. 32, p. 435–464, doi:10.1146/annurev.earth.32.101802.120553.
Murray, J.B., van Wyk de Vries, B., Marquez, A., Williams, D.A., Byrne, P., Muller, J.P., and Kim, J.R., 2010, Late-stage water eruptions from Ascraeus Mons volcano, Mars: Implications for its structure and history: Earth and Planetary Science Letters, v. 294, p. 479–491, doi:10.1016/j.epsl.2009.06.020.
Nahm, A.L., and Schultz, R.A., 2010, Evaluation of the orogenic belt hypothesis for the formation of the Thaumasia Highlands, Mars: Journal of Geophysical Research, v. 115, E04008, doi:10.1029/2009JE003327.
Neumann, G.A., Zuber, M.T., Wieczorek, M.A., McGovern, P.J., Lemoine, F.G., and Smith, D.E., 2004, Crustal structure of Mars from gravity and topography: Journal of Geophysical Research, v. 109, E08002, doi:10.1029/2004JE002262.
Nimmo, F., and Tanaka, K., 2005, Early crustal evolution of Mars: Annual Review of Earth and Planetary Sciences, v. 33, p. 133–161, doi:10.1146/annurev.earth.33.092203.122637.
Okubo, C.H., and Schultz, R.A., 2004, Mechanical stratigraphy in the western equatorial region of Mars based on thrust fault–related fold topography and implications for near-surface volatile reservoirs: Geological Society of America Bulletin, v. 116, p. 594–605, doi:10.1130/B25361.1.
Okubo, C.H., and Schultz, R.A., 2006, Variability in Early Amazonian Tharsis stress state based on wrinkle ridges and strike-slip faulting: Journal of Structural Geology, v. 28, p. 2169–2181, doi:10.1016/j.jsg.2005.11.008.
Peulvast, J.P., and Masson, P.L., 1993, Melas Chasma: Morphology and tectonic patterns in Central Valles Marineris (Mars): Earth, Moon, and Planets, v. 61, p. 219–248, doi:10.1007/BF00572246.
Peulvast, J.P., Mège, D., Chiciak, J., Costard, F., and Masson, P.L., 2001, Morphology, evolution and tectonics of Valles Marineris wall slopes (Mars): Geomorphology, v. 37, p. 329–352, doi:10.1016/S0169-555X(00)00085-4.
Phillips, R.J., Zuber, M.T., Solomon, S.C., Golombek, M.P., Jakosky, B.M., Banerdt, W.B., Smith, D.E., Williams, R.M.E., Hynek, B.M., Aharonson, O., and Hauck, S.A., 2001, Ancient geodynamics and global-scale hydrology on Mars: Science, v. 291, p. 2587–2591, doi:10.1126/science.1058701.

Phillips, R.J., Zuber, M.T., Smrekar, S.E., Mellon, M.T., Head, J.W., Tanaka, K.L., Putzig, N.E., Milkovich, S.M., Campbell, B.A., Plaut, J.J., Safaeinili, A., Seu, R., Biccari, D., Carter, L.M., Picardi, G., Orosei, R., Mohit, P.S., Heggy, E., Zurek, R.W., Egan, A.F., Giacomoni, E., Russo, F., Cutigni, M. , Pettinelli, E., Holt, J.W., Leuschen, C.J., and Marinangeli, L., 2008, Mars north polar deposits: Stratigraphy, age, and geodynamical response: Science, v. 320, p. 1182–1185 , doi:10.1126/science.1157546.

Pierazzo, E., and Melosh, H.J., 1999, Hydrocode modeling of Chicxulub as an oblique impact event: Earth and Planetary Science Letters, v. 165, p. 163–176, doi:10.1016/S0012-821X(98)00263-5.

Platz, T., Münn, S., Walter, T.R., Procter, J.N., McGuire, P.C., Dumke, A., and Neukum, G., 2011, Vertical and lateral collapse of Tharsis Tholus, Mars: Earth and Planetary Science Letters, v. 305, p. 445–455, doi:10.1016/j.epsl.2011.03.012.

Plescia, J.B., 2000, Geology of the Uranius group volcanic constructs: Uranius Patera, Ceraunius Tholus, and Uranius Tholus: Icarus, v. 143, p. 376–396, doi:10.1006/icar.1999.6259.

Plescia, J.B., 2004, Morphometric properties of Martian volcanoes: Journal of Geophysical Research, v. 109, E03003, doi:10.1029/2002JE002031.

Plescia, J.B., and Golombek, M.P., 1986, Origin of planetary wrinkle ridges based on the study of terrestrial analogs: Geological Society of America Bulletin, v. 97, p. 1289–1299.

Plescia, J.B., and Saunders, R.S., 1982, Tectonic history of the Tharsis region: Journal of Geophysical Research, v. 87, p. 9775–9791, doi:10.1029/JB087iB12p09775.

Polit, A.T., Schultz, R.A., and Soliva, R., 2009, Geometry, displacement–length scaling, and extensional strain of normal faults on Mars with inferences on mechanical stratigraphy of the Martian crust: Journal of Structural Geology, v. 31, p. 662–673, doi:10.1016/j.jsg.2009.03.016.

Purucker, M., Ravat, D., Frey, H., Voorhies, C., Sabaka, T., and Acuña, M., 2000, An altitude-normalized magnetic map of Mars and its interpretation: Geophysical Research Letters, v. 27, p. 2449–2452.

Rawling, E.J., Mitchell, K.L., and Wilson, L., 2003, Recent silicic lava flows on Olympus Mons?, *in* Lunar and Planetary Science Conference XXXIV: Houston, Texas, Lunar and Planetary Institute, abstract 1337 (CD-ROM).

Reese, C.C., Solomatov, V.S., Baumgardner, J.R., Stegman, D.R., and Vezolainen, A.V., 2004, Magmatic evolution of impact-induced Martian mantle plumes and the origin of Tharsis: Journal of Geophysical Research, v. 109, E08009, doi:10.1029/2003JE002222.

Ruiz, J., 2011, Giant impacts and the initiation of plate tectonics on terrestrial planets: Planetary and Space Science, v. 59, p. 749–753.

Sandwell, D.T., and Smith, W.H.F., 2009, Global marine gravity from retracked Geosat and ERS-1 altimetry: Ridge segmentation versus spreading rate: Journal of Geophysical Research, v. 114, B01411, doi:10.1029/2008JB006008.

Savant, S.S., and de Silva, S.L., 2005, A GIS-based spatial analysis of volcanoes in the central Andes: Insights into factors controlling volcano spacing: Eos (Transactions, American Geophysical Union), Fall Meeting supplement, Abstract V21D-0648.

Schellart, W.P., 2008, Kinematics and flow patterns in deep mantle and upper mantle subduction models: Influence of the mantle depth and slab to mantle viscosity ratio: Geochemistry Geophysics Geosystems, v. 9, Q03014, doi:10.1029/2007GC001656.

Schellart, W.P., Lister, G.S., and Toy, V.G., 2006, A Late Cretaceous and Cenozoic reconstruction of the Southwest Pacific region: Tectonics controlled by subduction and slab rollback processes: Earth-Science Reviews, v. 76, p. 191–233, doi:10.1016/j.earscirev.2006.01.002.

Schultz, P.H., and Anderson, R.R., 1996, Asymmetry of the Manson impact structure: Evidence for impact angle and direction, *in* Koeberl, C., and Anderson, R.R., eds., Manson and Company: Impact Structures in the United States: Geological Society of America Special Paper 302, p. 397–417.

Schultz, P.H., and D'Hondt, S., 1996, Cretaceous-Tertiary (Chicxulub) impact angle and its consequences: Geology, v. 24, p. 963–967, doi:10.1130/0091-7613(1996)024<0963:CTCIAA>2.3.CO;2.

Schultz, R.A., 1989, Strike-slip faulting of ridged plains near Valles Marineris, Mars: Nature, v. 341, p. 424–426, doi:10.1038/341424a0.

Schultz, R.A., 1998, Multiple-process origin of Valles Marineris basins and troughs, Mars: Planetary and Space Science, v. 46, p. 827–834, doi:10.1016/S0032-0633(98)00030-0.

Schultz, R.A., 2000, Fault-population statistics at the Valles Marineris Extensional Province, Mars: Implications for segment linkage, crustal strains, and its geodynamical development: Tectonophysics, v. 316, p. 169–193, doi:10.1016/S0040-1951(99)00228-0.

Schultz, R.A., and Lin, J., 2001, Three-dimensional normal faulting models of the Valles Marineris, Mars, and geodynamic implications: Journal of Geophysical Research, v. 106, p. 16,549–16,566, doi:10.1029/2001JB000378.

Schultz, R.A., and Tanaka, K.L., 1994, Lithospheric-scale buckling and thrust structures on Mars: The Coprates rise and south Tharsis ridge belt: Journal of Geophysical Research, v. 99, p. 8371–8385, doi:10.1029/94JE00277.

Schultz, R.A., Okubo C.H., and Wilkins, S.J., 2006, Displacement–length scaling relations for faults on the terrestrial planets: Journal of Structural Geology, v. 28, p. 2182–2193, doi:10.1016/j.jsg.2006.03.034.

Schultz, R., Soliva, A.R., Fossen, H., Okubo, C.H., and Reeves, D.M., 2008, Dependence of displacement–length scaling relations for fractures and deformation bands on the volumetric changes across them: Journal of Structural Geology, v. 30, p. 1405–1411, doi:10.1016/j.jsg.2008.08.001.

Schultz, R.A., Hauber, E., Kattenhorn, S.A., Okubo, C.H., and Watters, T.R., 2010, Interpretation and analysis of planetary structures: Journal of Structural Geology, v. 32, p. 855–875, doi:10.1016/j.jsg.2009.09.005.

Scott, D.H., and Dohm, J.M., 1990, Faults and ridges—Historical development in Tempe Terra and Ulysses Patera regions of Mars, *in* 20th Lunar and Planetary Science Conference Proceedings: Houston, Texas, Lunar and Planetary Institute, v. 20, p. 503–513.

Scott, D.H., and Tanaka, K.L., 1986, Geological Map of the Western Equatorial Region of Mars: U.S. Geological Society Miscellaneous Investigation Series Map I-1802A, scale 1:15,000,000.

Scott, D.H., Dohm, J.M., and Rice, J.W., Jr., 1995, Map of Mars Showing Channels and Possible Paleolake Basins: U.S. Geological Society Miscellaneous Investigation Series Map I-2461, scale 1:30,000,000.

Scott, E., and Wilson, L., 2003, Did the Alba Patera and Syria Planum regions of Mars lose their lithospheric roots in convective overturn events?: Journal of Geophysical Research, v. 108, 5035, 12 p., doi:10.1029/2002JE001492.

Scott, E.D., Wilson, L., and Head, J.W., III, 2002, Emplacement of giant radial dikes in the northern Tharsis region of Mars: Journal of Geophysical Research, v. 107, no. E4, 5019, doi:10.1029/2000JE001431.

Sharp, R.P., 1973, Mars: Troughed terrain: Journal of Geophysical Research, v. 78, p. 4063–4072.

Shea, T., and van Wyk de Vries, B., 2008, Structural analysis and analogue modeling of the kinematics and dynamics of rockslide avalanches: Geosphere, v. 4, p. 657–686, doi:10.1130/GES00131.1.

Skinner, J.A., Hare, T.A., and Tanaka, K.L., 2006, Digital renovation of the Atlas of Mars 1:15,000,000-scale global geologic series maps, *in* Lunar and Planetary Science Conference XXXVII: Houston, Texas, Lunar and Planetary Institute, p. 2331.

Sleep, N.H., 1994, Martian plate tectonics: Journal of Geophysical Research, v. 99, p. 5639–5655, doi:10.1029/94JE00216.

Smith, D.E., and 18 others, 1999, The global topography of Mars and implications for surface evolution: Science, v. 284, p. 1495–1503, doi:10.1126/science.284.5419.1495.

Solomon, S.C., and Head, J.W., III, 1982, Evolution of the Tharsis Province of Mars: The importance of heterogeneous lithospheric thickness and volcanic construction: Journal of Geophysical Research, v. 87, p. 9755–9774, doi:10.1029/JB087iB12p09755.

Solomon, S.C., Aharonson, O., Aurnou, J.M., Banerdt, W.B., Carr, M.H., Dombard, A.J., Frey, H.V., Golombek, M.P., Hauck, S.A., II, Head, J.W., III, Jakosky, B.M., Johnson, C.L., McGovern, P.J., Neumann, G.A., Phillips, R.J., Smith, D.E., and Zuber, M.T., 2005, New perspectives on ancient Mars: Science, v. 307, p. 1214–1220, doi:10.1126/science.1101812.

Spencer, J.R., and Fanale, F.P., 1990, New models for the origin of Valles Marineris closed depressions: Journal of Geophysical Research, v. 95, p. 14,301–14,313, doi:10.1029/JB095iB09p14301.

Squyres, S.W., and 18 others, 2004, In situ evidence for an ancient aqueous environment at Meridiani Planum, Mars: Science, v. 306, p. 1709–1714, doi:10.1126/science.1104559.

Squyres, S.W., Aharonson, O., Clark, B.C., Cohen, B.A., Crumpler, L., de Souza, P.A., Farrand, W.H., Gellert, R., Grant, J., Grotzinger, J.P., Haldemann, A.F.C., Johnson, J.R., Klingelhöfer, G., Lewis, K.W., Li, R., McCoy, T., McEwen, A.S., McSween, H.Y., Ming, D.W., Moore, J.M., Morris, R.V., Parker, T.J., Rice, J.W., Jr., Ruff, S., Schmidt, M., Schröder, C., Soderblom, L.A., and Yen, A., 2007, Pyroclastic activity at Home Plate in Gusev Crater, Mars: Science, v. 316, p. 738–742, doi:10.1126/science.1139045.

Šrámek, O., and Zhong, S., 2010, Long-wavelength stagnant lid convection with hemispheric variation in lithospheric thickness: Link between Martian crustal dichotomy and Tharsis?: Journal of Geophysical Research–Planets, v. 115, E09010, doi:10.1029/2010JE003597.

Šrámek, O., and Zhong, S., 2012, Martian crustal dichotomy andTharsis formation by partial melting coupled to early plume migration: Journal of Geophysical Research–Planets, v. 117, E01005, doi:10.1029/2011JE003867.

Stegman, D.R., Farrington, R., Capitanio, F.A., and Schellart, W.P., 2010, A regime diagram for subduction styles from 3-D numerical models of free subduction: Tectonophysics, v. 483, p. 29–45, doi:10.1016/j.tecto.2009.08.041.

Stern, R.J., 2005, Evidence from ophiolites, blueschists, and ultrahigh-pressure metamorphic terranes that the modern episode of subduction tectonics began in Neoproterozoic time: Geology, v. 33, p. 557–560, doi:10.1130/G21365.1.

Stern, R.J., 2008, Modern style plate tectonics began in Neoproterozoic time: An alternative interpretation of Earth's tectonic history, *in* Condie, K.C., and Pease, V., eds., When Did Plate Tectonics Begin on Planet Earth: Geological Society of America Special Paper 440, p. 265–280.

Stevenson, D.J., 2001, Mars' core and magnetism: Nature, v. 412, p. 214–219, doi:10.1038/35084155.

Tanaka, K.L., 1985, Ice-lubricated gravity spreading of the Olympus Mons aureole deposits: Icarus, v. 62, p. 191–206, doi:10.1016/0019-1035(85)90117-4.

Tanaka, K.L., and Davis, P.A., 1988, Tectonic history of the Syria Planum province of Mars: Journal of Geophysical Research, v. 93, p. 14,893–14,917, doi:10.1029/JB093iB12p14893.

Tanaka, K.L., and MacKinnon, D.K., 2000, Pseudokarst origin for Valles Marineris, *in* Lunar and Planetary Space Science Conference XXXI: Houston, Texas, Lunar and Planetary Institute, Abstract 1780.

Tanaka, K.L., Golombek, M.P., and Banerdt, W.B., 1991, Reconciliation of stress and structural histories of the Tharsis region of Mars: Journal of Geophysical Research, v. 96, p. 15,617–15,633, doi:10.1029/91JE01194.

Taylor, M.H., and Yin, A., 2009, Active faulting on the Tibetan Plateau and surrounding regions: Relationships to earthquakes, contemporary strain, and late Cenozoic volcanism: Geosphere, v. 5, no. 3, p. 199–214, doi:10.1130/GES00217.1.

Taylor, M., Yin, A., Ryerson, F.J., Kapp, P., and Ding, L., 2003, Conjugate strike-slip faulting along the Bangong-Nujiang suture zone accommodates coeval east-west extension and north-south shortening in the interior of the Tibetan Plateau: Tectonics, v. 22, no. 4, 1044, doi:10.1029/2002TC001361.

ten Brink, U., 1991, Volcano spacing and plate rigidity: Geology, v. 19, p. 397–400, doi:10.1130/0091-7613(1991)019<0397:VSAPR>2.3.CO;2.

Turcotte, D.L., and Schubert, G., 2002, Geodynamics: New York, Cambridge University Press, 456 p.

van Hunen, J., and van den Berg, A.P., 2008, Plate tectonics on the early Earth: Limitations imposed by strength and buoyancy of subducted lithosphere: Lithos, v. 103, p. 217–235, doi:10.1016/j.lithos.2007.09.016.

van Hunen, J., van Keken, P.E., Hynes, A., and Davies, G.F., 2008, Tectonics of early Earth: Some geodynamic considerations, *in* Condie K.C., and Pease, V., eds., When Did Plate Tectonics Begin on Planet Earth: Geological Society of America Special Paper 440, p. 157–171.

Vogt, P.R., 1974, 1974, Volcano spacing, fractures, and thickness of the lithosphere: Earth and Planetary Science Letters, v. 21, p. 235–252, doi:10.1016/0012-821X(74)90159-9.

Wadge, G., and Lopes, R.M.C., 1991, The lobes of lava flows on Earth and Olympus Mons, Mars: Bulletin of Volcanology, v. 54, p. 10–24, doi:10.1007/BF00278203.

Watson, E.B., and Harrison, T.M., 2005, Zircon thermometer reveals minimum melting conditions on earliest Earth: Science, v. 308, p. 841–844, doi:10.1126/science.1110873.

Watters, T.R., 1991, Origin of periodically spaced wrinkle ridges on the Tharsis Plateau of Mars: Journal of Geophysical Research. Planets, v. 96, p. 15,599–15,616, doi:10.1029/91JE01402.

Watters, T.R., 1993, Compressional tectonism on Mars: Journal of Geophysical Research–Planets, v. 98, p. 17,049–17,060, doi:10.1029/93JE01138.

Webb, B.M., and Head, J.W., 2002, Noachian tectonics of Syria Planum and the Thaumasia Plateau (abstract): 2002 Annual Lunar and Planetary Science Conference, v. XXXIII, p. 1358.

Werner, S.C., 2009, The global Martian volcanic evolutionary history: Icarus, v. 201, p. 44-68, doi:10.1016/j. icarus.2008.12.019.

Whaler, K., and Purucker, M., 2005, A spatially continuous magnetization model for Mars: Journal of Geophysical Research, v. 110, E09001, doi:10.1029/2004JE002393.

Williams, J.-P., Paige, D.A., and Manning, C.E., 2003, Layering in the wall rock of Valles Marineris: Intrusive and extrusive magmatism: Geophysical Research Letters, v. 1623, doi:10.1029/2003GL017662.

Williams, J.P., Nimmo, F., Moore, W.B., and Paige, D.A., 2008, The formation of Tharsis on Mars: What the line-of-sight gravity is telling us: Journal of Geophysical Research, v. 113, E10011, doi:10.1029/2007JE003050.

Wilson, L., and Head, J.W., III, 2002, Tharsis-radial graben systems as the surface manifestation of plume-related dike intrusion complexes: Models and implications: Journal of Geophysical Research, v. 107, no. E8, 5057, doi:10.1029/2001JE001593.

Wise, D.U., Golombek, M.P., and McGill, G.E., 1979, Tharsis province of Mars: Geologic sequence, geometry, and a deformation mechanism: Icarus, v. 38, p. 456–472, doi:10.1016/0019-1035(79)90200-8.

Witbeck, N.E., Tanaka, K.L., and Scott, D.H., 1991, The Geologic Map of the Valles Marineris Region, Mars: U.S. Geological Survey Miscellaneous Investigations Series Map I-2010.

Wyrick, D.Y., and Smart, K.J., 2009, Dike-induced deformation and Martian graben systems: Journal of Volcanology and Geothermal Research, v. 185, p. 1–11, doi:10.1016/j.jvolgeores.2008.11.022.

Wyrick, D., Ferrill, D.A., Morris, A.P., Colton, S.L., and Sims, D.W., 2004, Distribution, morphology, and origins of Martian pit crater chains: Journal of Geophysical Research, v. 109, E06005, doi:10.1029/2004JE002240.

Yin, A., 2010a, Testing a slab rollback model for the development of the Tharsis rise: Geological Society of America Abstracts with Programs, v. 42, no. 5, p. 645.

Yin, A., 2010b, Evidence for a Crustal-scale Thrust Belt along the Northwestern Margin of the Tharsis Rise: Implications for Possible Plate Subduction on Mars: Abstract EP21A-0734 presented at 2010 Fall Meeting, AGU, San Francisco, California, 13–17 Dec.

Yin, A., 2010c, Cenozoic tectonics of Asia: A preliminary synthesis: Tectonophysics, v. 488, p. 293–325, doi:10.1016/j.tecto.2009.06.002.

Yin, A., 2011a, Impact-induced subduction and slab rollback for the tectonic origin of the Tharsis rise on Mars, *in* 42nd Lunar and Planetary Science Conference, 7–11 March 2011: Abstract 1525.

Yin, A., 2011b, Structural analysis of the southern Valles Marineris trough zones and implications for large-scale left-slip faulting on Mars, *in* 42nd Lunar and Planetary Science Conference, Abstract 1529.

Yin, A., 2012, Structural analysis of the Valles Marineris fault zone: Possible evidence for large-scale strike-slip faulting and a primitive form of plate tectonics on Mars: Lithosphere, v. 4, p. 286–330, doi:10.1130/L192.1.

Yin, A., and Harrison, T.M., 2000, Geologic evolution of the Himalayan-Tibetan orogen: Annual Review of Earth and Planetary Sciences, v. 28, p. 211–280.

Yin, A., and Taylor, M.H., 2011, Mechanics of V-shaped conjugate strike-slip faults and the corresponding continuum mode of continental deformation: Geological Society of America Bulletin, v. 123, p. 1798–1821, doi:10.1130/B30159.1.

Yoshino, T., Yamamoto, H., Okudaira, T., and Toriumi, M., 1998, Crustal thickening of the lower crust of the Kohistan arc (N. Pakistan) deduced from Al zoning in clinopyroxene and plagioclase: Journal of Metamorphic Geology, v. 16, p. 729–748, doi:10.1111/j.1525-1314.1998.00168.x.

Zhong, S., 2009, Migration of Tharsis volcanism on Mars caused by differential rotation of the lithosphere: Nature Geoscience, v. 2, p. 19–23, doi:10.1038/ngeo392.

Zhong, S., and Roberts, J.H., 2003, On the support of the Tharsis Rise on Mars: Earth and Planetary Science Letters, v. 214, p. 1–9, doi:10.1016/S0012-821X(03)00384-4.

Zhong, S., and Roberts, J.H., 2004, Plume-induced topography and geoid anomalies and their implications for the Tharsis rise on Mars: Geophysical Research Letters, v. 109, E03009, doi:10.1029/2003JE002226.

Zuber, M.T., 2001, The crust and mantle of Mars: Nature, v. 412, p. 220–227, doi:10.1038/35084163.

Zuber, M.T., Solomon, S.C., Phillips, R.J., Smith, D.E., Tyler, G.L., Aharonson, O., Balmino, G., Banerdt, W.B., Head, J.W., III, Johnson, C.L., Lemoine, F.G., McGovern, P.J., Neumann, G.A., Rowlands, D.D., and Zhong, S., 2000, Internal structure and early thermal evolution of Mars from *Mars Global Surveyor* topography and gravity: Science, v. 287, p. 1788–1793, doi:10.1126/science.287.5459.1788.

MANUSCRIPT RECEIVED 4 JANUARY 2012
REVISED MANUSCRIPT RECEIVED 21 SEPTEMBER 2012
MANUSCRIPT ACCEPTED 30 SEPTEMBER 2012

Printed in the USA